# THE FINAL STEP IN PHAGE LYSIS: THE ROLE OF THE RZ-RZ1 SPANIN COMPLEX IN THE DISRUPTION OF THE OUTER MEMBRANE

A Dissertation

by

JOEL DALLAS BERRY

Submitted to the Office of Graduate Studies of
Texas A&M University
in partial fulfillment of the requirements for the degree of

DOCTOR OF PHILOSOPHY

May 2010

Major Subject: Biochemistry

# THE FINAL STEP IN PHAGE LYSIS: THE ROLE OF THE RZ-RZ1 SPANIN COMPLEX IN THE DISRUPTION OF THE OUTER MEMBRANE

A Dissertation

by

JOEL DALLAS BERRY

Submitted to the Office of Graduate Studies of
Texas A&M University
in partial fulfillment of the requirements for the degree of

DOCTOR OF PHILOSOPHY

Approved by:

| | |
|---|---|
| Chair of Committee, | Ryland F. Young |
| Committee Members, | Andreas Holzenburg |
| | James C. Sacchettini |
| | Paul Straight |
| Head of Department, | Gregory D. Reinhart |

May 2010

Major Subject: Biochemistry

# ABSTRACT

The Final Step in Phage Lysis: The Role of the Rz-Rz1 Spanin Complex in the Disruption of the Outer Membrane. (May 2010)

Joel Dallas Berry, B.S., Mississippi State University

Chair of Advisory Committee: Dr. Ryland F. Young

The purpose of the work described in this dissertation is to better understand the role of Rz and Rz1 function with respect to phage lysis. We determined using both a genetic and biochemical approach that the Rz protein is an inner membrane protein containing a single N-terminal transmembrane domain (TMD) with an $N_{in}/C_{out}$ topology. Consistent with previous work on Rz1 (Taylor *et al.*, 1996), the Rz1 lipoprotein was found to be localized to the outer membrane (OM).

Following localization, both Rz and Rz1 form homodimers *in vivo* due to intermolecular disulfide formation. Despite being localized to apposing membranes, the two proteins form a complex. A small number of phages encode a potential single protein equivalent of Rz-Rz1. This protein, termed a spanin, is predicted to tether the inner and outer membranes by a single polypeptide chain. Based on complementation, it was concluded that gp11 from the phage T1 is a functional equivalent of Rz-Rz1. Gp11, and by analogy the Rz-Rz1 two-component spanin complex, threads the meshwork of the PG layer. The presence of an Rz-Rz1 complex, which forms in the presence of peptidoglycan (PG), is supported by *in vivo* results.

The soluble periplasmic domains of Rz and Rz1, which are dimeric and monomeric respectively, were purified. Circular dichroism analysis indicates that Rz is structured, with significant α-helical content, whereas Rz1, in which 10 out 39 residues are proline, is unstructured. Mixing the proteins results in the formation of a complex with significant new α-helical content. Negative-stain images reveal ~ 25 nm x ~ 4 nm rod-shaped structures.

Holin independent activity of Rz and Rz1 is found to disrupt whole cells. Furthermore, time lapse microscopy of λ and λ$Rz_{am}$ lysis allows us to conclude that Rz and Rz1 are essential for lysis. These results suggest a model for Rz-Rz1 function which begins with Rz and Rz1 forming a complex through direct interaction prior to holin and endolysin function. Holin-mediated hole formation allows the endolysin to degrade PG which sterically hinders Rz-Rz1 activity. Removal of PG by endolysin degradation thus triggers Rz-Rz1 OM disruption via fusion of the inner and outer membranes.

## ACKNOWLEDGMENTS

I would like to start by thanking my family for their guidance and support over the years. Certainly without their assistance I would not be where I am today. I would also like to thank my fiancé Harmony Turk. It is her strong will and ability to make me laugh that helped keep me going when progress was slow. Thanks to my committee members: Andreas Holzenburg, James C. Sacchettini, and Paul Straight for generously providing their time and expertise over the last seven years. Thanks to Doug Struck as well. His mastery of experimental design and ability to ask the right questions had a profound impact on me early in my career. I would also like to thank all of the Young lab members, past and present, for allowing me to bend their ears with my thoughts from time to time. Thanks especially to Rebecca White, John Deaton, and Min Xu for their patience and expertise while they were helping me make my first steps as a molecular biologist/biochemist. Thanks as well to the Young lab administrative assistant Daisy Wilbert. She is very instrumental in many aspects of the Young lab, but I would like to thank her especially for assistance in arranging many committee meetings. I would also like to thank one of my collaborators, Christos Savva, for his greatly appreciated help with the Rz/Rz1 complex characterization. Lastly, I would like to thank my mentor Ry Young. His enthusiasm for science and great teaching are unrelenting. Although he is the busiest person I have ever known, somehow he manages to find time to offer great ideas for experiments as well as the occasional funny story.

# TABLE OF CONTENTS

CHAPTER Page

# LIST OF FIGURES

FIGURE Page

# LIST OF TABLES

# CHAPTER I

## INTRODUCTION

Bacteriophages (phages) are viruses of bacteria. Greater than 90% of phages have a large (>14 kb) double-stranded nucleic acid (dsDNA) genome. The vast majority of large dsDNA phages are of the order Caudovirales, or tailed-phages, which have as their distinguishing characteristics (a) a single linear dsDNA chromosome and (b) an apparatus for attaching to the host exterior and injecting that DNA into the host cytoplasm. Entry of the viral DNA into the host cytoplasm begins a cascade of phage encoded molecular processes. One process is the production and assembly of progeny phage. To ensure progeny release, all phages must overcome the host cell envelope. The process by which a phage destroys the cell envelope leading to dissolution of the host cell is referred to as phage lysis.

Phage lysis is an exceedingly common and influential biological process. Phages are the most abundant life form on earth resulting in ~ $10^{29}$ infection cycles per day. A recent study concluded that phage turnover of prokaryotic life in the deep-sea has a major impact on the global biogeochemical cycle (Danovaro *et al.*, 2008). Furthermore, phage production and lysis is associated with the production and release of bacterial toxins (Wagner *et al.*, 2002, Summer *et al.*, 2007b) . The predominance of phage lysis in the natural world and its role in bacterial pathogenesis merits its investigation.

---

This dissertation follows the style and formatting of *Molecular Microbiology*.

## Lysis by large dsDNA phages

### Two-component lysis

The lysis program of all large dsDNA phages targets the host cell  All of these phages encode at least two proteins for host lysis. The holin is a small inner membrane (IM) protein, which produces 'hole(s)' in the IM at an allele specific time. The holin is often described as a molecular clock (Young & Blasi, 1995, Grundling *et al.*, 2001) because the timing of its activity appears to be the "rate-limiting step" of lysis. The endolysin is a peptidoglycan (PG) degrading enzyme. The PG is the primary line of defense against lysis due to intracellular osmotic pressure. Two classes of topologically distinct endolysins have been identified to date. Soluble endolysins accumulate in the cytoplasm and are reliant on holin activity to gain access to the PG. An additional class of endolysin is defined by the presence of an N-terminal signal anchor release (SAR) domain. The SAR domain is a specialized signal sequence which targets the endolysin for secretion to the periplasm. Following secretion, the SAR endolysin remains tethered to the IM until being released spontaneously or by collapse of the proton motive force due to holin-mediated hole formation (Xu *et al.*, 2004). Although the initial localization of an endolysin can vary, the end result is always the same. Holin-mediated hole formation results in active-soluble endolysins gaining access to the PG. In the absence of an intact PG layer, the cell envelope succumbs to internal osmotic pressure and the cell lyses.

A third lysis component

Most large dsDNA phage which infect a Gram-negative host have an additional pair of lysis genes (Summer *et al.*, 2007a). The *Rz* and *Rz1* genes, first identified in the tailed-phage lambda (λ), have an unusual genetic architecture. The smaller *Rz1* reading frame is entirely embedded in the +1 register with respect to the *Rz* reading frame. A null mutation in the λ *Rz* or *Rz1* gene results in an identical conditional-lysis block. If the growth media is supplemented with millimolar (mM) levels of divalent cations, phage release is blocked due to the formation of meta-stable spherical cells as opposed to lysis (Zhang & Young, 1999). Divalent cations are known to stabilize the outer membrane (OM) (Leive, 1974) through interactions with the negatively charged groups of the lipopolysaccharide (LPS) molecule (Osborn & Munson, 1974). However, in the absence of additional divalent cations the holin and endolysin are necessary and sufficient to cause lysis. The molecular basis of Rz and Rz1 function is currently unknown, but the identical lysis block caused by *Rz* or *Rz1* null mutations indicates the two proteins are involved in the same biological pathway.

Although the phenotype is conditional in the laboratory, conservation of the *Rz/Rz1* genes indicates they provide a selective advantage. The divalent cation dependent phenotype coupled with the fact λ *Rz/Rz1* equivalents do not occur in phages which lack an OM is highly suggestive that their function is not necessary in the absence of an outer membrane (OM). It is the contention of this dissertation that the biological role of Rz and Rz1 is solely to disrupt the OM. λ, a prototype of molecular biology, has

also served as the prototype of large dsDNA phage lysis. The goal of this dissertation is to update the canonical model for phage lysis by describing the biological role of the λ spanin proteins, i.e., Rz and Rz1. Since the lysis gene products of tailed phages are systematically attacking each layer of the cell envelope, it is essential to discuss each individual component and its function in further detail.

**Structure and barrier function of the cell envelope**

For phages that infect Gram-negative bacteria, the cell envelope imposes a physical barrier which prevents progeny release at the end of their respective infection cycle. The three structural components of the Gram-negative cell envelope are the cytoplasmic or IM, PG, and OM (Fig. 1.1). The envelope consists of three independent physical barriers, but the PG is typically regarded as the primary defense against rupture due to internal osmotic pressure (Holtje, 1998) and thus phage release. The lysis systems of coliphages such as λ, T4, and P2 are the best described so only the cell envelope of their Gram-negative host *Escherichia coli* (*E. coli*) will be described here. Many of the features which will be discussed are common to the majority of other Gram-negative species.

The OM is an asymmetric barrier, with an inner leaflet of phospholipids and an outer leaflet composed of LPS (Bayer, 1974). The barrier function of the OM was first realized as it became apparent that Gram-negative cells were less susceptible to drug action than a Gram-positive organism. The OM's role as a barrier was further supported

by the discovery that treatment of *E. coli* with ethylenediaminetetraacetate (EDTA) leads to the release of the LPS layer and thus increased susceptibility to drug action (Leive, 1974). The barrier function of the OM is enhanced by the presence of millimolar concentrations of divalent cations like $Mg^{++}$ and $Ca^{++}$ (Leive, 1974). Divalent cations compensate for the anionic character of both phosphate and carboxyl groups in the LPS.

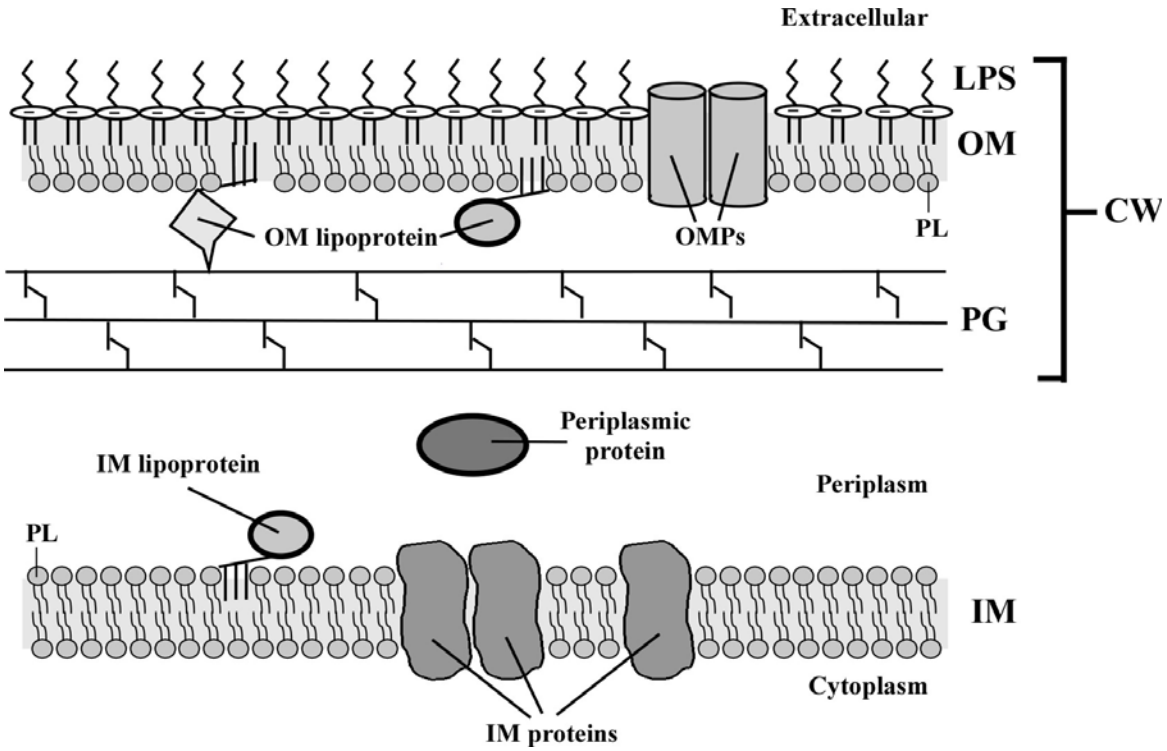


Figure 1.1. The *E. coli* cell envelope. See text for details. The following abbreviations are used: IM, inner membrane; PG, peptidoglycan; OM, outer membrane; LPS, lipopolysaccharide; CW, cell wall; PL, phospholipid; OMPs, outer membrane proteins. The OM lipoprotein, LPP, contacts the PG layer to indicate the LPP-PG covalent linkage (Braun et al., 1974).

While the exact mechanism of stabilization is still debated, available evidence suggests that divalent cations are participating in the formation of ionic bridges between adjacent

LPS molecules (Schindler & Osborn, 1979). In contrast, the IM is a symmetric bilayer in that the inner and outer leaflets are both composed entirely of phospholipids.

The IM and OM are theoretically capable of impeding phage release in the absence of an intact PG layer. Cells in which the PG layer has been compromised by external addition of lysozyme can remain intact but become much more susceptible to lysis by osmotic shock (Birdsell & Cota-Robles, 1967) In addition, cells lacking an intact PG layer, are equally susceptible to osmotic shock both with and without an intact OM. Based on this evidence it was concluded that the rigidity of the IM and OM are comparable. The study however did not account for possible improvements in OM stability due to the presence of elevated levels of divalent cations

The space between the IM and OM is the periplasm. More than one group has concluded that the osmotic strength of the periplasm is equal to that of the cytoplasm (Cayley *et al.*, 2000, Stock *et al.*, 1977) The PG is located in the periplasm and it is a large and highly insoluble macromolecule made up of oligopeptide cross-linked polysaccharide strands (Holtje, 1998). The thickness of the periplasm is still a matter of controversy but one of the most reliable estimates, based on thin-sections of rapidly frozen whole cells, is 21 ± 3 nm (Matias *et al.*, 2003). Also located in the periplasmic space are the membrane-derived oligosaccharides (MDO). The E.coli MDO consist of 8-10 glucose units which are highly branched and variably decorated with sn-1-phosphoglycerol and phosphoethanolamine residues derived from the membrane phospholipids. The polyanionic character of MDO allows the cell to maintain the

isoosmotic balance between the cytoplasmic and periplasmic spaces when growth is occurring in medium of low osmolarity (Kennedy & Rumley, 1988).

Several classes of proteins reside in the cell envelope. Soluble proteins in the periplasm are localized there by secretion, mostly through the Sec translocon (Oliver, 1996), accompanied by proteolytic removal of an N-terminal signal sequence by signal peptidase I (SPI) (Park, 1996). Both membranes have integral membrane proteins with distinct secondary structure. All IM proteins have alpha-helical transmembrane domains (TMDs) (Park, 1996). In contrast, most of the integral membrane proteins of the OM span the membrane with beta-barrel structures (Nikaido, 1996). Members of a distinct class of membrane proteins, the lipoproteins can be found in both the IM and OM. Lipoproteins are secreted through the Sec translocon but are processed at a Cysteine (Cys) residue by Signal Peptidase II (SPII). Lipoproteins are further modified by lipoylation at the newly exposed N-terminal Cys residue. Lipoproteins destined for the periplasmic leaflet of the OM are first released from the IM by an ATP-binding cassette transporter, LolCDE IM lipoproteins avoid the LolCDE step due to the presence of aspartic residues located at the +2 and +3 positions of the mature lipoprotein (Hara *et al.*, 2003, Tokuda & Matsuyama, 2004). The LolCDE released lipoprotein then interacts with a soluble periplasmic chaperone, LolA. The LolA-lipoprotein complex interacts with an OM receptor, LolB. This interaction leads to lipoprotein transfer to the periplasmic leaflet of the OM (Tokuda & Matsuyama, 2004). The most abundant protein in *E. coli* is the OM lipoprotein Lpp, formerly known as Braun's lipoprotein. Lpp is present at about 750,000 copies per cell, with about a one-third being covalently

bound to the PG via oligopeptide linkages to the ε-amino group of its C-terminal lysine (Braun *et al.*, 1974). The significance of the Lpp-PG linkage is best understood when one considers that the cellular turgor pressure is also exerted on the OM due to the isoosmotic relationship of the cytoplasm and periplasm (Stock et al., 1977). Thus together, the OM, Lpp, and PG form a cohesive unit or cell wall (CW) (Leive, 1974). The cell wall resists the pressure of several atmospheres due to the outwardly directed intracellular turgor pressure.

## The holin-endolysin system

### The λ paradigm

The molecular events leading up to host lysis are currently described by the holin-endolysin system in the case of dsDNA phage. Among these phages, the lysis system of λ is by far the best characterized on both the genetic and biochemical levels. λ is an ideal model in part because it is a temperate phage. A temperature-sensitive allele of the λ cI repressor (*cI857*), which maintains the lysogenic state, can be exploited to synchronously induce the lytic cycle of an entire culture under carefully controlled physiological conditions.

The four λ lysis genes *S*, *R*, *Rz* and *Rz1* are tightly linked on the phage genome and are the first of all the late genes to be transcribed upon Q driven anti-termination at the late promoter, pR', approximately 8 minutes post infection (Fig. 1.2A).

Transcription from pR' is constitutive and leads to the continuous translation and accumulation of all the lysis gene products up to the normal lysis time of 50 minutes. The endolysin, encoded by the *R* gene, is a 17 kDa soluble transglycosylase which cleaves the β(1→4) glycosidic bond of the PG backbone forming glycan chains (Bienkowska-Szewczyk *et al.*, 1981). R function is entirely dependent on the holin protein because it accumulates fully folded in the cytoplasm but lacks the necessary N-terminal signal sequence for transport to the periplasm (Fig. 1.2B). The holin protein, or S105, is one of two proteins translated from the *S* gene. S105 is a 105 residue IM protein constituting a short N-terminal periplasmic domain followed by three TMDs and a positively charged cytoplasmic tail. The holin protein is so named due to the model which describes first an oligomerization of S105 followed by a spontaneous conformational change or "triggering event" to form holes in the IM. Thus in addition to collapsing the IM potential, the holin permits the non-specific release of cytoplasmic contents, including R. Holin proteins also have the distinct property of triggering in response to collapse of the proton motive force (pmf) through exposure to energy poisons such as cyanide (Reader & Siminovitch, 1971).

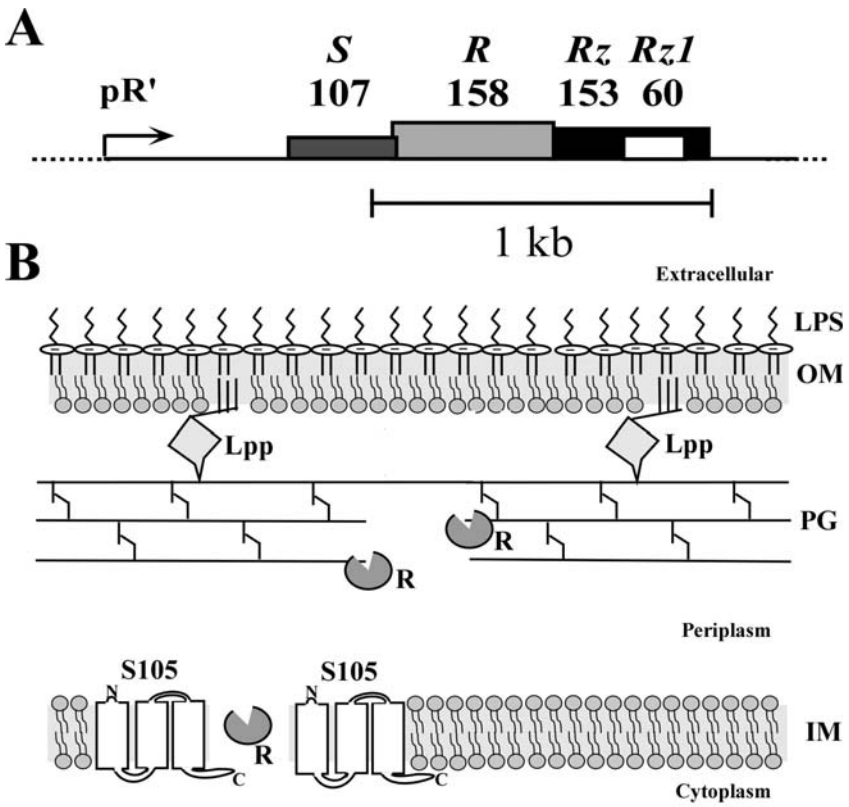


Figure 1.2. The holin-endolysin system.
A. The λ lysis cassette. Drawn to scale is the region of the λ genome beginning with the late promoter pR' and extending through the *Rz* gene. The corresponding codon number of each gene is indicated.
B. The canonical model for tailed-dsDNA phage lysis. Only lysis proteins with a described function are shown. See text for details.

The structure of the hole is still undetermined but its existence is backed by a wealth of experimental evidence (Young & Wang, 2006). One of the defining genetic characteristics of the *S* gene is that its disruption, as in λ*Sam7R*$^{+}$, leads to unabated phage accumulation well beyond the characteristic 50 minute endpoint of the vegetative growth period. However, if the membranes of these un-lysed cells are made permeable through chloroform exposure the cells lyse within minutes due to R activity. Thermal

induction of λ*S*$^{+}$*Ram* does not result in lysis, but does result in cell death at 50 minutes because S105 function collapses the pmf (Young, 1992).

The most conclusive evidence to support S105 hole formation *in vivo* comes from cryo-EM examination of rapidly frozen whole cells. Micrographs revealed large gaps in the IM of cells induced for *S105* expression and frozen ten minutes past the normal time of triggering. The gaps appear to be dependent only on *S105* expression alone because control cells revealed no gaps. Tomography reconstruction of a single cell confirmed that the gaps are in fact large irregularly shaped holes. Analysis indicates that ~ 2 holes are formed per cell and they ranged in size from 88 nm to 1.2 μm, with an average diameter of ~ 340nm (Dewey *et al.*, 2009). These results are consistent with another *in vivo* localization study which utilized an S105ΦGFP fusion. The fusion protein was found to form large patches of fluorescence at the time of triggering, whereas prior to hole formation the S105ΦGFP proteins were observed to be evenly distributed throughout the membrane (White and Young, unpublished). S105 oligomerization is supported by the *in vivo* DSP crosslinking (Wilson, 1982) of oligomeric states and by the observation that, upon SDS-PAGE and Western blotting, the purified protein itself produces a ladder of successive oligomers up to a tetramer (Smith *et al.*, 1998b).

Throughout the entire λ lytic growth cycle, R is fully functional and its activity is limited only by the presence of the IM. Thus, the timing of S105 hole formation determines the time of lysis. Timing of S105 hole formation is regulated on both the translational and protein structure levels. Translation of the S gene results in two gene

products. The holin, S105, is translated from Met3 of the S reading frame and the anti-holin, S107, from Met1 (Fig. 1.3A). A missense mutation of M3L results in the production of a non-hole forming inhibitor of S105. Mutating Met1 to a Lys residue accelerates lysis by about 5 to 8 minutes compared to the normal time (Blasi *et al.*, 1989). The ratio of S105 to S107 produced during a phage infection is determined by a stem loop structure upstream of Met1 called the sdi (site directed initiation) (Chang *et al.*, 1995). A single additional positive charge contributed by Lys2 of S107 is responsible for its inhibition of S105 function**.** The current model of S107 inhibition dictates that the additional positive charge prevents TM1 from assuming an N-out topology (Fig. 1.3B) (Blasi *et al.*, 1990). This model is consistent with the dominant-negative character of S105ΔTM1 (White *et al.*, 2009).

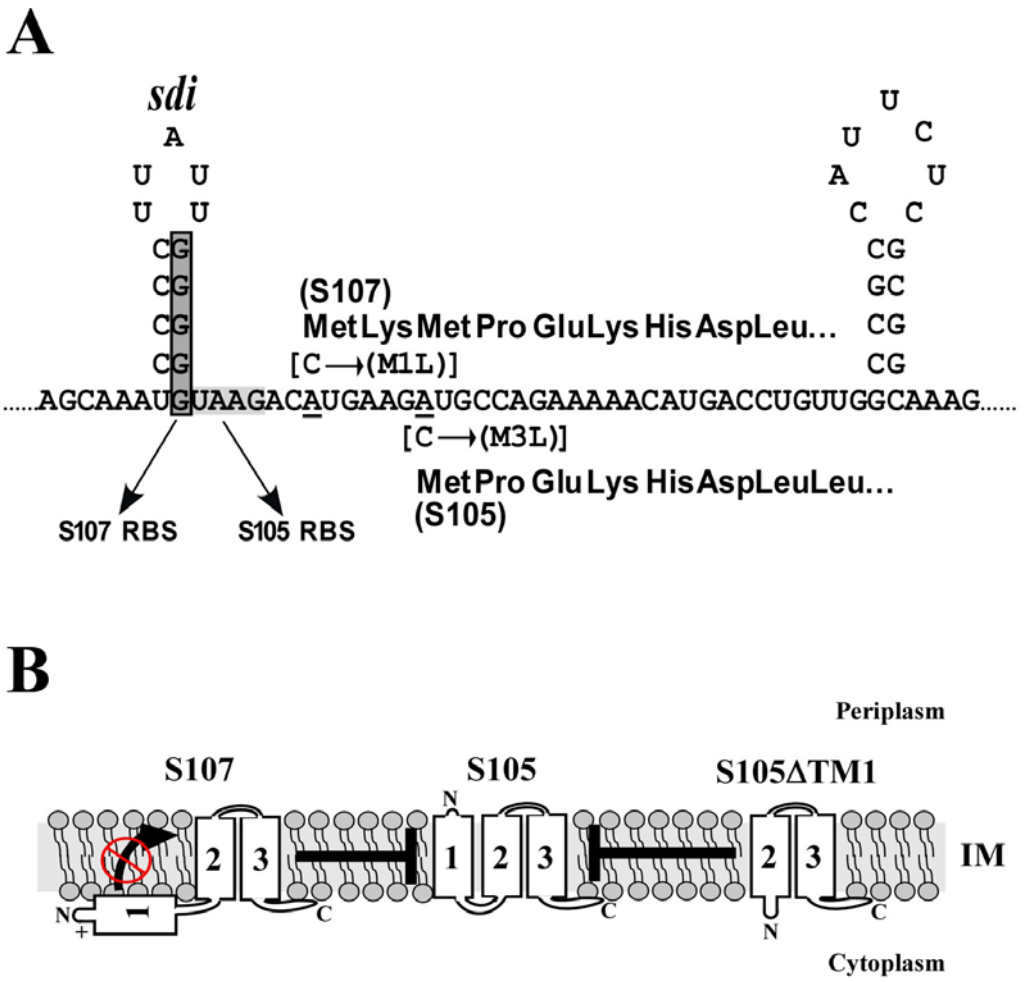


Figure 1.3. The dual-start motif and topological models for S105 inhibitors.
A. Shown is the region of the λ pR' transcript beginning just upstream of the *S107* and *S105* reading frames. The ratio of S105 and S107 produced during the course of phage infection is determined by the site-directed initiation (sdi) stem-loop structure. In this example, the sdi stem-loop is present and translation of *S105* is favored since the *S107* ribosome binding site (RBS) is not available for binding to the complementary sequence of the 16S rRNA (Chang et al., 1995). The mutations leading to a block of *S107* (M1L) or *S105* (M3L) translation are indicated above and below the mRNA sequence, respectively.
B. The predicted inhibitory topologies of S107 and S105ΔTM1. The additional positive charge, contributed by Lys2, at the N-terminus of S107 is speculated to prevent TM1 from flipping through the IM to achieve an $N_{out}$ topology (Blasi & Young, 1996). S105ΔTM1 is an inhibitor of S105 and is predicted to have a $N_{in}/C_{in}$ topology (White et al., 2009).

S105 primary structure is also a key determinant of lysis timing. A single missense mutation in S105 can have drastic affects on lysis timing. For example, the Ala at position 52 when converted to a Gly accelerates the time of lysis to 20 minutes (Johnson-Boaz *et al.*, 1994). However if the same Ala is converted to a Val then lysis is delayed indefinitely (Johnson-Boaz et al., 1994, Raab *et al.*, 1988). In fact, many single missense mutations have been isolated or created by mutagenesis throughout the three TMDs of S105 which effect lysis timing (Zheng *et al.*, 2008, Raab *et al.*, 1986). These results and genetic experiments demonstrating the dominance/recessiveness of various S105 alleles (Raab et al., 1988) have lead to a model for S105 behavior which is intimately related to helical packing of the three TMDs.

It is now clear that the holin oligomerizes to produces a large non-specific hole in the IM at an allele specific time to allow endolysin release. The endolysin then proceeds to cleave glycosidic bonds of the PG which are critical for the maintenance of cell shape and viability. However, the holin-endolysin model for phage lysis is not sufficient to describe lysis if the OM is stabilized by divalent cations. Under this circumstance the Rz/Rz1 genes are essential. The spherical cell phenotype is consistent with holin and endolysin function. Presumably, the cell morphology is changing from rod to spherical as a result of extensive endolysin mediated PG degradation. It is only when the OM, although mechanically fragile, is stabilized sufficiently that it can withstand the force of osmotic pressure. The spherical cell phenotype indicates that the selective pressure, which has led to conservation of Rz/Rz1 genes among phage which infect a Gram-negative host, is OM disruption.

Variations of the λ theme

Many endolysins are not soluble-cytoplasmic proteins. The "SAR endolysins" from the phages 21 ($R^{21}$) and P1 (Lyz) for example have been shown to possess N-terminal SAR (signal anchor release) domains (Sun *et al.*, 2009, Xu et al., 2004). SAR domains are very similar to hydrophobic TMDs with the exception that they are rich in relatively nonhydrophobic residues such as Gly, Ala, Ser, and Thr. The SAR domain targets the endolysin for secretion to the periplasm by the sec system. The membrane tethered endolysin is inactive. When the endolysin is released from the IM it refolds into an active form. Its release can be induced by the collapse of the proton motive force (pmf) with energy poisons such as dinitrophenol (Xu et al., 2004). Holin-mediated hole formation collapses the pmf and thus also results in SAR endolysin release. SAR endolysin release also occurs more slowly on a spontaneous basis. The endolysin-specific spontaneous release can serve a practical purpose. It provides a holin independent pathway to investigate Rz and Rz1 function (Chapter III).

Holins represent a large and diverse group of proteins which at this time are classified based on their number of TMDs as well as the resulting topology (Young, 2005). The three holin classes are illustrated by the respective prototypical member in Figure 1.4. Class I holins like λS105 have three TMDs and an $N_{out}/C_{in}$ topology. Class II members like the phage 21 holin, $S^{21}$, have two TMDs and an $N_{in}/C_{in}$ topology. The T4 holin, T, represents class III and it has a single N-terminal TMD and an $N_{in}/C_{out}$

topology. $S^{21}$ is different from the other two classes for reasons aside from TMD number and topology alone.

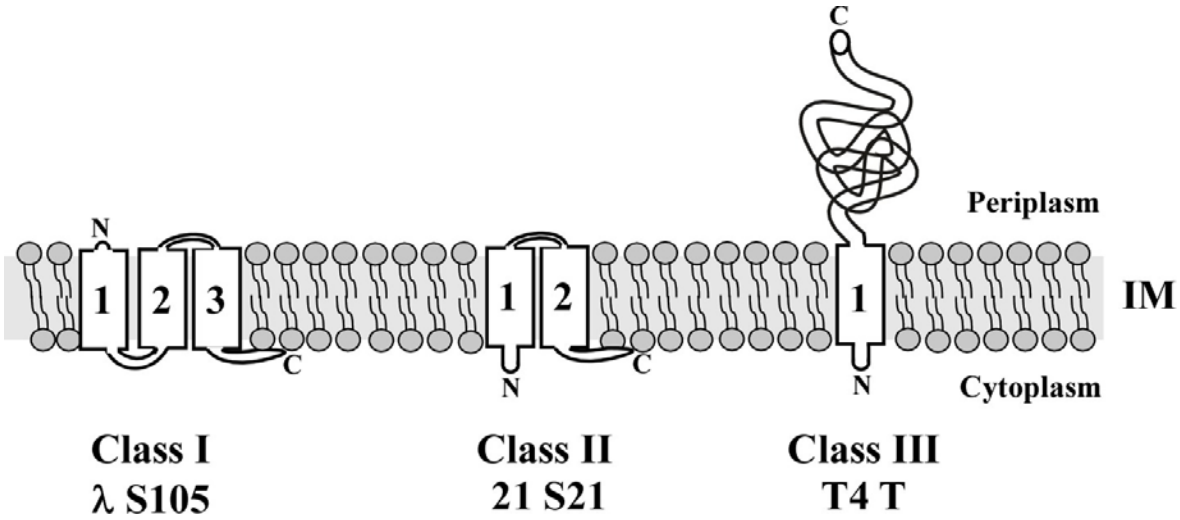


Figure 1.4. The three holin classes. Illustrated are the topologies for the three prototype members of the Class I-III holins, respectively. Class I holins have three TMDs in a $N_{out}/C_{in}$ topology, Class II holins have 2 TMDs with a $N_{in}/C_{in}$ topology, and Class III holins have a single TMD with a $N_{in}/C_{out}$ topology. TMDs are numbered beginning from the N-terminus and topologies are with respect to the periplasm being out and the cytoplasm being in.

Dynamic membrane topology is not unique to SAR endolysins. The first TMD of $S^{21}$ was found to be sensitive to protease cleavage after cells were converted to spheroplasts (Park *et al.*, 2006). Also supporting a periplasmic localization for the N-terminal SAR domain was the observation that $S^{21}$ forms disulfide linked homodimers if the Ser at position 16 was substituted with Cys. It was concluded that the first TMD of $S^{21}$ leaves the bilayer following membrane insertion resulting in an Nout/Cin topology.

An experiment conducted by Park et al. 2007 demonstrated that $S^{21}$ produces holes smaller than λS. Through the use of a GFP mutant carrying a signal sequence for export to the periplasm, it was shown that unlike λS, triggering of $S^{21}$ did not allow diffusion of the periplasmic GFP to the cytoplasm. The diameter of the $S^{21}$ hole was narrowed down to values below ~15 nm after it was determined that the $S^{21}$ holin could not complement the lysis defect of $\lambda S_{am}R^{+}$(Park *et al.*, 2007). It was this discovery that lead to the term "pinholin" to describe $S^{21}$ and other small hole forming holins.

Canonical holins like λS105 can function with cytoplasmic endolysins and SAR endolysins. However, a pinholin such as $S^{21}$, while lethal on its own, can not bring about lysis unless paired with a SAR endolysin (Park et al., 2007). So the function of both S105 and $S^{21}$ is the same, the difference being that $S^{21}$ just serves to depolarize the membrane and cause the synchronous release of SAR endolysins. So where do the spanin proteins fit into all this? It is impossible to answer this question without knowing the mechanism of spanin function. However, spanin genes can be found along with genes which make up pinholin and SAR endolysin lysis systems. In fact, the phage 21 contains an embedded *Rz/Rz1* gene pair and the gene products are closely related to λ Rz and Rz1 based on primary structure (Summer et al., 2007a).

## History of the λ *Rz* and *Rz1* genes

### The discovery of *Rz* and *Rz1*

Young et al. conducted Tn903, a transposable kanamycin resistant element, mutagenesis of λ and isolated two classes of mutants which adversely affected growth (i.e. plaque formation) while maintaining the ability to assemble phage particles and establish themselves as lysogens. Of these two classes, only one represented by two mutant phages designated λdk6 and λdk23 could not form plaques when plated on a *supF* host which suppresses the non-functional *Sam7* allele. Both phages carried the *Sam7* to increase phage production in a non-suppressing host. The location of the Tn903 insertions for both phages was determined by heteroduplex mapping and restriction digestion. Both mapped to a near identical location on the chromosome which was just distal to the right end of the *R* gene. The λ physical map had no gene at this location so the phages were tested to determine if they defined a new complementation group. Complementation experiments confirmed that the Tn:903 insertion mutants represented a new group and it was designated *Rz* due to its close proximity to the *R* gene (Young et al., 1979). Subsequent sequencing of the cloned lysis gene region from λdk23 confirmed that Tn903 was in fact inserted between nucleotides 43 and 44 of the *Rz* reading frame (Taylor *et al.*, 1983).

At the time *Rz* was discovered it was known that null mutations in either of the previously identified lysis genes, *S* and *R*, also resulted in loss of plaque formation

without affecting production of viable phage (Harris *et al.*, 1967, Campbell & Delcampillo-Campbell, 1963). This knowledge coupled with the fact that $S^+$ allele recombinants of λdk6 and λdk23 only gained the ability to form pinpoint plaques was highly suggestive that the Rz gene product had a role in lysis. The role of Rz in lysis was examined by testing the ability of λdk6$S^+$ to produce bulk lysis of a liquid culture approximately 30 minutes post infection. λdk6$S^+$ failed the test as it merely resulted in only a slight decrease in optical density at the time of lysis as opposed to the characteristic precipitous drop in optical density after λ$S^+$ infection. However, interpretation of this finding was initially clouded by a contradictory result. When lysis was monitored as a result of λdk6$S^+$ lysogenic induction the growth curve was indistinguishable from that of λ$S^+$.

It was subsequently determined that the difference in the one-step growth curves of the infection versus the lysogenic induction were due solely to the presence or absence of 10 mM $MgCl_2$, respectively. The addition of Mg to the liquid growth media is only necessary in the case of the infection because its sole purpose is to aid in phage adsorption. As expected, addition of 10 mM $MgCl_2$ to solid media abolished pinpoint plaque formation of λdk6$S^+$ thus establishing a Mg dependent lysis defect. The $Mg^{++}$ dependent growth defect in liquid or on solid media is explained by the observation that λdk6$S^+$ infection in liquid media terminates in the formation of metastable spherically shaped cells as opposed to lysis. The formation of spherical cells explains why the growth curve of a host following λdk6$S^+$ infection plateaus following an initial slight decrease. The slight decrease does not indicate partial lysis but rather that the spherical

cells do not scatter light with the same efficiency as rod shaped cells. Young et. al (1979) went on to define *Rz* as an essential gene but it would gradually lose this distinction over time. To date the Rz gene is still widely considered a non-essential accessory lysis gene.

The first attempt to clone *Rz* for overexpression from a T7 promoter inadvertently resulted in the discovery of an embedded open reading frame (Hanych et al., 1993). This abortive attempt to subclone a segment of the lambda lysis gene region resulted in a 4 b.p. deletion within the 5' end of the *Rz* reading frame. The deletion, which resulted in a frame shift mutation of *Rz*, went undetected until after the resulting plasmid, pSB54, was induced for expression. Aside from the lack of an *Rz* gene product, what also caught the attention of the authors was the appearance of a 6.5 kDa $^{35}$S-Methione labeled species following sodium dodecyl sulfate polyacrylamide electrophoresis (SDS-PAGE). This band was not present in control samples and it was subsequently concluded the 6.5 kiloDalton (kDa) species may correspond to a 60 codon reading frame entirely embedded within *Rz* in a +1 frame (Fig. 1.5A). The embedded reading frame has a strong ribosome binding site within 8 nt of the AUG and it coded for a basic protein (pI 9.06) with a predicted molecular weight of 6,589 Da. Induction of a plasmid carrying only this 60 codon reading frame also resulted in accumulation of the 6.5 kDa protein. The newly discovered open reading frame was given the name *Rz1* (Fig. 1.5C) (Hanych et al., 1993).

Biochemical analysis of Rz and Rz1

Early biochemical investigation of the *Rz* and *Rz1* gene products was limited entirely to their sub-cellular localization and the extent, if any, of post-translational modifications. *Rz* encodes a 153 residue basic (pI 9.3) protein with a predicted molecular mass of 17229 Da (Fig. 1.5B) (Taylor et al., 1983). Plasmid pBH21 was generated by sub-cloning the lambda genomic region containing *Rz*, and thus its embedded partner *Rz1*, downstream of the T7 promoter and strong RBS of vector pT7-7 (Hanych et al., 1993). Accumulation of a $^{35}$S-Methione labeled protein with a relative mobility ($M_r$) of 17 kDa was identified both in vivo and in vitro upon induction of pBH21 expression. The $M_r$ of the Rz product is identical whether expressed *in vivo* or *in vitro*. From this the authors concluded that the putative cleavable signal sequence at the N-terminus is in fact a TM domain**.**

Utilizing pBH21, Haynch et al. (1993) localized the Rz protein to the IM, intermediate zone (IZ), and OM fractions after isopycnic density gradient centrifugation.. From these results it would appear that Rz is a membrane protein which in the least is localized to both the inner and outer membranes. However, two key aspects of the experimental design complicate interpretation. Rz and the Rz1 6.5 kDa gene product both clearly accumulate upon *in vivo* induction of pBH21.

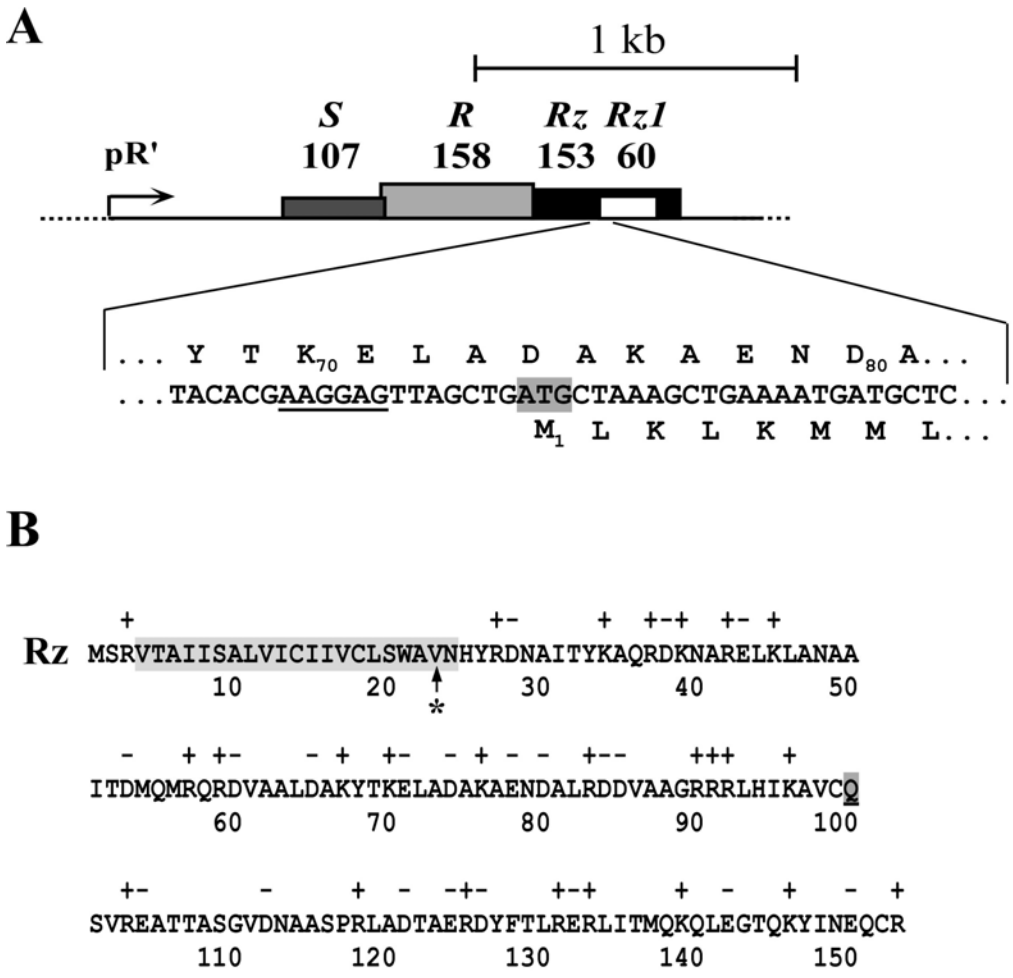


Figure. 1.5. The embedded *Rz1* reading frame and the primary structures of Rz and Rz1.
A. *Rz1* is entirely embedded in the +1 frame of *Rz*. Shown below the λ lysis cassette is a close up of the nucleotide region where the *Rz* reading frame first overlaps that of *Rz1*. The respective translation products for *Rz* and *Rz1* are shown above and below the nucleotide sequence. The *Rz1* shine-dalgarno is underlined and the start codon is highlighted.
B. The *Rz* gene translation product. Charged residues are indicated. The putative N-terminal transmembrane domain is highlighted and the asterisk marks the potential signal peptidase I cleavage site (Bendtsen *et al.*, 2004). The location of the amber stop codon substitution is highlighted and underlined (Zhang & Young, 1999).
C. The *Rz1* gene translation product. Charged residues are indicated. The N-terminal lipoprotein signal sequence (Juncker *et al.*, 2003) is highlighted in grey and the processed Cys residue is highlighted in black. The location of the amber stop codon substitution is highlighted and underlined (Zhang & Young, 1999).

C

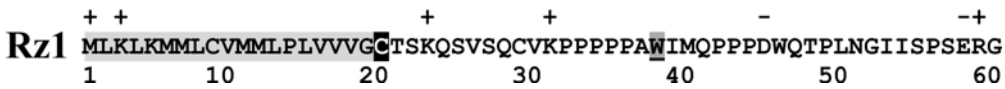


Fig. 1.5 Continued.

It is unclear if the authors were aware of the *Rz1* open reading frame located in pBH21 at the time of publication, but they do not account for what, if any, affect its presence could have on the localization of Rz. Secondly, the over-expression of Rz for subsequent localization could lead to artifactual results due to membrane toxicity. The sub-cellular localization of Rz and Rz1 when expressed alone or together at physiologically relevant concentrations is thus warranted and is addressed in Chapter III of this dissertation.

Using a computer based prediction program it was determined that the N-terminus of Rz1 may contain a lipoprotein signal sequence (Kedzierska *et al.*, 1996). Treatment of cells, induced for the plasmid borne expression of Rz1, with the SpaseII specific inhibitor globomycin resulted in the accumulation of an Rz1 species with a slightly lower $M_r$. It was concluded that this larger protein represented the prolipoprotein form of Rz1 (Taylor *et al.*, 1996). A conclusive demonstration of Rz1 lipid modification began with treatment of cells, induced for Rz1 expression, with [9, 10-$^3$H] palmitic acid. Subsequent analysis of labeled products by western blotting and autoradiography indicated the mature form of Rz1 is modified by [9, 10-$^3$H] palmitic acid (Kedzierska et al., 1996). Membranes from the induced lysogen W3350$\lambda cI857S_{am}7$ were separated by

isopycnic gradient centrifugation and fractions were resolved by SDS-PAGE. A western blot probed with the Rz1 antibody indicated the mature Rz1 is associated with the OM. (Kedzierska et al., 1996). In this case, Rz1 localization is determined after accumulation due to vegetative growth, but the Rz reading frame is intact in the W3350*λcI857S*$_{am}$*7* lysogen. Taylor et al. (1996) were well aware of this problem, but previous attempts to modify an *Rz* expression vector to prevent concomitant expression of *Rz1* proved unsuccessful. Localizing Rz and Rz1 independently of one another following lysogenic induction would require λ mutants in which the embedded *Rz1* reading frame was interrupted without affecting the *Rz* frame and vice versa.

Genetic analysis of *Rz* and *Rz1*

The Rz1 gene product was successfully identified as an OM lipoprotein but its possible function during vegetative growth of λ was still undetermined. Zhang and Young (1999) began by constructing a set of amber nonsense alleles of *Rz* and *Rz1* using site-directed mutagenesis. The resulting plasmids carried the allele pairs *Rz*$^{+}$*Rz1*$_{W38am}$, *Rz*$_{Q100am}$*Rz1*$^{+}$, and *Rz*$_{Q100am}$*Rz1*$_{W38am}$ as well as the entire lysis gene cassette under control of the native pR' promoter. The position of the nonsense mutations were carefully chosen so that changes in one reading frame were silent in the other. The different allelic pairs of Rz and Rz1 were then crossed back onto the λ chromosome producing a set of recombinant phage. As expected the λ*Rz*$_{Q100am}$*Rz1*$^{+}$ and λ*Rz*$_{Q100am}$*Rz1*$_{W38am}$ phages displayed a $Mg^{++}$ dependent growth defect in liquid culture and on solid media. Less

expected was the finding that λ*Rz*$^{+}$*Rz1*$_{W38am}$ also exhibited the $Mg^{++}$ dependent phenotype (Fig. 1.6). From a genetic perspective, Rz and Rz1 null alleles having an identical phenotype indicates they participate in the same biological pathway This made possible a situation which is unique in all of biology, two genes encoded by the same DNA, in overlapping reading frames, which have the same physiological function. A co-infection experiment was performed with λ*Rz*$^{+}$*Rz1*$_{W38am}$ and *Rz*$_{Q100am}$*Rz1*$^{+}$ to ensure the *Rz1*$_{am}$ mutation was not simply acting in a cis manner to disrupt Rz expression. The *Rz*$_{am}$ and *Rz1*$_{am}$ alleles complemented one another by restoring lysis in liquid media containing 10mM $Mg^{++}$. This result demonstrated unequivocally that the *Rz1* gene produces a diffusible gene product which functions in the lysis pathway.

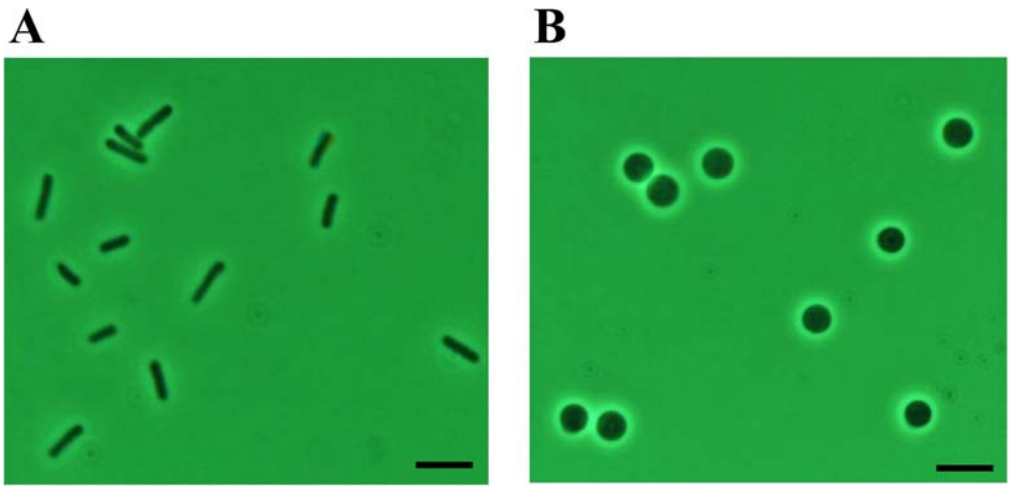


Figure. 1.6. The λ*Rz1*$_{am}$ divalent cation dependent lysis block. Inset scale bars equal 5μm.
A. Phase contrast micrograph of λ*Rz1*$_{am}$ infected cells grown in LB supplemented with 10 mM $MgCl_2$ just prior to the time of lysis.
B. $Mg^{++}$-stabilized spherical cell phenotype. Phase contrast micrograph of λ*Rz1*$_{am}$ infected cells grown in LB supplemented with 10 mM $MgCl_2$ ten minutes past normal time of lysis. Note: λ*Rz*$_{am}$ infected cells grown in LB supplemented with 10 mM $MgCl_2$ produce spherical cells indistinguishable from those shown in Fig. 1.6B.

To summarize, interruption of the Rz gene by Tn903, i.e. λdk23, or by converting codon 100 to TAG results in an identical conditional lysis defect as to that observed in the case of Rz1 interruption by mutation of codon 38 to TAG.

$\lambda Rz^{+}Rz1^{+}$ (wild type) plating efficiencies for $\lambda Rz_{Q100am}Rz1^{+}$ were recovered when grown in the presence of $Mg^{++}$ on a *supF58*. This indicates that Rz can tolerate a tyrosine at position 100. Although $\lambda Rz^{+}Rz1_{W38am}$ plated with wild type efficiency on the *supE44* host in the presence of $Mg^{++}$, plating on the *supF58* host failed to recover plaque formation of wild type efficiency either in the presence or absence of $Mg^{++}$. This indicates that the Rz1W38Y mutant functions abnormally since it blocks plaque formation even in the absence of $Mg^{++}$. The Rz1W38Y mutant is dominant-recessive to Rz1W38Q but recessive to the wild type Rz1. All of the aforementioned $Mg^{++}$ dependent or independent phenotypes for the *Rz* and *Rz1* suppressed nonsense alleles were reproducible in liquid media.

Another example of an Rz1 mutant functioning abnormally is found with the P2 homolog *LysC*. The *rpoC* gene of *E.coli* encodes the β' subunit of the bacterial DNA-dependent RNA polymerase (RNAP). The 397 mutation results in the replacement of the last 50 residues of the β' subunit with 23 incorrect residues. An *E.coli* host which carries the *rpoC397* mutation does not support growth of P2. The mechanism by which *rpoC397* blocks P2 growth is unknown. Markov et al. (2004) hoped to isolate suppressor mutations which would map to a P2 transcription factor. Instead, two suppressor mutations in *LysC* were isolated based on their ability to restore plaque

growth of P2 on a host carrying the *rpoC397* mutation. The two LysC mutants named *gor* and *trl* resulted in the missense mutations P25L and P25T, respectively. Plasmid reconstitution of P2 lysis indicated a premature onset of lysis in the *rpoC397* host compared to $rpoC^{+}$. It was concluded that premature lysis could be responsible for the P2 growth defect. Lysis which occurs too early results in immature (non-infective) phage particles. This conclusion was supported by the discovery that P2 reconstituted lysis on *rpoC397* with a plasmid carrying *LysC (gor)* significantly delayed lysis onset. The delay in lysis restores the production of infective particles and thus recovery of plaque formation. A key question brought about by these results remains unanswered. How could a single missense mutation in an OM lipoprotein (LysC P25L) delay the onset of lysis which is normally under the control of a small IM protein (P2 Y holin)?

**The spanin genes: a bioinformatic perspective**

Spanin genes are ubiquitous and diverse

Null mutations in Rz or Rz1 produce conditional-lethal phenotype under standard laboratory conditions. The conditionality of the Rz/Rz1 phenotype coupled with the lack of a described function in phage lysis culminated over time in a lack of genomic annotation for many *Rz/Rz1* equivalents. Prior to 2007, potential λRz and/or λRz1 equivalents were identified in phages P2 (Markov *et al.*, 2004), T7 (Casjens *et al.*, 1989, Bartel *et al.*, 1996), and P22 (Casjens et al., 1989) based on genetic evidence. Both P22

and T7 contain an entirely embedded reading frame coding for a putative OM lipoprotein in the +1 register. P2 *LysB* also contains an internal lipoprotein reading frame (*LysC*) in a +1 register, but the *LysC* stop codon is located downstream of the *LysB* stop codon. The *LysC* reading frame is described as an "overlapping" arrangement since it is only partially embedded within *LysB* (Fig. 1.7).

An initial survey of primarily λ and P22 like phages revealed 10 *Rz1* like reading frames within the presumed *Rz* orthologs. All of the *Rz1* like reading frames contained a potential SpaseII cleavage site and the mature reading frames were generally proline rich. The mature sequences could be aligned and clearly grouped into two families based on the location of proline rich sequences (Zhang & Young, 1999). While this initial survey was small in nature it provided the basis for a more comprehensive search of sequenced phage genomes for *Rz/Rz1* equivalents.

Utilizing protein and translation blast searches, approximately half of the 130 then currently annotated dsDNA phages of gram-negative bacteria were found to have proteins with sequence similarity to λ Rz/Rz1, P2 LysB/LysC or T7 18.5/18.7 (Summer et al., 2007a) Equivalents were eventually identified in all except 17 of the remaining genomes based on a manual inspection strategy. This strategy took advantage of the established "tight" physical linkage of the *Rz*/*Rz1* genes and the ability to identify a potential TMD or lipoprotein signal sequence using web based algorithms. Potential candidates had to meet the following criteria: 1. The *Rz* gene must precede *Rz1* and contain a potential N-terminal TM domain. 2. The *Rz1*gene must be a potential OM lipoprotein and be closely associated with *Rz* within the genome. Most of the *Rz1*

equivalents identified through blast and manual inspection were of the embedded (45 total) or overlapped (51 total) genetic architecture. All of the embedded or overlapped *Rz1* reading frames were in the +1 register with respect to *Rz*. A third genetic arrangement of *Rz/Rz1* gene pairs was also discovered. Eighteen pairs were found to be totally separated but very closely associated. For example, T4's *pseT.3* and *pseT.2* reading frames only overlap at the stop and start codons, respectively (Fig. 1.7). Infection with a T4 phage carrying a complete deletion of pseT.3 and *pseT.2* resulted in a λ*Rz*$^{-}$*/Rz1*$^{-}$ like $Mg^{++}$ dependent lysis defect in liquid or on solid media. Termination of the lytic cycle in the development of spherical cells indicates that pseT.3 and pseT.2 have the same biological function as λRz and λRz1, respectively.

A total of seven phage, including T1 (Fig. 1.7) contained a potential single gene equivalent of λ *Rz/Rz1*. In each case, the translation product of the gene was predicted to encode an outer membrane lipoprotein with a C-terminal transmembrane domain (Fig. 1.8). Based on the predictions for T1 gp11, it was concluded that a single gp11 molecule could localize to both the IM (C-terminal TM domain) and OM (lipoylated N-terminus) constituting a periplasm spanning protein or "spanin" (Summer et al., 2007a). Alignments and family assignments of the putative single (e.g. T1 gp11) and two-component (e.g. λRz/Rz1) spanin equivalents revealed extensive diversity on the primary structure level. Considered together, the extent of sequence and architectural diversity indicates a polyphyletic origin for these functionally related proteins (Summer et al., 2007a).

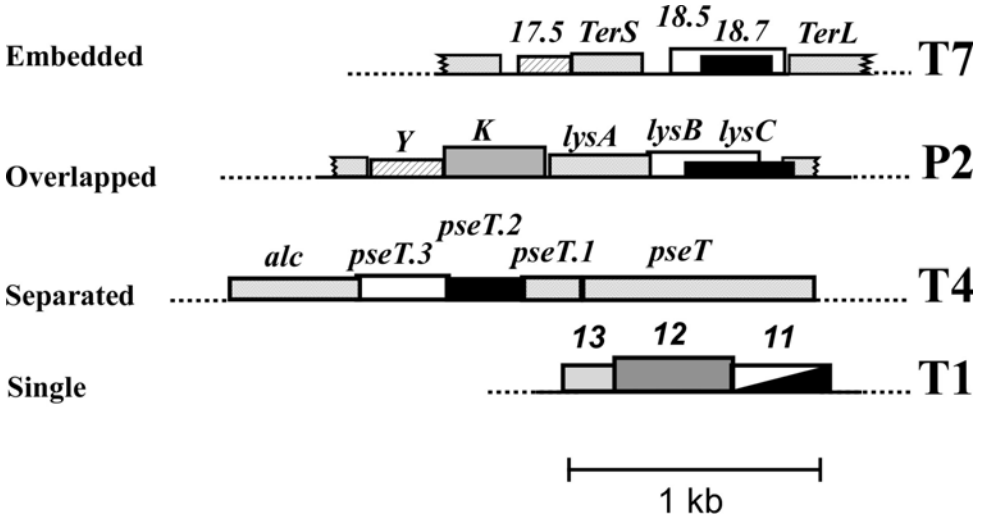


Fig. 1.7. Architectural diversity of *Rz/Rz1* equivalents. Shown to scale are the locations of the *Rz/Rz1* equivalents and surrounding genes within the T7, P2, T4, and T1 genomes. Reprinted with permission from Summer et al. (2007).

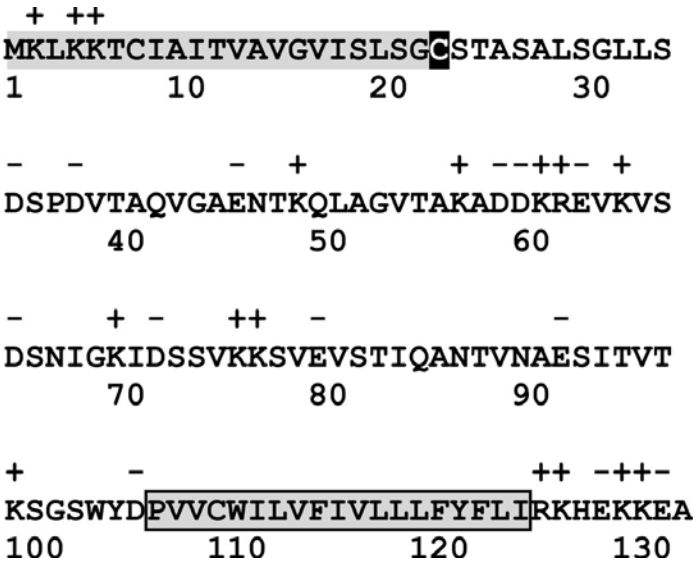


Figure. 1.8. Primary structure of the phage T1 gene product 11. Charged residues are indicated. The putative N-terminal lipoprotein signal sequence is highlighted in grey and the processed Cys residue is highlighted in black. The location of the putative C-terminal TMD is highlighted and boxed (Summer et al., 2007a).

Features of the predicted *Rz/Rz1* proteins

Reasonable alignments could only be generated for the more populated λ, T7, and P2 families of *Rz* and *Rz1* gene pairs due to sequence diversity. The Rz proteins of the λ and T7 families showed no primary structure relationship but the secondary structure predictions for both families are nearly identical. The periplasmic domains consist of two strongly predicted stretches of alpha-helix separated only by a short region of predicted beta-sheet and non-helical linker region. The short periplasmic domains (35-50 residues) of the Rz1 proteins from λ and T7 families can be divided into three domains. The N-terminal proximal domain is characterized by a high proline percentage (7% to 28%) in comparison to other *E. coli* lipoproteins. The central domain is characterized by an invariant PXAWXM in the λ family and a VDXSLMXP motif in the T7 family. The C-terminal domain is not conserved. The P2 family Rz1 lipoproteins, which are considerably longer (65-76 residues), also contain region of continuous alpha-helix prediction. Interestingly, the increase in predicted alpha-helix conformation coincides with a lack of C-terminal alpha-helix prediction in the P2 family Rz partners. The length of the Rz periplasmic domains based on predicted alpha-helix conformation is consistent with an extended protein that would stretch out across the periplasm toward the OM and thus Rz1 (Summer et al., 2007a).

**A function for spanins**

Prior to the discovery of *Rz*, a basic 17 kDa protein with endopeptidase activity was purified from λ lysates and ascribed to the R gene product. The endopeptidase activity was specific for the meso-DAP-D-Ala crosslinking peptide bonds of the PG (Taylor, 1971). Ten years later the R gene product was conclusively demonstrated to be a murein transglycosylase (Bienkowska-Szewczyk et al., 1981). The endopeptidase activity was thus displaced and tentatively assigned to Rz. It was argued that an Rz endopeptidase activity was consistent with the $Mg^{++}$ dependent phenotype. In Rz's absence, the PG, while severely destabilized due to R activity, could maintain enough structural stability to resist lysis if the OM is stabilized by divalent cations (Bienkowska-Szewczyk & Taylor, 1980, Young et al., 1979). After it was determined that Rz1 shares the same phenotype as Rz it was speculated the putative Rz endopeptidase activity might be localized to the inner leaflet of the OM through a Rz1 interaction. Here Rz would cleave the peptide bonds linking Lpp to the murein (Young, 2005). To date there has been no experimental evidence presented in the literature which directly links Rz or an equivalent with endopeptidase activity. Furthermore, Rz and Rz1 nor any of their equivalents contain the common sequence motifs associated with known endopeptidases. These facts have not prevented the incorrect annotation of many Rz orthologs and unrelated equivalents as endopeptidases.

Krupovič et al. (2008) proposed an alternative mechanism for spanin-mediated OM disruption. The model states that P37 and P36, the phage PRD1 Rz and Rz1

equivalents respectively, transfer the mechanical stress of hole formation to the OM. The model however is based on several critical assumptions: (a) hole formation results in a lateral movement of the holin protein, (b) the Rz protein is localized adjacent to the holin, and (c) the spanin complex is formed prior to PG degradation.

Taylor et al. (1996) proposed an Rz independent role for Rz1 in the formation of membrane fractions with intermediate density. This proposal stems from reports by Kucharczyk et al. (1991) and Fletcher and Earhart (1980), both of whom observed an increased inability to separate inner and outer membranes due to λ or T4 late gene expression respectively. Traditionally, difficulty in separating membranes by isopycnic sucrose density gradient (ISDG) centrifugation is manifested as an increase in intermediate density membrane fractions. The change in cell envelope structure during λ vegetative growth was initially attributed to the S protein (Kucharczyk *et al.*, 1991) but the same group would eventually identify the Rz1 protein as the responsible player. Both induction of the lysogen λ*CI857 Sam7* and the plasmid borne over-expression of *Rz1* alone were found to increase the accumulation intermediate density membrane fractions (Taylor et al., 1996). Subsequently, SDS-PAGE purified Rz1 was reconstituted into membrane vesicles and found to exhibit membrane fusogenic activity *in vitro* (Bryl *et al.*, 2000).

A region of the cell envelope where the IM and OM are adhered or fused would exhibit a density intermediate to a vesicle that consists of entirely inner or OM. What is less clear is how Rz1 could bring about changes in cell envelope structure without the aid of Rz? One possibility is that the overexpression of Rz1 could lead to membrane

toxicity induced perturbations in cell envelope structure. Perhaps a more relevant question is whether the changes in membrane density brought about by λ*CI857 Sam7* induction are due to both Rz and Rz1?

**Questions to be addressed**

As described above, the function of the spanin proteins in phage lysis is undetermined. We suggest that the function of the spanin proteins is to disrupt the OM for the following reasons: (a). phages which infect only a Gram-positive host do not carry the *Rz/Rz1* genes, and (b) the null phenotype of both is only apparent in liquid culture or on solid media when the OM is stabilized by the presence of mM levels of divalent cations. Although the work described in the following three chapters does not provide a mechanism for Rz/Rz1 function it does address some key biochemical questions including Rz/Rz1 protein localization (Chapter III), Rz-Rz1 complex formation *in vivo* and *in vitro* (Chapters II-IV) , complex stoichiometry (Chapter II) and the structure of the reconstituted complex *in vitro* (Chapter V). In addition, we will also the address the functional equivalence of single component spanin proteins (Chapter II) and the holin dependence of spanin function, as it pertains to the Krupovic et al. (2008) model (Chapter III). Lastly, we will propose a model for spanin function which ultimately results in the fusion of the inner and outer membranes of the cell envelope (Chapters III and V).

# CHAPTER II

# THE RZ AND RZ1 PROTEINS ARE ESSENTIAL BUT THEY ARE SUBJECT TO NONESSENTIAL INTERMOLECULAR DISULFIDE BONDING*

## Introduction

To what extent the OM of a gram-negative host impedes phage release at the end of the lytic cycle is not entirely understood. What has been clear for some time is that sufficient concentrations of divalent cations improve the function of OM as a permeability barrier to many different molecules (Leive, 1974). The fortification of the OM by divalent cations also appears to improve its ability to impede phage release. Null mutations in the λ lysis gene Rz or Rz1 were found to cause an identical block in host cell lysis as perceived by light microscopy (Zhang & Young, 1999). The manifest lysis block, originally described by Young et al. (1979), is a divalent cation dependent, persistent spherical-cell phenotype. The transition from rod to sphere occurs at the end of the lytic cycle during the course of time which normally corresponds to dissolution of the host cell. The null phenotype suggests the biological role of Rz and Rz1 is disruption of the OM.

---

* Part of this chapter is reprinted with permission from "Rz/Rz1 lysis gene equivalents in phages of Gram-negative hosts" by Summer, E.J., Berry, J., Tran, T.A., Niu, L., Struck, D.K., and Young, R., 2007. *J. Mol. Bio.*, 373, 1098-1112, 2007 by Elsevier Ltd.

It is unknown if the transition to a spherical cell is a normal step lysis. Groman and Suzuki (1962) observed induced lysogens swelling and rounding up prior to lysis. This observation led Young et al. (1979) to conclude that the spherical cell could be an intermediate step of lysis which is susceptible to blockage by divalent cations in the absence of Rz. Understanding the mechanism of Rz-Rz1 OM disruption will inevitably require a better understanding of the divalent cation dependent phenotype. Given that the phenotype is our only insight into Rz-Rz1 function at this time, the microscopic examination of λ lysis under carefully controlled physiological conditions is a top priority.

Also of interest is the redox state of the Rz and Rz1 cysteine residues in the oxidative environment of the periplasm. The Rz protein has two periplasmic cysteine residues, one located near the center of the periplasmic domain at position 99 and another at the penultimate, 152, position (Fig. 1.5B). The Rz1 protein has a single periplasmic cysteine at position 29 (Fig. 1.5C). Many periplasmic proteins are known to participate in the formation of **intra**molecular disulfide bonds. The formation and/or isomerization of disulfide bonds normally serve one of two purposes. They can contribute to the folding and overall stability of the protein or they can serve to regulate the proteins activity as in the case of the muralytic enzyme from phage P1 (Kadokura *et al.*, 2003, Xu *et al.*, 2005). There are however no reports of a native protein from *E. coli* or a phage which serves as substrate for the formation of **inter**molecular disulfide bonds for either purpose.

Summer et al. (2007) conducted a thorough bioinformatic search of the genomes belonging to phages which infect a Gram-negative host for potential *Rz/Rz1* equivalents. It was a determined that seven of these phages, most notably phage T1, contain a single gene equivalent of *Rz* and *Rz1*. The reading frame of T1 *gp11* is located just downstream of the T1 holin and endolysin genes, a location where *Rz/Rz1* equivalents are often found. It encodes a 131 residue protein with strong predictions for an N-terminal lipoprotein signal sequence followed by a short periplasmic domain and ending in a strongly predicted single C-terminal transmembrane domain (Fig. 1.8). Based on these predictions gp11 in its mature form would be tethered to the OM by its lipoylated N-terminal cysteine and tethered to the IM by its C-terminal TM domain. A first step in assessing the reliability of these predictions will be determining if gp11 is in fact a functional equivalent of Rz and Rz1.

A comprehensive genetic analysis of Rz and Rz1 function has never been undertaken. What little genetic information is available is cryptic at best. For example, suppression of the λ*Rz1W38am* phage in a *supF* host results in a divalent cation independent lysis defect. The cells adopt a spherical morphology at the time of lysis but the Rz1W38Y mutation for some reason eliminates the need to stabilize the OM with millimolar (mM) concentrations of divalent cations such as $Mg^{++}$ (Zhang & Young, 1999). The function of S and R appears to be unaffected given that the cells are spherical. Future work aimed at the identification and characterization of Rz-Rz1 activity will undoubtedly require the use of other non-functional Rz1 mutants.

Here we describe our efforts to accomplish four goals: (a) Refine the description of morphological changes which occur during cell lysis through time lapse microscopy. (ii) Assess the redox state of the Rz and Rz1 periplasmic cysteine residues through SDS-PAGE and Western blotting following whole cell acid precipitation. (iii) Test the ability of the putative T1 single gene equivalent gp11 to complement λ$Rz_{am}Rz1_{am}$. (iv) Conduct a search for non-functional alleles of Rz1 through alanine scanning mutagenesis of conserved residues.

**Materials and methods**

Bacterial growth, induction, and TCA precipitation

Bacterial cultures were grown in standard LB media supplemented with $MgCl_2$ (10 mM), ampicillin (100 μg/ml), and kanamycin (40 μg/ml) when appropriate. Culture growth and lysis profiles were monitored as previously described (Smith *et al.*, 1998). Briefly, overnight cultures were diluted 300:1 and grown with aeration at 30ºC for lysogenic cultures and 37ºC for non-lysogens. Lysogens were thermally induced at A550 ~0.3 by aeration at 42ºC for 20 min, followed by continued growth at 37ºC. When indicated, isopropyl β-D-thiogalactosidase (IPTG) was added to a final concentration of 1mM. The bacterial strains and plasmids used in this study are listed in Table 2.1. A more complete description of the phage mentioned in Table 2.1 can be found in the materials and methods section of Chapter III of this dissertation.

Table 2.1. Strains and plasmids

| **Strains** | **Description** | **Source** |
|---|---|---|
| XL-1 Blue | *recA endA1 gyrA96 thi1 hsdR17 supE44 relA1 lac* [F' *proAB lacZ*$_{\Delta M15}$::*Tn*10] | Stratagene |
| RY17299 | MG1655 Δ*tonA* | Laboratory stock |
| RY17299(λ901 *Rz*$^{+}$*Rz1*$^{+}$) | Lysogen carrying λ900*S*$_{am7}$*Rz*$^{+}$*Rz1*$^{+}$ prophage | This study |
| RY17299(λ901 *Rz*$_{am}$*Rz1*$^{+}$) | | This study |
| RY17299(λ901*Rz*$^{+}$*Rz1*$_{am}$) | | This study |
| RY17299(λ901*Rz*$_{am}$*Rz1*$_{am}$) | | This study |
| MC4100 | F$^{-}$ *araD139* Δ[*argF-lac*]$_{U169}$ *rpsL150 relA1 flb5301 deoC1 ptsF25 rbsR* | (Casadaban, 1976) |
| MC4100(λ900) | Lysogen carrying λ900*S*$^{+}$*Rz*$^{+}$*Rz1*$^{+}$ prophage | (Zhang & Young, 1999) |
| MC4100(λ900*Rz*$_{am}$*Rz1*$^{+}$) | | (Zhang & Young, 1999) |
| MC4100(λ900*Rz*$^{+}$*Rz1*$_{am}$) | | (Zhang & Young, 1999) |
| MC4100(λ900*Rz*$_{am}$*Rz1*$_{am}$) | | (Zhang & Young, 1999) |

| **Plasmid** | **Description** | **Source** |
|---|---|---|
| pRE | Derivative of pJF118EH with *lacI*$^{Q}$ and P$_{tac}$ promoter replaced with pR' promoter region from λ, transcriptionally activated by λ Q | (Park et al., 2006) |
| pRE-gp11 | Gene 11 from phage T1 cloned in pRE | This study |
| pRE-RzRz1 | *Rz*$^{+}$*Rz1*$^{+}$ cloned in pRE | This study |

Table 2.1. Continued

| Plasmid | Description | Source |
|---|---|---|
| pRE-Rz | *Rz*$^{+}$ cloned in pRE with *Rz1*$_{W38am}$ null mutation | This study |
| pRE-Rz1 | *Rz1*$^{+}$ cloned in pRE | This study |
| pRE-Rz$_{C99S}$ | pRE-Rz carrying C99S mutation in *Rz* | This study |
| pRE-Rz$_{C152S}$ | pRE-Rz carrying C152S mutation in *Rz* | This study |
| pRE-Rz$_{C99S,C152S}$ | pRE-Rz carrying C99S and C152S mutations in *Rz* | This study |
| pRE-Rz1$_{C29S}$ | pRE-Rz1 carrying C29S mutation in *Rz1* | This study |
| pRE-Rz1P34A | pRE-Rz1 carrying P34A mutation in *Rz1* | This study |
| pRE-Rz1W38A | pRE-Rz1 carrying W38A mutation in *Rz1* | This study |
| pRE-Rz1M40A | pRE-Rz1 carrying M40A mutation in *Rz1* | This study |
| pRE-Rz1L50A | pRE-Rz1 carrying L50A mutation in *Rz1* | This study |
| pRE-Rz1S57A | pRE-Rz1 carrying S57A mutation in *Rz1* | This study |

The *RzRz1* genes and T1 *gp11* are either expressed in their native context in the λ genome from prophage induction or from derivatives of the medium-copy plasmid pRE carrying the λ late promoter, pR'. In all cases, the λ late gene activator Q is either supplied *in trans* from an induced prophage or from pQ, a very low copy vector carrying *Q* cloned under the control of the $P_{lac/ara-1}$ promoter (Lutz & Bujard, 1997, Grundling et al., 2001).

At the indicated time, precipitation of cellular protein was achieved by the rapid addition of one ml of culture into a solution of trichloroacetic acid (TCA) to achieve a final concentration of 10% TCA. Precipitation reactions were mixed thoroughly by vortexing and left on ice for 15 minutes. Precipitated protein was collected by centrifugation in a tabletop microcentrifuge at 18,000 x rcf for 10 minutes. Excess TCA was removed by twice resuspending pellets in one ml of cold acetone before pelleting protein in the microcentrifuge at 18,000 x rcf. TCA pellets were air dried and resuspended in 1X SDS-PAGE sample loading buffer which contained 100 mM Beta-Mercaptoethanol unless otherwise indicated.

SDS-PAGE and Western blotting

SDS-PAGE and Western blotting were performed as described previously (Gründling *et al.*, 2000a; Bernhardt *et al.*, 2002). SeeBlue Plus2 (Invitrogen) prestained standard was included as a molecular mass standard. Samples destined for western blotting with anti-Rz serum were resolved by SDS-PAGE on 10% resolving/4% stacking Tris-tricine polyacrylamide gels. Samples destined for western blotting with anti-Rz1 serum were resolved by SDS-PAGE on 16.5% resolving/4% stacking Tris-tricine polyacrylamide gels. Proteins were transferred to PVDF membrane (Pall Life Sciences) using a Hoefer TE unit at 0.1 mA overnight at 4º C. Antibodies (Sigma Genosys) were generated in rabbits against the synthetic peptides CELADAKAENDALRDD, corresponding to the Rz residues 71-85 (modified with an N-terminal Cys for

conjugation) and SQCVKPPPPPAWIMQ, corresponding to Rz1 residues 27-41 and used at a dilution of 1:1000. The secondary antibody, goat-anti-rabbit-HRP (Thermo Scientific), was used at a dilution of 1:5000. Chemiluminescence was detected using a Bio-Rad XR Gel Doc system.

Standard DNA manipulations, PCR, site directed DNA mutagenesis and DNA sequencing

Isolation of plasmid DNA, DNA amplification by PCR, DNA transformation, and DNA sequencing were performed as previously described (Tran *et al.*, 2005). Oligonucleotides (primers) were obtained from Integrated DNA Technologies (Coralville, Ia.) and were used without further purification. Restriction and DNA-modifying enzymes were purchased from New England Biolabs (Ipswich, Ma.); all reactions using these enzymes were performed according to the manufacturer's instructions. Site-directed mutagenesis was performed using the QuikChange kit from Stratagene (La Jolla, Calif.) as described previously (Grundling *et al.*, 2000). Oligonucleotide (primer) sequences are listed in Table 2.2.

Table 2.2. Oligonucleotide sequences

| **Primer** | **Sequence** |
|---|---|
| gp11ForBamHI | CGCGGATCCAGGAGGTGGTGAGATTATGAAAGAGTTT |
| gp11RevHindII | CGGCGGAAGCTTACGCCTCCTTTTTTTCGT |
| gp11A1toCFor | GAAGAATACGCATATTGCGTTACGGAACTATAATGAAAC TTAAGAAA |

Table 2.2. Continued

| Primer | Sequence |
|---|---|
| gp11A1toCRev | TTTCTTAAGTTTCATTATAGTTCCGTAACGCAATATGCGTATTCTTC |
| gp11A2toCFor | GAAGAATACGCATATTGCGTTACGGCACTATAATGAAACTTAAGAAA |
| gp11A2toCRev | TTTCTTAAGTTTCATTATAGTGCCGTAACGCAATATGCGTATTCTTC |
| RzC99SFor | TTGCACATCAAAGCAGTCTCTCAGTCAGTGCGTGAAGCC |
| RzC99SRev | GGCTTCACGCACTGACTGAGAGACTGCTTTGATGTGCAA |
| RzC152SFor | AAGTATATTAATGAGCAGTCCAGATAGGGATCCGTCGAC |
| RzC152SRev | GTCGACGGATCCCTATCTGGACTGCTCATTAATATACTT |
| Rz1C29SFor | TCAAAGCAGTCTGTCAGTCAGTCCGTGAAGCCACCACCGCCTCCG |
| Rz1C29SRev | CGGAGGCGGTGGTGGCTTCACGGACTGACTGACAGACTGCTTTGA |
| Rz1P34AFor | CAGTGCGTGAAGCCACCAGCGCCTCCGGCGTGGATAATG |
| Rz1P34ARev | CATTATCCACGCCGGAGGCGCTGGTGGCTTCACGCACTG |
| Rz1W38AFor | CCACCACCGCCTCCGGCGGCGATAATGCAGCCTCCC |
| Rz1W38ARev | GGGAGGCTGCATTATCGCCGCCGGAGGCGGTGGTGG |
| Rz1M40AFor | CCTCCGGCGTGGATAGCGCAGCCTCCCCCCGACTGGCAG |
| Rz1M40ARev | CTGCCAGTCGGGGGGAGGCTGCGCTATCCACGCCGGAGG |
| Rz1L50AFor | GACTGGCAGACACCGGCGAACGGGATTATTTCACCC |
| Rz1L50ARev | GGGTGAAATAATCCCGTTCGCCGGTGTCTGCCAGTC |
| Rz1S57AFor | CTGAACGGGATTATTTCACCCGCAGAGAGAGGCTGAAAGCTTGGC |
| Rz1S57ARev | GCCAAGCTTTCAGCCTCTCTCTGCGGGTGAAATAATCCCGTTCAG |

Plasmid construction

All plasmids used and generated in the course of this study are listed in Table 2.1. The construction of plasmids pRE-Rz and pRE-Rz1 is described in the materials and methods section of Chapter III. The plasmids pRE-RzC99S, pRE-RzC152S, and

pRE-RzC99S,C152S were generated by site-directed mutagenesis using the pRE-Rz as a template. The plasmids pRE-Rz1C29S, pRE-Rz1P34A, pRE-Rz1W38A, pRE-Rz1M40A, pRE-Rz1L50A, and pRE-Rz1S57A were also generated by site-directed mutagenesis using pRE-Rz1 as a template. Primer pairs used for site-directed mutagenesis are listed in Table 2.2. The plasmid pRE-gp11* was constructed by first amplifying the region of the T1 genome starting 64 nt upstream of the start codon to 44 nt downstream of the stop codon using primers gp11ForBamHI and gp11RevHindIII. The PCR product was then ligated to the pRE backbone after both had been digested with BamHI and HindIII. Due to toxicity as a result of *gp11* expression the ribosome binding site of pRE-gp11 was weakened from its native form of AAGGAA to ACGGCA through site-directed mutagenesis. The sequences of the two primer pairs used to weaken the ribosome binding site are listed in Table 2.2 and the resulting plasmid was named pRE-gp11.

Time lapse imaging of λ lysis

At 50 minutes post thermal induction, a 10μl sample of the indicated culture was placed on a glass slide and covered with a cover slip, both of which were pre-warmed to 37ºC. Host cell lysis was imaged using an EC Plan-NEOFLUOR 40X/0.75 Ph2 objective installed on a Zeiss Axio Observer A1 microscope equipped with a heated stage, PECON temperature control unit, and an AXIOCam HSM camera. The heated stage was equilibrated to 37ºC and equipped with an air pump which passed air heated to

37ºC over the top of the mounted glass slide. Time lapse video was captured at 2 frames per second for a duration of five minutes. Video was edited using the AXIO vision 4 software package. All images were stored as zvi format files and converted to tiff or jpeg format as necessary.

**Results**

The λ$Rz_{am}$ lysis defect

Although much of the molecular basis of phage lysis has been described in great detail, a clear picture of morphological changes at the time of lysis is sorely lacking. In fact, most accounts of the morphological changes associated with phage lysis are gained from personal communication with current or past members of the phage research community. We set out to gain a clearer perspective of the lysis defect by observing both λ and λ$Rz_{am}$ lysis in the **absence** of 10 mM $Mg^{++}$ with thermally induced λ lysogens that were cultured under carefully controlled physiological conditions (see materials and methods). Fig. 2.1A-C shows the time course of 3 independent λ lysis events in LB at 37ºC. No changes are observed in the overall structure of the cell (Fig. 2.1A and B) until a single point on the periphery of the cell abruptly ruptures. Cell contents are then rapidly expunged through the breach as determined by a visible reduction in phase contrast. Lysis shown in Fig. 2.1C is the same with the exception that a slight swelling

is visible at the pole just prior to envelope rupture in the same location. The entire process is over in a matter of seconds (Fig. 2.1A-C).

Observation of λ$Rz_{am}$ lysis in the absence of 10 mM $Mg^{++}$ reveals the formation of spherical cells. Fig. 2.2A- and B shows two independent lysis block events post λ$Rz_{am}$ induction. The process begins as a single, localized and swollen deformation on the cell periphery, which can occur at the midcell (Fig. 2.2A) or the pole (Fig. 2.2B). The deformation then propagates toward one or both poles depending on where it originated until the cells rod shape is no longer distinguishable. Complete spherical conversion from the first appearance of a deformation takes substantially longer than the entire lysis process of λ$Rz^{+}$. The total time of conversion, ~ 4sec for midcell originating deformation (Fig. 2.2 A) to ~25sec for pole originating deformation (Fig. 2.2B), appears to vary based primarily on the length of the cell and point of origin for the first observable deformation.

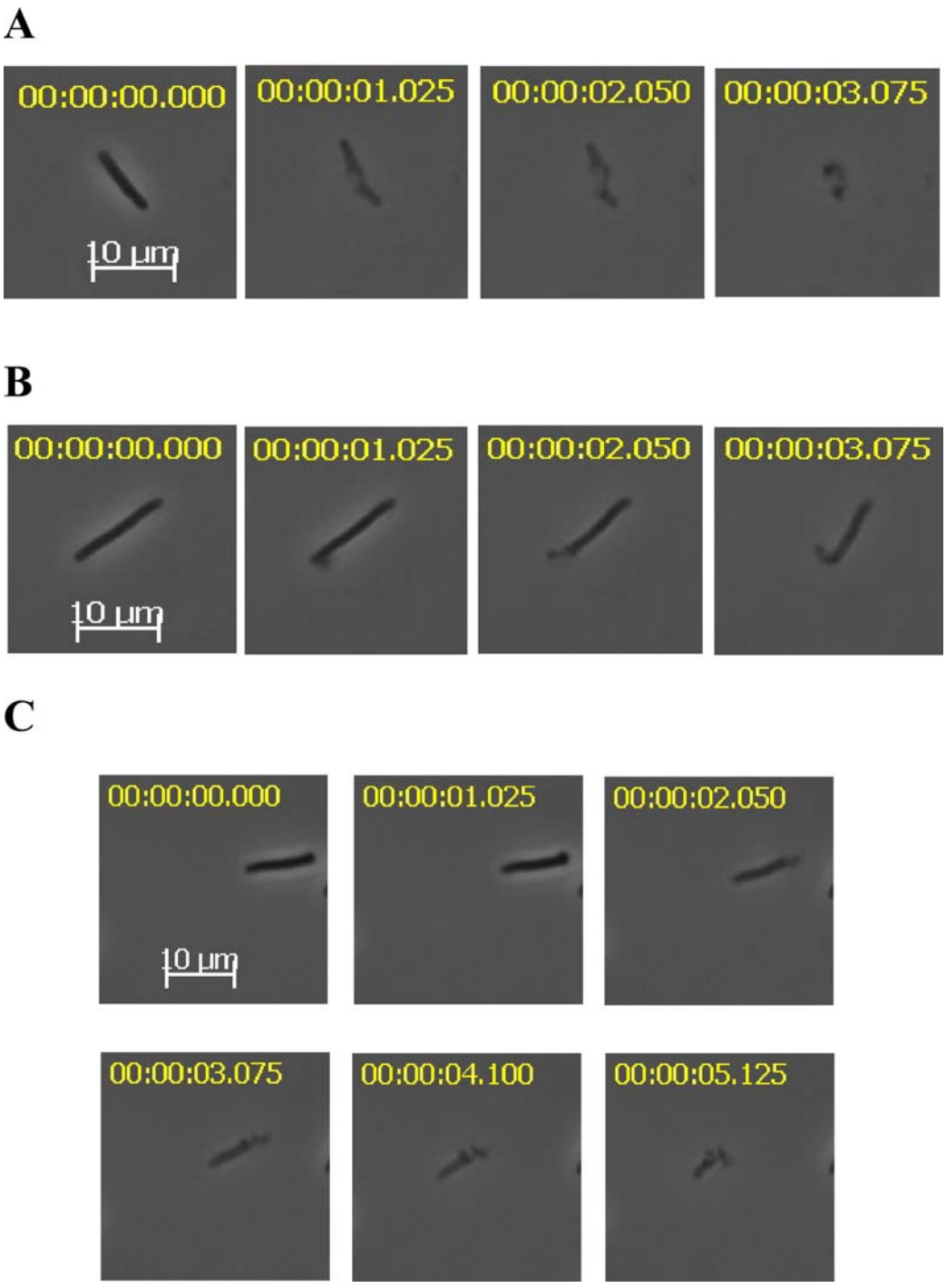


Figure 2.1. λ lysis is rapid.
A-C. A culture of MC4100(λ900) growing logarithmically in LB lacking mM levels of divalent cations was thermally induced and the resultant lysis events were captured by time lapse microscopy as described in *Materials and methods*.

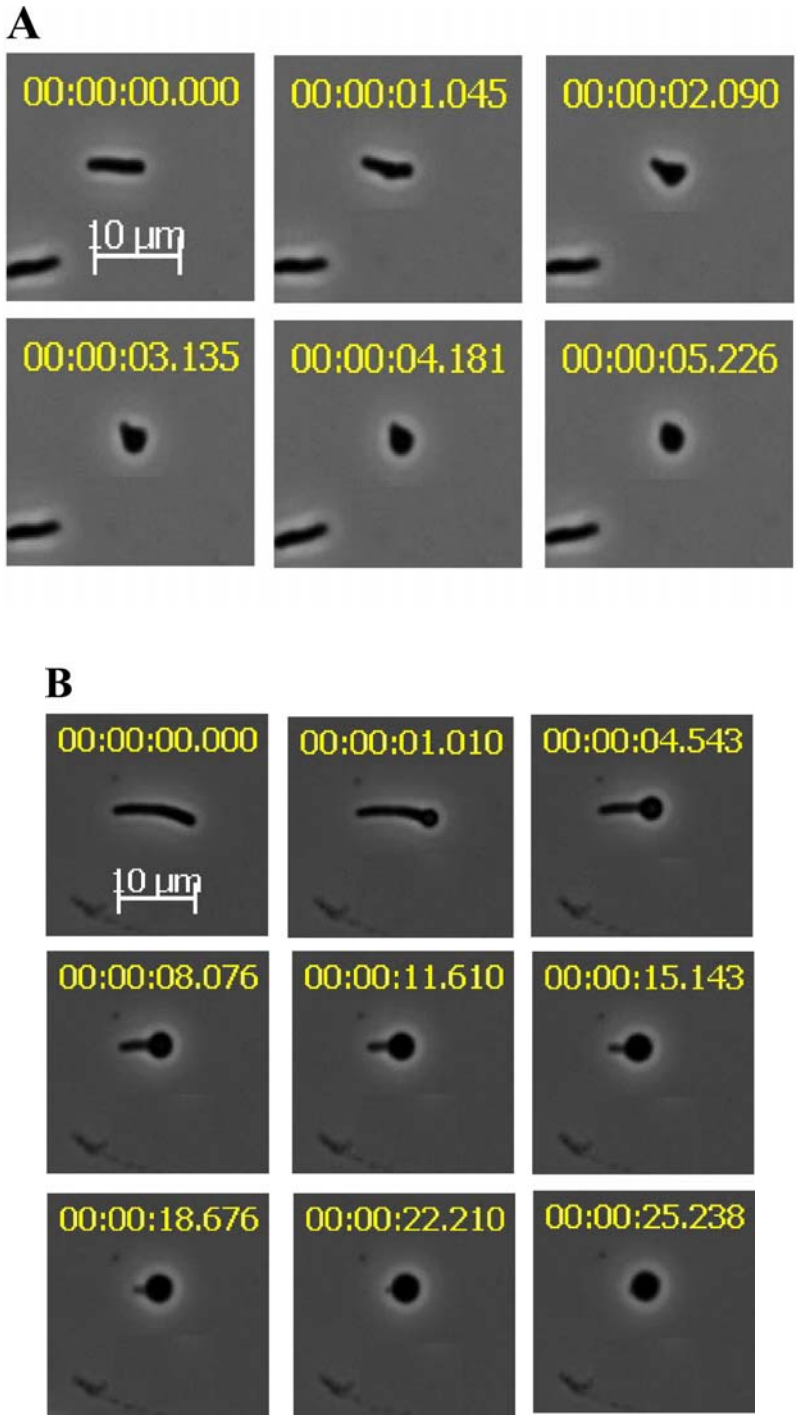


Figure 2.2. λ$Rz_{am}$ lysis is blocked.
A-B. A culture of MC4100(λ900$Rz_{am}Rz1^{+}$) growing logarithmically in LB lacking mM levels of divalent cations was thermally induced and the resultant lysis block events were captured by time lapse microscopy as described in *Materials and methods*.

The Rz and Rz1 periplasmic cysteine residues

It is well known that cysteine residues which reside in the oxidative environment of the periplasm often participate in the formation of **intra**molecular disulfide bonds. These disulfide bonds are often necessary for a protein to function properly. Although **inter**molecular disulfide bond formation has never been reported under native conditions in *E. coli*, we entertained the possibility that the single cysteine of Rz1 forms essential **inter**molecular homo or hetero linkages. Fig. 2.3A and Fig. 2.4A show that RzC99S, RzC152S, RzC99SC152S, and Rz1C29S can functionally replace Rz and Rz1, respectively.

Although the Rz and Rz1 periplasmic cysteine residues are non-essential, we had noted previously based on non-reducing SDS-PAGE and Western blotting that both Rz and Rz1 have a Mr consistent with a homodimer (data not shown). Since the putative Rz and Rz1 homodimers were sensitive to reducing agent we were forced to consider the possibility that the proteins were forming **inter**molecular disulfide linked dimers. We tested this idea by transactivating (see materials and methods) the induction of *Rz* and *Rz1* Cys to Ser substitution mutants through thermal induction of a MG1655λ*cI857Sam7R*$^{+}$ lysogen carrying the amber alleles of *Rz* and/or *Rz1*. Samples of the culture were TCA precipitated to ensure the state of the cysteine functional groups was not disturbed prior to preparation for SDS-PAGE.

A

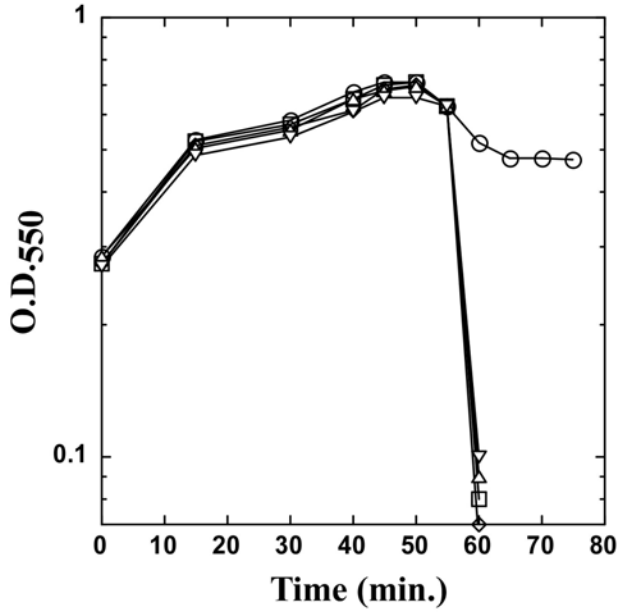


Figure 2.3. The non-essential periplasmic Cys residues of Rz participate in intermolecular disulfide bond formation.
A. MC4100(λ900$Rz_{am}Rz1^{+}$) carrying the indicated plasmid was grown in LB media supplemented with 10 mM $MgCl_2$. At time O the culture was thermally induced and lysis was monitored as described in *Materials and Methods*. Plasmids: pRE, (○); pRE-Rz, (□); pRE-$Rz_{C99S}$, (◇); pRE-$Rz_{C152S}$, (△); pRE-$Rz_{C99S,C152S}$, (▽).
B. A culture of MC4100(λ$S_{am7}R^{+}$) carrying the indicated alleles of *Rz* and *Rz1* as well as the indicated plasmid were thermally induced and samples were TCA precipitated 60 minutes post-induction. Identical samples were resuspended in 1X SDS-PAGE sample loading buffer with (reduced) or without 100 mM β-mercaptoethanol (non-reduced) and subjected to SDS-PAGE followed by Western blotting with the anti-Rz antibody. The allelic status of *Rz* and *Rz1* within each lysogen as it corresponds to a given sample is indicated above each lane. A (+) sign indicates the wt allele and a (-) sign indicates an amber allele. Each lysogen was carrying the indicated plasmid: pRE, (-); pRE-Rz, (+); pRE-$Rz_{C99S}$, (99); pRE-$Rz_{C152S}$, (152); pRE-$Rz_{C99S,C152S}$, (99,152). MW standards are indicated to the side of each blot. A single asterisk indicates the position of a reproducible Rz degradation product and a double asterisk indicates the position of the Rz homodimer.

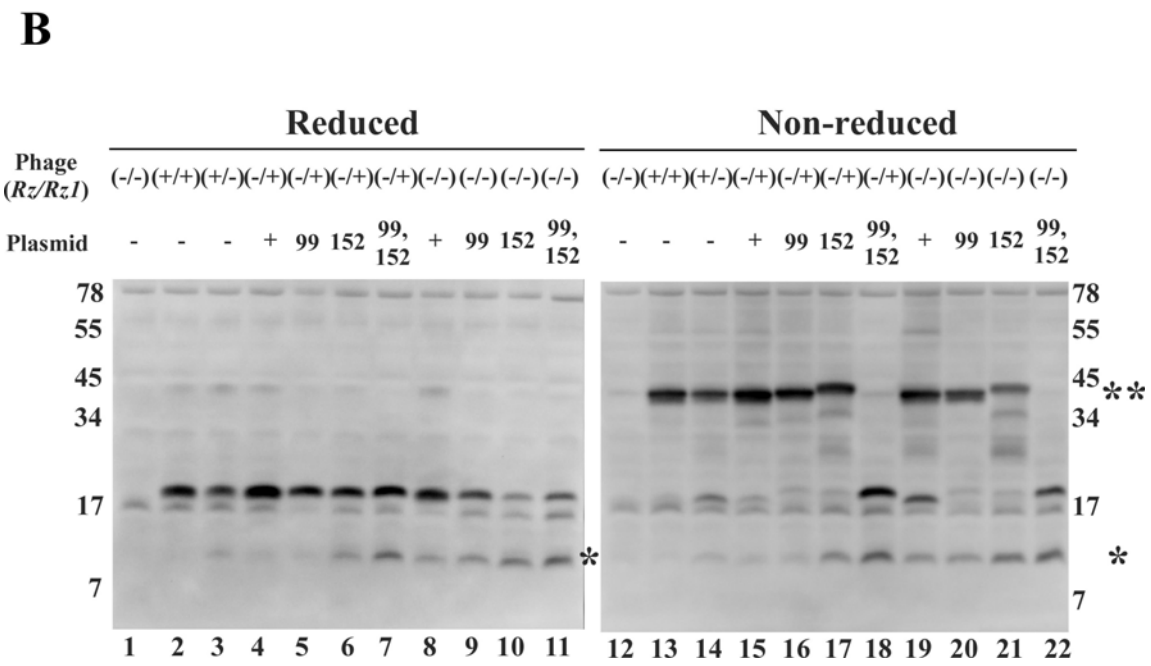


Fig. 2.3. Continued.

Fig. 2.3B shows anti-Rz western blots of identical samples prepared for SDS-PAGE in the presence or absence of reducing agent. Fig. 2.3B lanes 2 and 13 show that when Rz is produced from the phage chromosome it forms a β-Mercaptoethanol (β-Me) sensitive dimer. The same result is observed when Rz is produced from the plasmid (Fig. 2.3B, compare lanes 4 and 15) and the absence of Rz1 has little affect (see below) (Fig. 2.3B, compare lanes 8 and 19). The RzC99S (Fig. 2.3B. compare lanes 5 and 16) and RzC152S (Fig. 2.3B. compare lanes 6 and 17) proteins also form a β-Me sensitive dimer. Once again the absence of Rz1 has little affect (Fig. 2.3B, compare lanes 9 and 20; Fig. 2.3B, compare lanes 10 and 21). The β-Me sensitive dimer persists until both cysteine residues at position 99 and 152 are replaced with serine (Fig. 2.3B, compare lanes 7 and 18). These results indicate that an Rz C99-C99 and C152-C152 linked

homodimer is occurring under physiological conditions. Also worth noting is the 12 kDa Rz degradation product, the position of which is indicated by an asterisk in Fig. 2.3B.The Rz degradation product only appears when the Rz1 protein is not present (Fig. 2.3B, compare lanes 4 and 8) indicating that the Rz product is more unstable in its absence. Interestingly, the degradation product is apparent in the presence of Rz1 for the RzC152 (Fig. 2.3B, lane 6) sample and even more so in the double mutant (Fig. 2.3B, lane7).

Fig. 2.4B shows anti-Rz1 Western blots of identical samples prepared for SDS-PAGE in the presence or absence of reducing agent. As in the case of Rz, the Rz1 protein forms a β-Me sensitive dimer whether produced from the phage (Fig. 2.4B, compare lanes 2 and 9) or the plasmid (Fig. 2.4B, compare lanes 4 and 11). The absence of Rz has no affect on dimer formation (Fig. 2.4B, compare lanes 6 and 13). The β-Me sensitive dimer is not observed in the case of Rz1C29S (Fig. 2.4B, compare lanes 5 and 12). The fact that Rz1C29S, unlike Rz1, does not form a β-Me sensitive dimer suggests that Rz1 is forming a C29-C29 linked homodimer under physiological conditions.

**A**

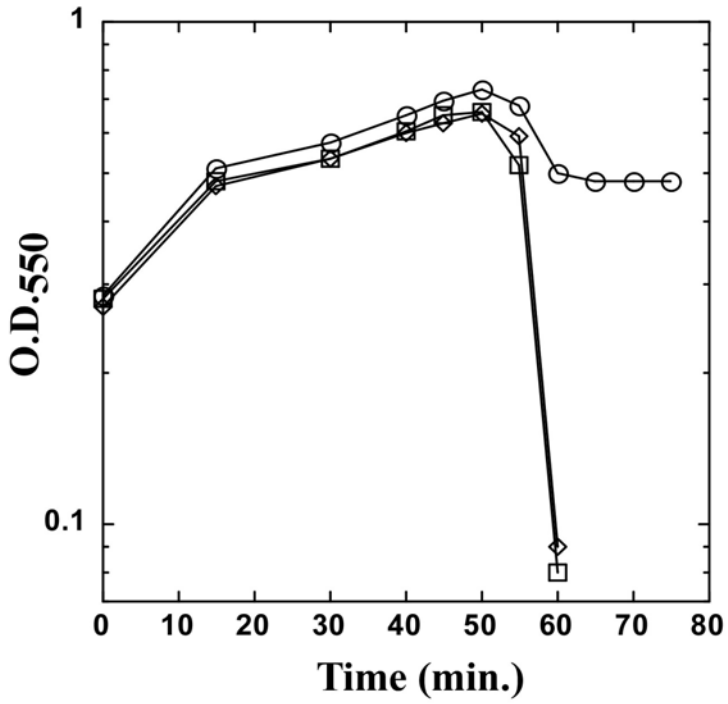


Figure 2.4. The non-essential periplasmic Cys residue of Rz1 participates in intermolecular disulfide bond formation.
A. MC4100(λ900$Rz^{+}Rz1_{am}$)carrying the indicated plasmid was grown in LB media supplemented with 10 mM $MgC_{l2}$. At time O the culture was thermally induced and lysis was monitored as described in *Materials and Methods*. Plasmids: pRE, (○); pRE-Rz1, (□); pRE-$Rz_{C99S}$, (◇).
B. A culture of MC4100(λ$S_{am7}R^{+}$) carrying the indicated alleles of *Rz* and *Rz1* as well as the indicated plasmid were thermally induced and samples were TCA precipitated 60 minutes post-induction. Identical samples were resuspended in 1X SDS-PAGE sample loading buffer with (reduced) or without 100 mM β-mercaptoethanol (non-reduced) and subjected to SDS-PAGE followed by Western blotting with the anti-Rz1 antibody. The allelic status of *Rz* and *Rz1* within each lysogen as it corresponds to a given sample is indicated above each lane. A (+) sign indicates the wt allele and a (-) sign indicates an amber allele. Each lysogen was carrying the indicated plasmid: pRE, (-); pRE-Rz1, (+); pRE-$Rz1_{C29S}$, (29). Selected MW standards are indicated to the side of each blot. A single asterisk indicates the position of the Rz1 homodimer.

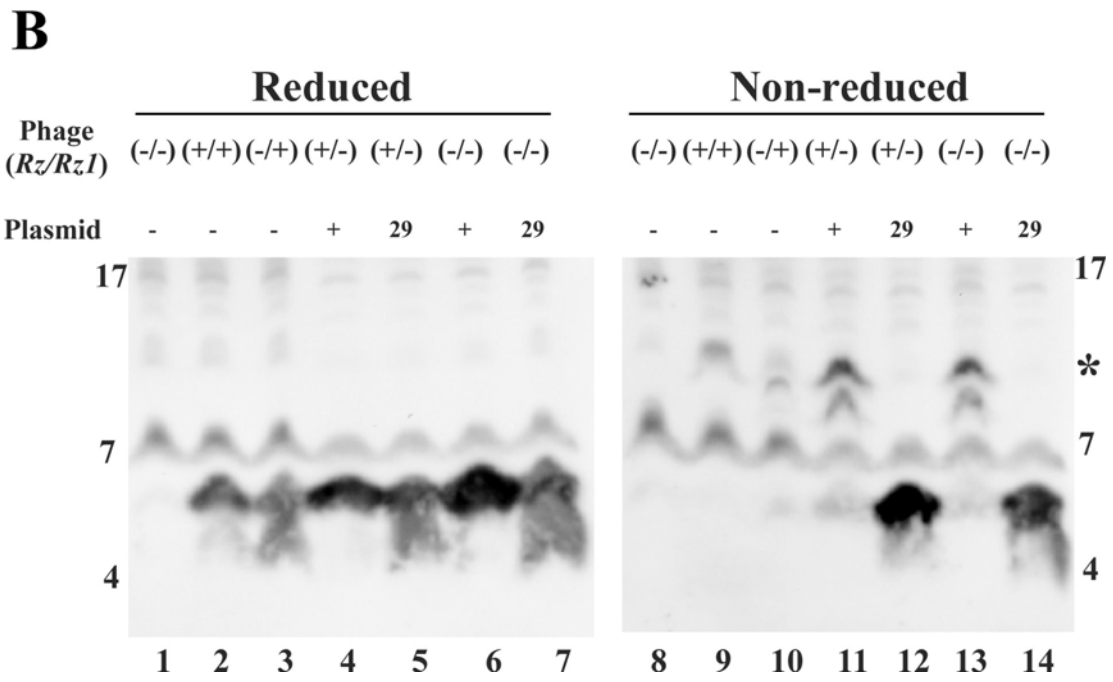


Fig. 2.4. Continued.

T1 gp11 is a functional equivalent of Rz and Rz1

The potential single gene equivalent, *gp11*, from phage T1 was cloned and tested for its ability to replace the function of the *Rz* and *Rz1* gene products. Fig. 2.5 shows that expression of *gp11* recovers lysis by λ900$Rz_{am}Rz1_{am}$ in the presence of 10 mM $Mg^{++}$. This demonstrates unequivocally that a single gene can complement the function of two.

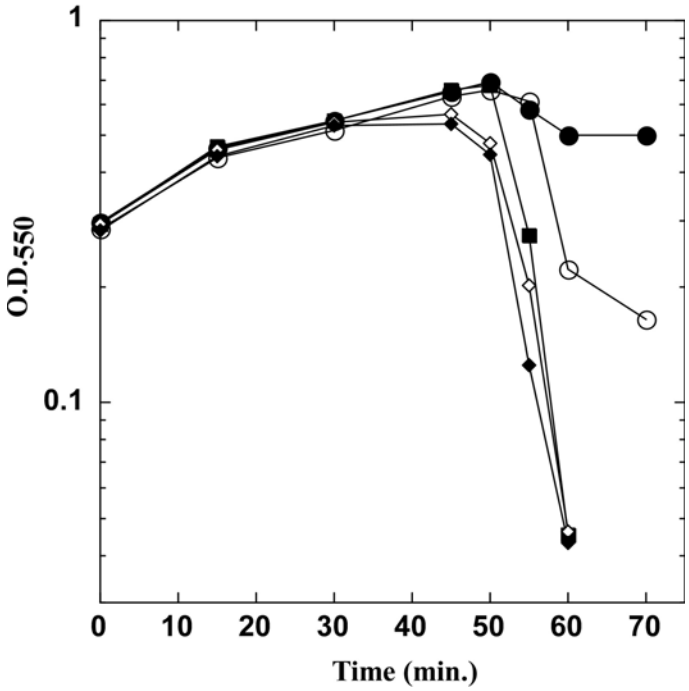


Figure 2.5. T1 gp11 is a functional equivalent of λ Rz and Rz1. A culture of MC4100(λ900$Rz_{am}Rz1_{am}$) carrying the indicated the indicated plasmid was thermally induced and the lysis profile was monitored as described in *Materials and methods*. Filled symbols indicate LB media supplemented with 10mM $MgCl_2$ and open symbols indicate standard LB media. Plasmids: pRE, (circle);pRE-RzRz1, (square); pRE-gp11, (diamond). This Figure is reprinted with permission of Summer et al. (2007).

Alanine scanning mutagenesis of conserved Rz1 residues

Fig. 2.6A shows that 5 residues are entirely conserved among members of the λ Rz1 protein family. A hunt for non-functional mutants of Rz1 was conducted by independently converting each conserved residue to an Ala. The resulting plasmids, each carrying one of the following mutations, P34A, W38A, M40A, L50A, or S57A, were subjected to complementation analysis. Fig. 2.6B shows that all alanine

substitution mutants were functional with the exception of Rz1M40A. The protein was subsequently confirmed to accumulate *in vivo* by Western blot using the anti-Rz1 antibody (Fig. 2.6C). The Rz1M40A mutant should provide a useful control for future *in vitro* work aimed at testing the membrane fusion hypothesis (see Chapter V).

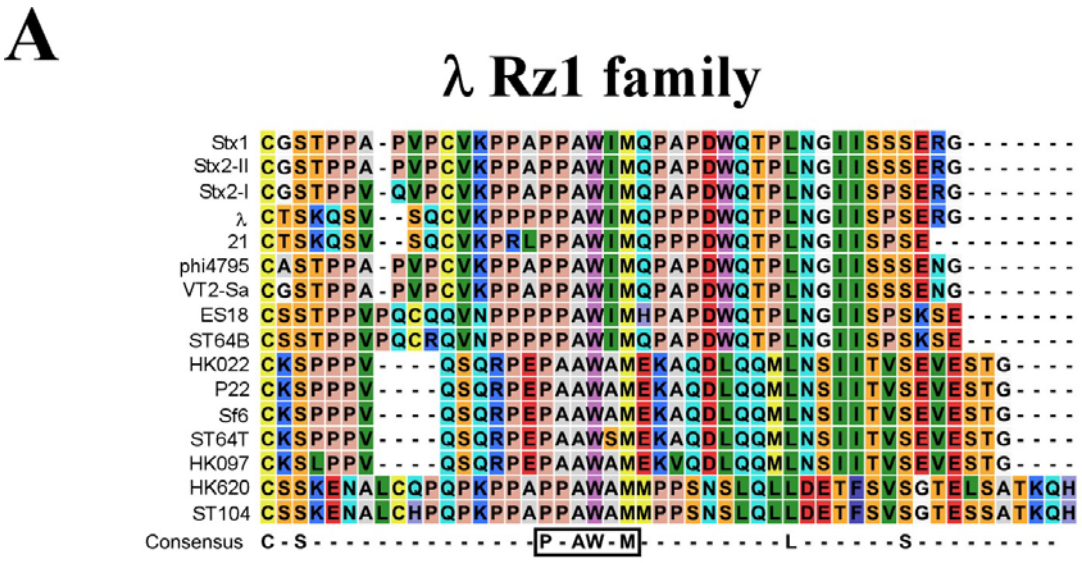


Figure 2.6. Alanine scanning mutagenesis of conserved Rz1 residues.
A. Alignment of the Rz1 proteins from the λ family. Consensus residues are indicated below the alignment and are based on 100% identity. Boxed region indicates domain described in text. Reprinted with permission of Summer et al. (2007).
B. Complementation of Rz1 Ala to Ser mutants. A culture of MC4100(λ900$Rz^{+}$ $Rz1_{am}$) carrying the indicated the indicated plasmid was thermally induced and the lysis profile was monitored as described in *Materials and Methods*. Cultures were grown in LB supplemented with 10 mM $MgCl_2$. Plasmids: pRE, (●); pRE-Rz1, (■); pRE-Rz1P34A, (◆); pRE-Rz1W38A, (▲); pRE-Rz1M40A, (▼ ); pRE-Rz1L50A, (◣); pRE-Rz1S57A, (◢).
C. Rz1M40A accumulates *in vivo*. Samples of the cultures described in (B) were TCA precipitated 5 minutes prior to lysis and subjected to SDS-PAGE and Western blotting with the anti-Rz1 antibody. Selected MW standards are indicated to the left of the blot. Lane assignments for MC4100(λ900$Rz^{+}$ $Rz1_{am}$) with the indicated plasmid: 1, (pRE); 2, (pRE-Rz1); 3, (pRE-Rz1P34A); 4, (pRE-Rz1W38A); 5, (pRE-Rz1M40A); 6, (pRE-Rz1L50A); 7, (pRE-Rz1S57A).

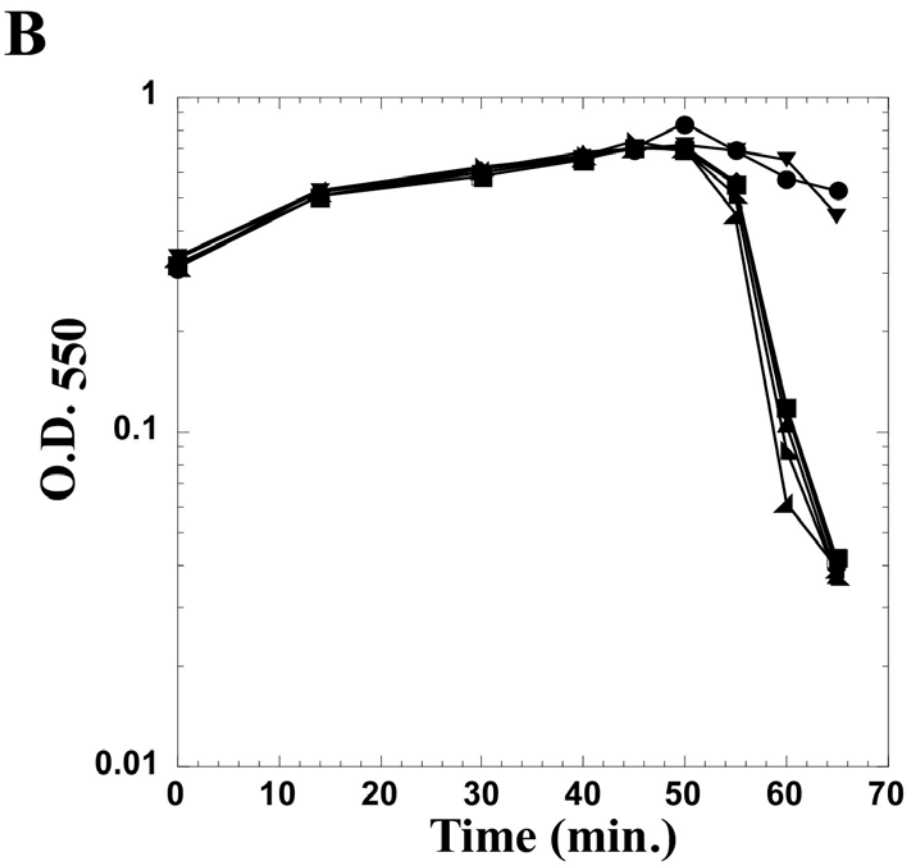


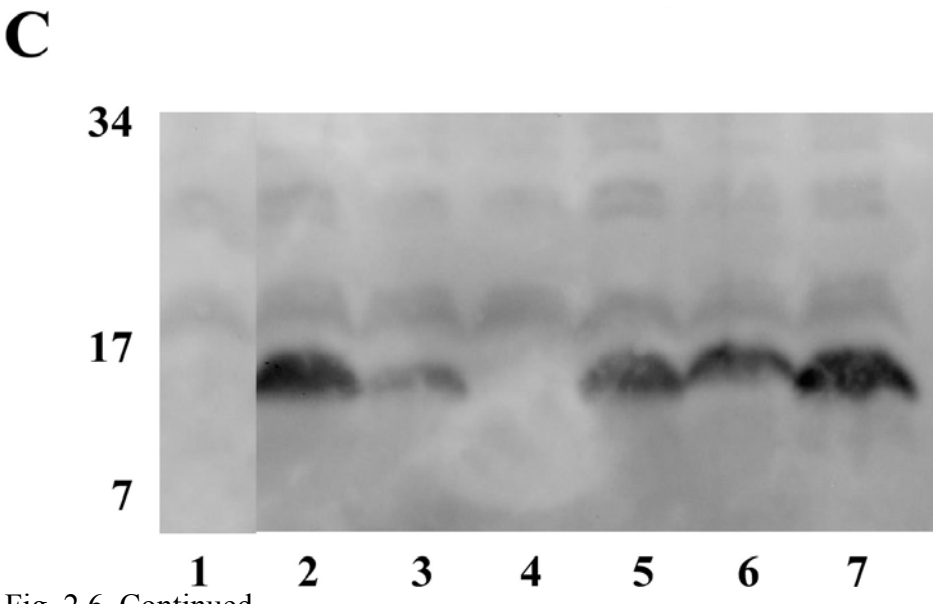


Fig. 2.6. Continued.

**Discussion**

Rz is required for rapid lysis

The results shown in Fig. 2.1A-C and Fig. 2.2A-B demonstrate conclusively that formation of spherical cells is not a normal occurrence during λ lysis. To our knowledge these results provide the clearest picture to date of how the molecular processes of λ lysis play out on a macroscopic level. It is now clear that λ lysis, under conditions close to those normally applied in the laboratory, begins with singular violent breach of the cell envelope. Furthermore, based on the observation of many lytic events not shown here, said breach is most often not preceded by any visible deformation of the cell envelope. The entire process beginning with envelope breach through expulsion of cellular contents due to osmotic and presumably other forces (i.e. genomic DNA expansion), is over in ~ 1 to 5 seconds.

An important conclusion based on the results shown in Fig. 2.2A and B is that the λ$Rz_{am}$ lysis defect occurs in the absence of 10 mM $Mg^{++}$. However, without the stabilizing affect of $Mg^{++}$, the OM is susceptible to mechanical breakage. This explains why the lysis defect is not evident during growth in liquid media, without 10 mM $Mg^{++}$, with constant and vigorous aeration due to shaking. It is important to note that the spherical cells observed under the microscope do in fact burst, due presumably to their inability to withstand the pressure of osmotic force for prolonged periods of time. Unlike λ lysis however the lytic events are no longer synchronized. Regardless, the

results shown in Fig. 2.2.A and B also indicate that Rz and thus Rz1 by association are not in fact accessory lysis proteins. The saltatory lysis observed in liquid media due to λ$Rz_{am}$ infection is nothing more than an artifact. The spherical cells are so mechanically fragile that the mere force of a shaking flask is sufficient to disrupt them.

We propose the following scenario of molecular events to explain the observed events shown in Fig. 2.2B. At ~ 55 minutes post lysogenic induction the holin oligomerizes and produces a large lesion (hole) in the IM. The endolysin escapes through this lesion(s) and begins degrading the PG in that immediate vicinity. The localized PG degradation produces a visible swelling in the cell envelope (Fig. 2.2B) within seconds of hole formation. As the endolysin diffuses away from the hole it continues to degrade PG until the rod shape of the host is no longer distinguishable.

Another major conclusion from these results is that Rz and thus the Rz-Rz1 complex is necessary to ensure rapid lysis. The mechanism by which Rz and Rz1 shunts the lytic pathway away from spherical cell formation toward the violent breach is of great interest and will be discussed further in Chapter V.

Rz and Rz1 form disulfide linked homodimers *in vivo*

To our knowledge, the results shown in Fig. 2.3B and Fig. 2.4B provide the first example of not one but two native phage proteins participating in intermolecular disulfide bond formation. Furthermore, a search of the literature did not turn up any examples of prokaryotic periplasmic proteins participating in this type of bond

formation. Given this information, it is truly surprising to identify not one but two proteins which form homodimers due to intermolecular disulfide formation. It is also surprising to find that the disulfide bonds are not essential for function in either case (Fig. 2.3A and Fig. 2.4A). Due to the findings discussed above, we consider it highly likely that the Rz-Rz1 complex at some point during the course of vegetative growth consists of a 2-Rz:2-Rz1 stoichiometry.

The non-essential nature of the disulfide bridges could indicate that they function in a stabilization capacity. This conclusion seems to be supported by the increase in Rz degradation product that is observed in the C152S and C99S,C152S mutants (Fig. 2.3B, compare lanes 6 and 7). Rz is more susceptible to degradation in the absence of Rz1 (Fig. 2.3B, compare lanes 4 and 8), possibly due to the loss of a complex formation. Perhaps more importantly, the absence of a degradation product in the presence of Rz1 serves as indirect evidence that the Rz-Rz1 complex (see Chapter III) is forming in the presence of the PG.

The ramifications of a single gene equivalent

T1 *gp11* was cloned and plasmid borne expression shown to complement the λ*Rz/Rz1*$^{-}$ $Mg^{++}$ dependent lysis defect (Fig. 2.5). Thus, a functional homolog of Rz and Rz1 is encoded by a single gene product (gp11), which based on strong predictions could physically connect the IM and OM. The major implication of single gene equivalent discovery was that the Rz and Rz1 proteins may be interacting through their periplasmic

domains at some point prior to and/or during lysis (Summer et al., 2007a). Actually, the idea of a Rz-Rz1 complex predated single gene equivalent discovery. From a genetics standpoint, the fact that the null phenotype of λ$Rz_{am}$ and λ$Rz1_{am}$ is the same implies an interaction. Furthermore, the T7 equivalents 18.5/18.7 were demonstrated to interact via their C-terminal ends through a yeast-two hybrid assay (Bartel et al., 1996). Further genetic evidence suggesting an interaction comes from complementation experiments with P2 *LysB/LysC*. The Rz-LysC and LysB-Rz1 pairings were non-functional. The P2 equivalents could only complement the λ $Rz^{-}/Rz1^{-}$ lysis defect as a cognate pair (Markov et al., 2004). The putative Rz-Rz1 interaction had never been demonstrated to form *in vivo* or *in vitro* prior to the work presented in this dissertation. The biochemical investigation of the Rz-Rz1 complex is addressed directly in Chapters III and IV of this dissertation.

# CHAPTER III

# THE FINAL STEP IN THE PHAGE INFECTION CYCLE: THE RZ AND RZ1 PROTEINS LINK THE INNER AND OUTER MEMBRANES*

## Introduction

*Rz* and *Rz1*, and their equivalents, are unique in biology. They are the only genes that share the same DNA in different reading frames (Fig. 3.1A) and are associated with the same phenotype. Moreover, nonsense mutations in either *Rz* or *Rz1* abolish lysis and plaque-formation if moderate concentrations of divalent cations are present, making them the only lambda genes with lethal or conditionally-lethal phenotypes on wt *E. coli* whose function remains undefined (Zhang and Young, 1999). Recently, a comprehensive bioinformatic search found *Rz/Rz1* equivalents in nearly all phages of Gram-negative hosts (Summer et al., 2007a). The diversity of *Rz-Rz1* equivalents was striking: 37 unrelated sequence families, including 8 families with the embedded structure found in lambda, but also families in which *Rz1* extends beyond *Rz* (overlapped structure; 23 families) and others where the two genes are completely separated (6 families).

---

*Reprinted with permission from "The final step in the phage infection cycle: the Rz and Rz1 lysis proteins link the inner and outer membranes" by Berry, J., Summer, E.J., Struck, D.K., and Young, R., 2008. *Molecular Microbiology*, 70, 341-351, 2008 by Blackwell Publishing Ltd.

The phenotype associated with *Rz* (or *Rz1*) mutations has been known for nearly three decades, but the molecular role of these two proteins in host lysis has not been elucidated. Although it was suggested that *Rz* might encode a murein-specific endopeptidase detected in lambda lysates (Taylor, 1971, Young et al., 1979, Bienkowska-Szewczyk & Taylor, 1980) , neither protein has been associated with an enzymatic activity. *Rz* encodes a 153 aa polypeptide with a hydrophobic N-terminus (Fig. 3.1B) that is predicted to be either a secretory signal or N-terminal transmembrane domain (TMD) by sequence analysis algorithms. No studies describing its sub-cellular localization under normal levels of expression have been reported. *Rz1* spans only 60 codons, with a predicted signal peptidase II cleavage site at Cys20 (Fig. 3.1C) (Hanych, 1993, Zhang & Young, 1999); its product was identified as a 6 kDa outer membrane lipoprotein by palmitate-labeling in vivo (Kedzierska et al., 1996).

There is some genetic evidence that the Rz and Rz1 proteins interact. First, the *Rz*/*Rz1* equivalents from phage P2, *lysB*/*lysC*, complement defects in the lambda genes, but only as a cognate pair (Markov et al., 2004). In addition, yeast two-hybrid analysis of a library of phage T7 genes found multiple positives between clones with the last 10 codons of *18.7*, the T7 *Rz1* equivalent, and the last 50 codons of *18.5*, the *Rz* equivalent (Bartel et al., 1996). These data suggest that Rz and Rz1 interact in a C-terminus to C-terminus fashion, which may account for the architectures of the embedded and overlapped *Rz*/*Rz1* genes, in that these unusual arrangements minimize the likelihood of recombinational separation of the interacting domains (Summer et al., 2007a).

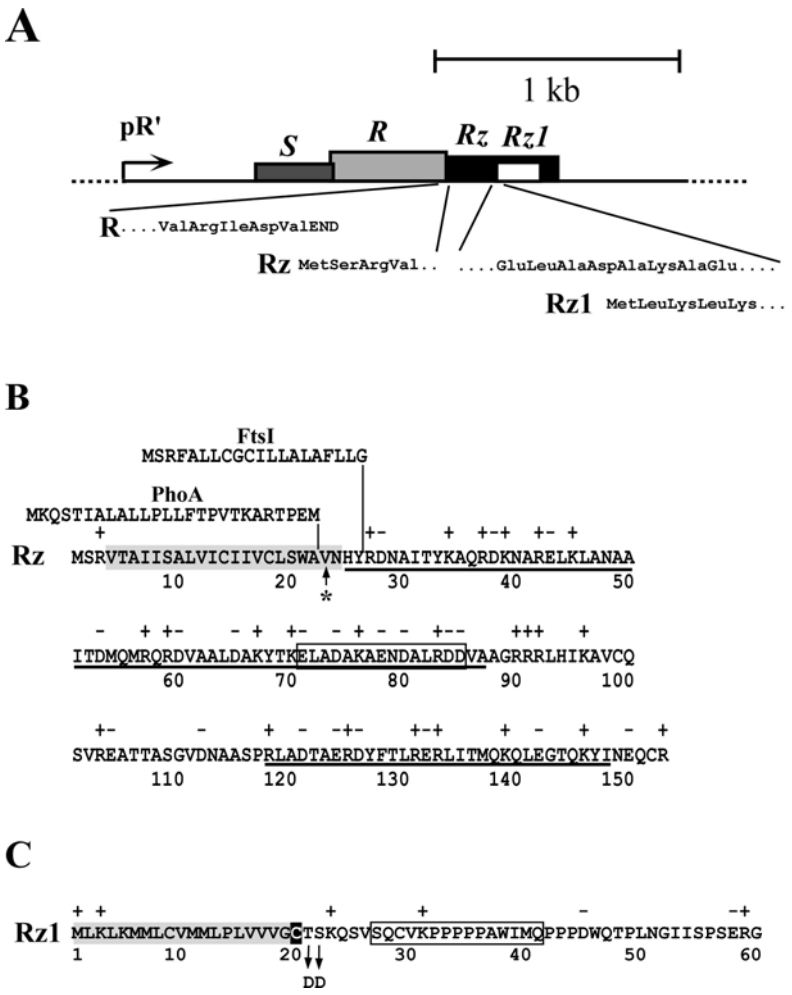


Figure 3.1. The Rz and Rz1 genes

A. The lambda lysis cassette. The four lysis genes are shown drawn to scale downstream of the lambda late promoter pR'. The insets show the initial codons of *Rz*, beginning at the end of the *R* endolysin gene, and *Rz1*, which is embedded entirely within *Rz* in the +1 reading frame.

B. Rz amino acid sequence. The TMD is boxed in grey and predicted α-helical regions are underlined. Above the Rz sequence, the sequences of the PhoA secretory signal and the FtsI N-terminal TMD are shown above the junction where they are substituted in the PhoA-Rz and the FtsI-Rz hybrid constructs. The asterisk indicates the position of a predicted signal peptidase I cleavage site (Bendtsen et al., 2004). The boxed italic text here and in (C) indicates the polypeptide sequence used for raising antibodies.

C. Rz1 amino acid sequence. The lipoprotein (signal peptidase II) signal sequence predicted by LipoP (Juncker et al., 2003) is boxed in grey, with the processed Cys residue highlighted in black. The positions of the two Asp substitutions that redirect Rz1 to the cytoplasmic membrane are indicated by arrows.

The discovery of a new class of proteins, the spanins, which are functionally equivalent to Rz/Rz1 pairs, provides new insight into Rz/Rz1 function (Summer et al., 2007a). Spanins have a lipoprotein signal peptide as well as a C-terminal TMD and, thus, should provide a physical connection between the inner and outer bacterial membranes. The ability of the T1 spanin gene to complement the *Rz-Rz1* lysis phenotype provides further support to the notion that Rz and Rz1 interact and, in fact, indicates that Rz-Rz1 complexes span the periplasm and connect the inner (IM) and outer (OM) membranes.

Recently, Rz-Rz1 equivalents were identified in the tectivirus PRD1, and in the same study, a role for the Rz-Rz1 proteins in lysis was proposed (Krupovic *et al.*, 2008). In this scheme, it was suggested that Rz-Rz1 interact not only with each other but also, as a complex, with the holin, to transmit the mechanical stress of the holin-mediated lesion in the cytoplasmic membrane to the outer membrane, resulting in its disruption.

Here we describe experiments that unambiguously resolve the sub-cellular localization of the λ Rz and Rz1 proteins when their genes are expressed from the λ late promoter, assess the ability of Rz-Rz1 to form complexes, and examine the requirement of holins for Rz/Rz1 function. The results are discussed in terms of a model for the participation of these proteins in a hitherto unrecognized final stage of the bacteriophage infection cycle.

## Materials and methods

### Bacterial growth and induction

The bacterial strains, bacteriophage, and plasmids used in this study are listed in Table 3.1. Bacterial cultures were grown in standard LB media supplemented with $MgCl_2$ (10 mM), ampicillin (100 μg/ml), kanamycin (40 μg/ml), and chloramphenicol (10 μg/ml) when appropriate. Culture growth and lysis profiles were monitored as previously described (Smith *et al.*, 1998). Briefly, overnight cultures were diluted 300:1 and grown with aeration at 30ºC for lysogenic cultures and 37ºC for non-lysogens. Lysogens were thermally induced at A550 ~0.3 by aeration at 42ºC for 20 min, followed by continued growth at 37ºC. When indicated, isopropyl β-D-thiogalactosidase (IPTG) was added to a final concentration of 1mM.

The *RzRz1* genes are either expressed in their native context in the λ genome from prophage induction or from derivatives of the medium-copy plasmid pRE carrying the λ late promoter, pR'. In all cases, the λ late gene activator Q is either supplied *in trans* from an induced prophage or from pQ, a very low copy vector carrying *Q* cloned under the control of the $P_{lac/ara-1}$ promoter (Lutz & Bujard, 1997, Grundling et al., 2001).

Table 3.1. Strains, phages, and plasmids

| **Strain** | **Description** | **Source** |
|---|---|---|
| XL-1 Blue | *recA endA1 gyrA96 thi1 hsdR17 supE44 relA1 lac* [F' *proAB lacZ*$_{\Delta M15}$::*Tn*10] | Stratagene |
| MC4100 | F$^-$ *araD139* Δ[*argF-lac*]$_{U169}$ *rpsL150 relA1 flb5301 deoC1 ptsF25 rbsR* | (Casadaban, 1976) |
| MG1655 | F$^-$ *ilvG rph1 rfb50* | Laboratory stock |
| RY17299 | MG1655 Δ*tonA* | Laboratory stock |
| RY17299 *lacI*$^{q1}$ | | (Park et al., 2006) |
| RY17299(λ901 *Rz*$^+$*Rz1*$^+$) | Lysogen carrying λ900*S*$_{am7}$*Rz*$^+$*Rz1*$^+$ prophage | This study |
| RY17299(λ901 *Rz*$_{am}$*Rz1*$^+$) | | This study |
| RY17299(λ901*Rz*$^+$*Rz1*$_{am}$) | | This study |
| RY17299(λ901*Rz*$_{am}$*Rz1*$_{am}$) | | This study |
| MC4100(λ900) | Lysogen carrying λ900*S*$^+$*Rz*$^+$*Rz1*$^+$ prophage | (Zhang & Young, 1999) |
| MC4100(λ900*Rz*$_{am}$*Rz1*$^+$) | | (Zhang & Young, 1999) |
| MC4100(λ900*Rz*$^+$*Rz1*$_{am}$) | | (Zhang & Young, 1999) |

| **Phage** | **Description** | **Source** |
|---|---|---|
| λ143 | λimm$^{434}$ *cI R*$_{am5}$ | Laboratory stock |
| λ800Δ(*SR*) | λΔ(*stf tfa)::cat cI*$_{857}$ Δ(*SR*); forms lysis-defective, Cam$^R$ prophage | (Smith *et al.*, 1998a) |

Table 3.1. Continued

| Phage | Description | Source |
|---|---|---|
| λ900 | λΔ(*stf tfa)::cat cI$_{857}$bor::kan;* carries Cam$^R$ and Kan$^R$; wt *RzRz1* | (Zhang & Young, 1999) |
| λ900*Rz$_{Q100am}$ Rz1$^+$* | | (Zhang & Young, 1999) |
| λ900*Rz$^+$ Rz1$_{W38am}$* | | (Zhang & Young, 1999) |
| λ901 | *S$_{am7}$* recombinant, isogenic to λ900 | This study |
| λ901*Rz$_{Q100am}$Rz1$^+$* | | This study |
| λ901*Rz$^+$Rz1$_{W38am}$* | | This study |
| λ901*Rz$_{Q100am}$ Rz1$_{W38am}$* | | This study |

| Plasmid | Description | Source |
|---|---|---|
| pQ | pSC101 origin with low-copy mutation; *Q* cloned under P$_{lac/ara-1}$ promoter | (Park *et al*., 2006) |
| pER157Rz$^+$Rz1$^-$ | pBR322 derivative; *Δtet S$^+$R$^+$Rz$^+$Rz1$_{W38am}$ bor::kan* | (Zhang & Young, 1999) |
| pJF118EH | ColE1 origin, P$_{tac}$, *lacI$^q$* and *amp$^R$*; medium copy P$_{tac}$ expression vector | (Furste *et al.*, 1986) |
| pJFLyz | pJF118EH carrying P1 *lyz* ,nucleotides 20225-21079 of the P1 genome | (Xu *et al*., 2005) |
| pJF-PhoAΦRz$^{IRS}$ | *phoAΦRz$^{IRS}$* from pRE-*phoAΦRz$^{IRS}$* cloned into pJF118EH | This study |
| pJF-PhoA | pJF118EH carrying *phoA* | (Xu *et al.*, 2004) |

Table 3.1. Continued

| Plasmid | Description | Source |
|---|---|---|
| pJF-FtsI$^{cmyc}$ | pJF118EH carrying *ftsI*$^{cmyc}$ | (Xu *et al.*, 2004) |
| pRE | Derivative of pJF118EH with *lacI*$^{Q}$ and $P_{tac}$ promoter replaced with pR' promoter region from λ; transcriptionally activated by lambda Q | (Park *et al.,* 2006) |
| pRE-RzRz1 | *Rz*$^{+}$*Rz1*$^{+}$ cloned in pRE | This study |
| pRE-Rz | *Rz*$^{+}$ cloned in pRE with *Rz1*$_{W38am}$ null mutation | This study |
| pRE-Rz1 | *Rz1*$^{+}$ cloned in pRE | This study |
| pRE-Rz$^{HIS}$ | pRE-Rz with GGHHHHHH inserted after codon 153 of *Rz* | This study |
| pRE-Rz1$^{HIS}$ | pRE-Rz1 with GGHHHHHH inserted after codon 60 of *Rz1* | This study |
| pRE-Rz$^{IRS}$ | *Rz* with IRS epitope tag inserted after codon 153 cloned in pRE | This study |
| pRE-Rz1$^{AU1}$ | *Rz1* with AU1epitope tag inserted after codon 60 cloned in pRE | This study |
| pRE-FtsIΦRz$^{IRS}$ | Codons 24 to 40 of *ftsI* replacing codons 4-26 of *Rz*$^{IRS}$ | This study |
| pRE-PhoAΦRz$^{IRS}$ | Codons 1-22 of *Rz* replaced by codons 1-26 of *phoA*, encoding the signal sequence | This study |

Table 3.1. Continued

| **Plasmid** | **Description** | **Source** |
|---|---|---|
| pRE-Rz1$^{AU1}_{T21D,S22D}$ | pRE-Rz1 carrying the T21D and S22D mutations | This study |
| pRE-PhoAΦRz$^{IRS}$Rz1$^{HIS}$ | *Rz1$^{HIS}$* inserted downstream of PhoAΦRz | This study |
| pRW | Derivative of pRE with *bor* gene flanking multiple cloning site, to provide downstream homology for recombination | R. White, unpublished |
| pRW-Lyz$_{C13S,C44S}$ | P1 *lyz$_{C13S, C44S}$* cloned into pRW | G. Kuty, unpublished |
| pRW- Lyz$_{C13S,C44S}$-RzRz1 | *RzRz1* inserted downstream of *lyz$_{C13S, C44S}$* | This study |

DNA techniques

Isolation of plasmid DNA, DNA amplification by PCR, DNA transformation, site-directed mutagenesis and DNA sequencing were performed as described previously (Tran et al., 2005). Sequences of primers are listed in Table 3.2.

Table 3.2. Primer sequences

| Primer | Sequence |
|---|---|
| RzFor | ATATGGTACCAGAGAGATTGATGTATGAGCAGAG |
| RzRev | CGCGGATCCCTATCTGCACTGC |
| Rz1For | ATATGGATCCAAGGAGTTAGCTGATGCTAAAGCT |
| Rz1Rev | CCCGCAAGCTTTCAGCCTCTCTC |
| RzHISRev | GCCGGATCCCTAGCCGCCGTGATGGTGATGATGGTG |
| Rz1HISRev | GCCAAGCTTCTAGCCGCCGTGATGGTGATGATGGTG |
| RzIRSRev | ATATGGATCCTCAAGAACGGATATATCTGCACTG |
| Rz1AU1Rev | ATATAAGCTTTCAAATATAACGATAGGTATCGCC |
| FtsIFor | GGTACCAGAGAGATTGATGTATGAGCAGATTTGCGTTGTTATGCGGC |
| FtsIRev | GGTAATGGCGTTATCACGTCCGAGCAGAAAAGCCAG |
| PhoAFor | AGAGAGATTGATGTATGAAACAAAGCACTATTGC |
| PhoARev | ATCACGGTAATGATTAACCATTTCTGGTGTGCG |
| PhoAFor-2 | CCGGAATTCAGGAGGTATACCATATGAAACAAAGCACTATTGCA |
| Rz1T21DFor | CTGGTCGTCGTCGGTTGCGACTCAAAGCAGTCTGTCAGT |
| Rz1T21DRev | ACTGACAGACTGCTTTGAGTCGCAACCGACGACGACCAG |
| Rz1S22DFor | GGTCGTCGTCGGTTGCGACGACAAGCAGTCTGTCAGTCAGT |
| Rz1S22DRev | ACTGACTGACAGACTGCTTGTCGTCGCAACCGACGACGACC |
| LyzC13SFor | GGAGGCGGTGCAATTAGCGCTATCGCGGTGATG |

Table 3.2. Continued

| Primer | Sequence |
|---|---|
| LyzC13SRev | CATCACCGCGATAGCGCTAATTGCACCGCCTCC |
| LyzFor | GCGCGCGGATCCATGAGGTCTTTATGAAGGGAAAAACAGCC |
| LyzRev | GGGCCCCTCGAGTTATTCATTGACCAGTCC |
| LyzC44SFor | TAACGCTGAAGGTAGCCGACGTGATCC |
| LyzC44SRev | GGATCACGTCGGCTACCTTCAGCGTTA |

Phage manipulation

The phage λ*Sam7* and its isogenic *Rz* and *Rz1* variants listed in Table 3.1 were obtained by crossing the *Rz* and/or *Rz1* mutant alleles onto λ, as previously described (Zhang & Young, 1999, Grundling et al., 2000). Lysogens were selected, their allele and single copy status confirmed by sequencing and PCR, respectively, as previously described (Zhang & Young, 1999).

Plasmid construction

All DNA manipulations were performed according to standard techniques described previously (Tran et al., 2005). The pRE plasmid is a derivative of pJF118EH containing the λ pR' promoter in place of the $P_{tac}$ promoter and $lac^{Iq}$ gene (Park et al.,

2006). The pQ plasmid contains a very low copy pSC101* origin, a Plac/ara-1 promoter and a copy of λ*Q* (Grundling et al., 2001). Induction of the pRE plasmid is achieved by providing the λ Q protein either by IPTG induction of the pQ plasmid or through thermal induction of a λ prophage. Nucleotides 45950 – 46427 of λ encoding the *Rz* ribosome binding site (RBS) through the end of *Rz1* were amplified by PCR using primers RzFor/Rev and inserted in between the kpnI and BamHI sites of pRE to generate pRE-RzRz1. The plasmid pRE-Rz was constructed by first amplifying the *Rz* gene region from the template pER157$Rz^{+}Rz1^{-}$ using primers RzFor/Rev. This plasmid contains a silent mutation in the *Rz* reading frame which converts codon 38 of the *Rz1* frame to an amber codon. The amplified *Rz* gene fragment was ligated into pRE between the kpnI and BamHI sites. pRE-$Rz^{IRS}$ was constructed in the same manner with the exception that the reverse primer RzIRSrev was designed to fuse the amino acid sequence RYIRS, which serves as an epitope tag, to the extreme C-terminus of *Rz*. The plasmid pRE-Rz1 was constructed by first amplifying nt 46173 – nt 46368 of λ using primers Rz1For/Rev and then inserting the fragment between the BamHI and HindIII sites of pRE. The plasmid pRE-$Rz1^{AU1}$ was constructed in the same manner with the exception that the reverse primer Rz1AU1rev was designed to fuse the amino acid sequence DTYRYI , which serves as an epitope tag, to the extreme C-terminus of *Rz1*. The plasmid pRE-$Rz1^{AU1}$T21DS22D was generated by converting Thr21 and Ser22 of Rz1 to Asp through site directed mutagenesis with the primer pairs Rz1T21DFor/Rev and Rz1S22DFor/Rev, respectively.

The plasmids pRE-Rz$^{HIS}$ and pRE-Rz1$^{HIS}$ were constructed in the same manner as the untagged versions with the exception that the reverse primers were substituted with RzHISRev and Rz1HISRev, respectively. PCR using these reverse primers fused the residues $Gly_2His_6$ to the extreme C-terminus of each gene. The resulting products were then ligated using the same restriction sites used for the non-tagged versions.

The Rz signal sequence hybrid constructs pRE-FtsIΦRz$^{IRS}$ and pRE-PhoAΦRz$^{IRS}$ were produced by applying a modified version of the QuickChange site directed mutagenesis protocol as described previously (Tran et al., 2005). For example, an initial PCR reaction, using pJF-FtsI$^{cmyc}$ as a template, was performed with primer pair FtsIFor/Rev to amplify the region of *FtsI* corresponding to the N-terminal transmembrane domain. These forward and reverse oligonucleotides each have 5' ends which anneal to the target plasmid pRE-Rz$^{IRS}$. The initial PCR products were then used to perform a reaction similar to QuickChange site directed mutagenesis using the target plasmid as a template to generate pRE-FtsIΦRz$^{IRS}$.

The plasmid pRE-PhoAΦRz$^{IRS}$ Rz1HIS was constructed by digesting pRE-Rz1HIS with BamHI and HindIII and inserting the fragment into pRE-PhoAΦRz$^{IRS}$ digested at the same sites. The plasmid pJF-PhoAΦRz was constructed by first amplifying the PhoAΦRz$^{IRS}$ fragment using primer pair PhoAFor2/RzIRSRev and digesting the resulting fragment with EcoRI and BamHI. The PhoAΦRz$^{IRS}$ fragment was then ligated into the pJF118EH generated with the same cut sites.

The plasmid pRW Lyz C13SC44S was constructed by first amplifying the Lyz gene using pJFLyz as a template and the primer pair LyzFor/Rev. The PCR product and

pRW were treated with BamHI and XhoI prior to ligation. The Cys residues at positions 13 and 44 of Lyz were then converted to Ser by site directed mutagenesis using the primer pairs LyzC13SFor/Rev and LyzC44SFor/Rev respectively. The plasmid pRW-RzRz1 Lyz C13SC44S was constructed by digesting both pRE-RzRz1 and pRW Lyz C13SC44S with KpnI and BamHI. The resulting RzRz1 fragment was then ligated to the pRW Lyz C13SC44S backbone.

SDS-PAGE and Western blotting

SDS-PAGE and Western blotting were performed as described previously (Gründling *et al.*, 2000a; Bernhardt *et al.*, 2002). SeeBlue Plus2 (Invitrogen) prestained standard was included as a molecular mass standard. Briefly, proteins were transferred to PVDF membrane (Pall Life Sciences) using a Hoefer TE unit at 0.1 mA overnight at 4º C. Antibodies (Sigma Genosys) were generated in rabbits against the synthetic peptides CELADAKAENDALRDD, corresponding to the Rz residues 71-85 (modified with an N-terminal Cys for conjugation) and SQCVKPPPPPAWIMQ, corresponding to Rz1 residues 27-41 (Fig. 3.1B and C), and used at a dilution of 1:1000. The secondary antibody, goat-anti-rabbit-HRP (Thermo Scientific), was used at a dilution of 1:5000. Chemiluminescence was detected using a Bio-Rad XR Gel Doc system.

Sodium carbonate extraction

A 200 ml culture of RY17299(λ901$Rz^{+}Rz1_{am}$) was induced, aerated 1 h, and harvested by centrifugation in a JA-10 rotor at 8,000 x g for 10 min. The cells were resuspended in 1 ml of French press buffer (100mM $Na_2HPO_4$, 100mM KCl, 5 mM EDTA, pH 8.0) supplemented with 5 µl Protease Inhibitor Cocktail (Sigma-Aldrich P8465). The cells were disrupted by passage through a French pressure cell (Spectronic Instruments, Rochester, N.Y.) at 16,000 lb/in$^2$, and cleared of unbroken cells by centrifugation in a Damon-IEC Spinette clinical centrifuge at 1,000xg for 10 min. Membranes from three equal portions were pelleted in a TLA 100.3 rotor at 150,000 x g for 1 h at 4 ºC. One pellet was resuspended in 1 ml of 1M $Na_2 CO_3$, pH 11, incubated on ice for 30 min, and fractionated into peripheral (supernatant) and integral (pellet) protein fractions by centrifugation in a TLA 100.3 rotor at 150,000 x g for 1 h. A second pellet was resuspended in 1 mL of 1% Empigen BB, 100 mM NaCl, 50 mM Tris-Cl, pH 8.0, incubated at room temperature with gentle agitation for 1 h, and centrifuged in a TLA 100.3 rotor at 150,000 x g for 1 h. As a control, the final membrane pellet was resuspended in 1 ml of French press buffer and then centrifuged at 150,000 x g for 1 h as before. In each case, the insoluble material was resuspended in 1X SDS-PAGE buffer and the soluble material was mixed with an equal volume of 2X SDS-PAGE buffer. All samples were heated to 100ºC for 5 min before analysis by SDS-PAGE and Western blotting.

Subcellular localization of Rz and Rz1

Fifty min after thermal induction, 250 ml cultures of the indicated strains were rapidly cooled to 4º C by swirling the growth flasks in an ice-$H_2O$ bath. All subsequent steps carried out at 4º C. Cells were harvested by centrifugation at 8,000 x g for 15 min in a Beckman JA-10 rotor. The supernatant was completely removed and the cells converted to spheroplasts as previously described (Osborn & Munson, 1974). The spheroplasts were transferred to a Beckman Ultra-Clear SW28 centrifuge tube and ruptured by sonication using a Sonicator Cell Disruptor W-375 (60% output, 3 x 15 sec bursts separated by 1 minute intervals to prevent heating). For harvesting of membranes and fractionation by density gradient, all sucrose solutions were prepared w/w and contained 5 mM EDTA, pH7.5. The lysate was layered on a two-step gradient consisting of 12 ml of 18% and 3 ml of 55% sucrose and centrifuged in a Beckman SW28 rotor at 100,000 x g for 2 h. The total membrane fraction was layered on a 5-step sucrose gradient and centrifuged as previously described (Osborn and Munson, 1974). Gradients were collected in 1 ml fractions from the top using a Model 640 ISCO Density Gradient Fractionator. The protein concentration of individual fractions was determined with the Bio-Rad protein assay (Bio-Rad) using BSA as the standard according to the manufacturer's instructions. NADH oxidase activity assays were performed as described previously (Owen, 1982). The refractive index of alternate fractions was determined with a refractometer (Spectronic Instruments, 334610). Approximately 800 μl of every third gradient fraction was diluted to a final sucrose concentration of less

than 10% with 1 mM EDTA, pH7.5 and centrifuged in a Beckman 70.1Ti rotor at 100,000 x g for 2 h at 4ºC. Membrane pellets were resuspended in 60 µl of 1X SDS-PAGE buffer and boiled for 5 min. The distribution of the major OMPs was determined by SDS-PAGE and Coomassie blue staining.

Isolation of Rz-Rz1 complexes

Twenty-five ml cultures of lysogenic cells harboring the indicated plasmids were harvested at 50 min after induction by centrifugation in an Eppendorf 5702 centrifuge at 2,800 x g for 15 min. The cells were converted to spheroplasts and lysed as described (Broome-Smith & Spratt, 1986, Tran et al., 2005), except that a 50 µl aliquot of spheroplasts was reserved for SDS-PAGE analysis and the Protease Inhibitor Cocktail used (Sigma-Aldrich, P8849) did not contain EDTA. A 500 µl volume of lysate was incubated with 50 µl of Dynabeads TALON (Invitrogen) at 4ºC for 2 h with gentle agitation. The beads were then collected magnetically and washed three times with lysis buffer containing 1 mg/ml BSA (MP Biomedicals). The beads were resuspended in 50 µl of 1X SDS-PAGE buffer and boiled for 5 min. All samples were cleared of beads and debris by brief centifugation in a tabletop microcentrifuge and analyzed by SDS-PAGE and Western blotting.

## Results

### Analysis of membranes in lambda inductions

Accepted methods for separating the IM and OM by isopycnic gradient centrifugation involve first converting the cells to spheroplasts and then disrupting the cells by sonication (Osborn & Munson, 1974). Failure to convert cells to spheroplasts or having the spheroplasts undergo lysis before mechanical disruption leads to poor separation of the IM and OM fractions. In our hands (and as reported previously (Reader & Siminovitch, 1971)), stable spheroplasts could not be formed from cells expressing the λ holin gene. To avoid this problem, we examined the sub-cellular distribution of Rz and Rz1 expressed at their normal, physiological levels using a set of isogenic prophages carrying a null mutation in the *S* holin gene. As a control, isopycnic sucrose gradient analysis was performed for an induced lysogen with null mutations in *S*, *Rz* and *Rz1* (λ901$Rz_{am}Rz1_{am}$) (Fig. 3.2A). Total protein, NADH oxidase (an IM-marker), and major OM proteins (OMPs) were normally distributed in two major peaks at the densities expected of IM and OM fractions. When isogenic $Rz^{+}$ lysogens were induced, Rz appeared as a 17 kDa membrane-associated protein (Fig. 3.2E). This species could be extracted with detergent but not by sodium carbonate, as expected for proteins integrated into the cytoplasmic membrane. When membranes from these induced lysogens were fractionated by isopycnic sucrose gradient centrifugation, Rz was found in the IM fraction, distributed identically to NADH oxidase activity (Fig. 3.2B).

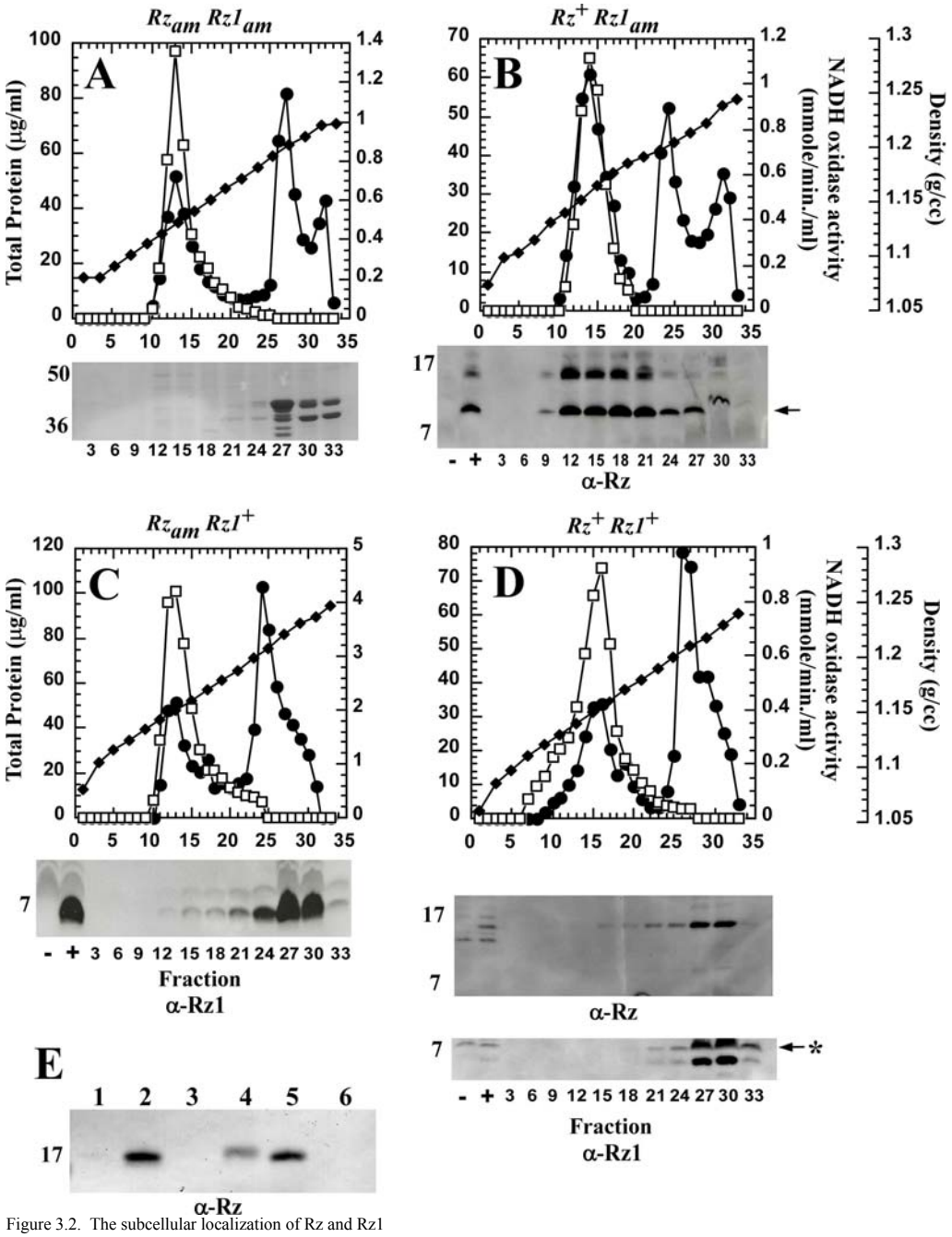


Figure 3.2. The subcellular localization of Rz and Rz1

A - E. Membranes from an induced culture of RY17299 carrying isogenic λ901 prophages with the indicated *RzRz1* alleles were analyzed by (A - D) sucrose density gradient or by carbonate extraction (E), as described in *Materials and Methods*. Symbols: total protein, filled circles; NADH oxidase activity, open boxes; density, filled diamonds. In all cases, the abscissa of the gradient distributions and gel or immunoblot insets is sample number, from the top of the gradient.

A. Coomassie-blue stained SDS gel showing major OMPs distributed in fractions 27-33.

B-D. Representative fractions were subjected to SDS-PAGE and Western blotting with anti-Rz and/or anti-Rz1 antibody as indicated below each respective blot, with selected MW standards indicated to the left. +, - : total membrane samples from induced lysogens with wt (+) or null (-) *Rz* or *Rz1* genes, as indicated. Arrow in panel (B) indicates the position of putative Rz degradation product (see text). The position of a reproducible background band is indicated by an asterisk (D).

E. Lane assignments: 1, soluble fraction from French-press disrupted cells; 2, total membrane fraction from disrupted cells; 3, soluble fraction from carbonate extraction; 4, insoluble fraction from carbonate extraction; 5, soluble fraction from 1% EBB extraction; 6, fraction insoluble in 1% EBB.

When parallel analyses were performed on membranes from an induced λ901$Rz_{am}Rz1^{+}$ lysogen, Rz1, the lipoprotein, was found to be located in the OM fractions (Fig. 3.2C). However, in the induction of the isogenic $Rz^{+}Rz1^{+}$ lysogen, the distribution of the Rz protein in particular changed dramatically, co-fractionating with Rz1 (Fig. 3.2D).

The Rz and Rz1 proteins form a complex

While there is genetic and phylogenetic evidence to suggest that Rz and Rz1 interact to form a complex, the physical association of these proteins has never been demonstrated. To show that Rz and Rz1 co-purify, we constructed alleles of *Rz* and *Rz*1 encoding C-terminal hexahistidine tagged products, confirmed that each was functional by complementation (data not shown), and prepared detergent-solubilized extracts from cells expressing the gene pairs $Rz_{his}/Rz1$ or $Rz/Rz1_{his}$,. Complexes were isolated by immobilized metal affinity chromatography (IMAC) and then analyzed by SDS-PAGE and Western blotting. As can be seen in Fig. 3.3C (lanes 11 and 12), the majority of Rz is bound to the affinity resin only when the *Rz* gene is co-expressed with $Rz1_{his}$. Surprisingly, the converse is not true; when *Rz1* is co-expressed with $Rz_{his}$, no Rz1 is retained by the affinity resin, Fig. 3.3C (lanes 9 and 10). However, in this experiment, only a small fraction of the $Rz_{his}$ protein present in the extracts binds to the resin. Since $Rz_{his}$ is quantitatively bound to the resin in the absence of Rz1, Fig. 3.3A (lanes 2 and 3), we interpret this to mean that, in the $Rz_{his}$ /Rz1 complex, the oligohistidine tag of $Rz_{his}$ is masked by Rz1 and is not free to interact with the IMAC resin. Further evidence that Rz

and Rz1 interact derives from the observation that when the *Rz* gene is expressed in the absence of *Rz1*, the Rz protein is subject to a specific proteolytic event resulting in a ~12kDa product recognized by antisera raised against a C-terminal epitope (Fig. 3.2B, arrow). This cleavage product is not detected in cells expressing the *Rz/Rz1* gene pair, suggesting that the protease-sensitive site in Rz is not exposed in Rz/Rz1 complexes (Fig. 3.2D).

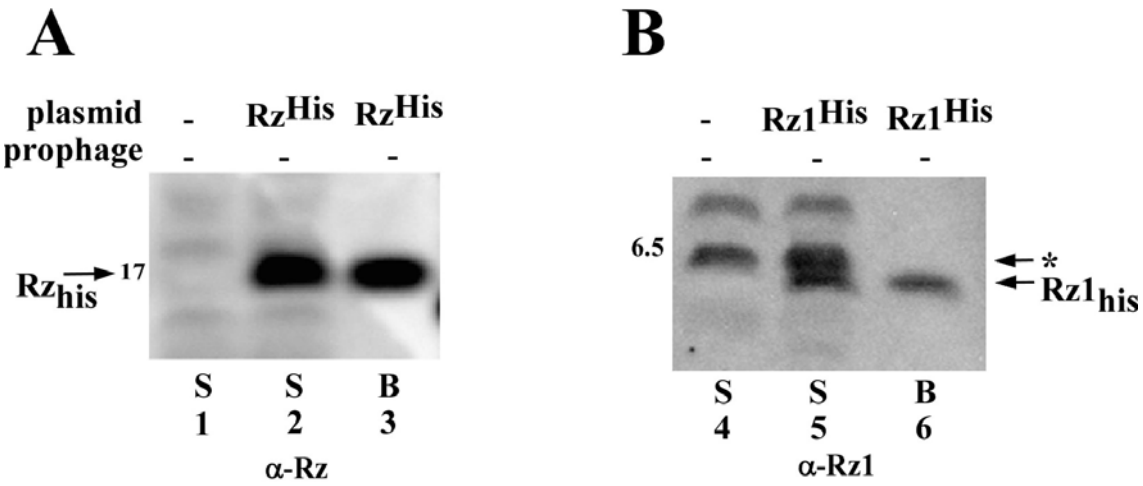


Figure 3.3. Rz and Rz1 form a complex. Induced RY17299 lysogens carrying single isogenic λ901 prophages with the indicated *Rz* and R*z1* alleles in trans to the indicated plasmids were converted to spheroplasts, lysed, and subjected to batch affinity fractionation with magnetic Talon beads. Total spheroplasts (S) and proteins bound to the beads (B) were analyzed by SDS-PAGE and Western blotting with the antibodies indicated below each panel. The position of relevant MW standards is indicated on the left of each panel. An asterisk indicates the position of a reproducible background band. The bands representing Rz, $Rz^{His}$, Rz1, $Rz1^{HIS}$ as well as the mature (mPhoAΦ$Rz^{IRS}$) and precursor (pPhoAΦ$Rz^{IRS}$) forms of the PhoA-Rz chimera are indicated with arrows.
A and B. Lanes: 1 and 4, $Rz_{am}Rz1_{am}$ lysogen with pRE; 2 and 3, $Rz_{am}Rz1_{am}$ lysogen with pRE-$Rz^{HIS}$; 5 and 6, $Rz_{am}Rz1_{am}$ lysogen with pRE-$Rz1^{HIS}$.
C. Lanes 7 and 8, $Rz_{am}Rz1_{am}$ lysogen with pRE-RzRz1; 9 and 10, $Rz_{am}Rz1$ lysogen with pRE-$Rz^{HIS}$; 11 and 12, $RzRz1_{am}$ lysogen with pRE-$Rz1^{HIS}$; 13 and 14, $Rz_{am}Rz1_{am}$ lysogen with pRE-PhoAΦ$Rz^{IRS}Rz1^{HIS}$.

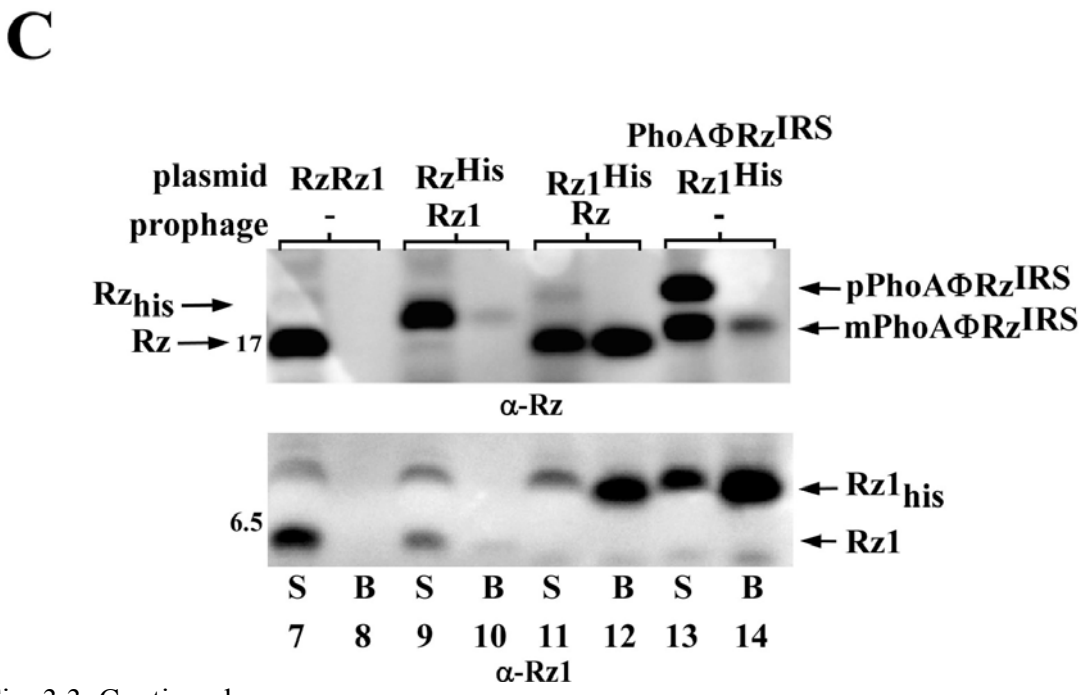


Fig. 3.3. Continued.

Rz/Rz1 complexes must connect the IM and OM to be functional

To provide evidence that the proposed connection between the IM and OM is required for the function of the Rz/Rz1 complex, we tested the ability of Rz and Rz1 derivatives with altered topological determinants to replace the wild type proteins. First, the N-terminal TMD of Rz was replaced with the canonical signal sequence of the soluble periplasmic protein PhoA. Roughly half of the PhoA$^{ss}$-Rz chimera accumulated as a processed species that formed a complex with Rz1 (Fig. 3.3C, lanes 13-14), but could not functionally replace Rz (Fig. 3.4A). In fact, the *phoA$^{ss}$-Rz* gene exhibited dominant-negative character, in that its expression in an induced *Rz$^{+}$Rz1$^{+}$* lysogen partially blocked lysis in the presence of 10mM $MgCl_2$ (Fig. 3.4B).

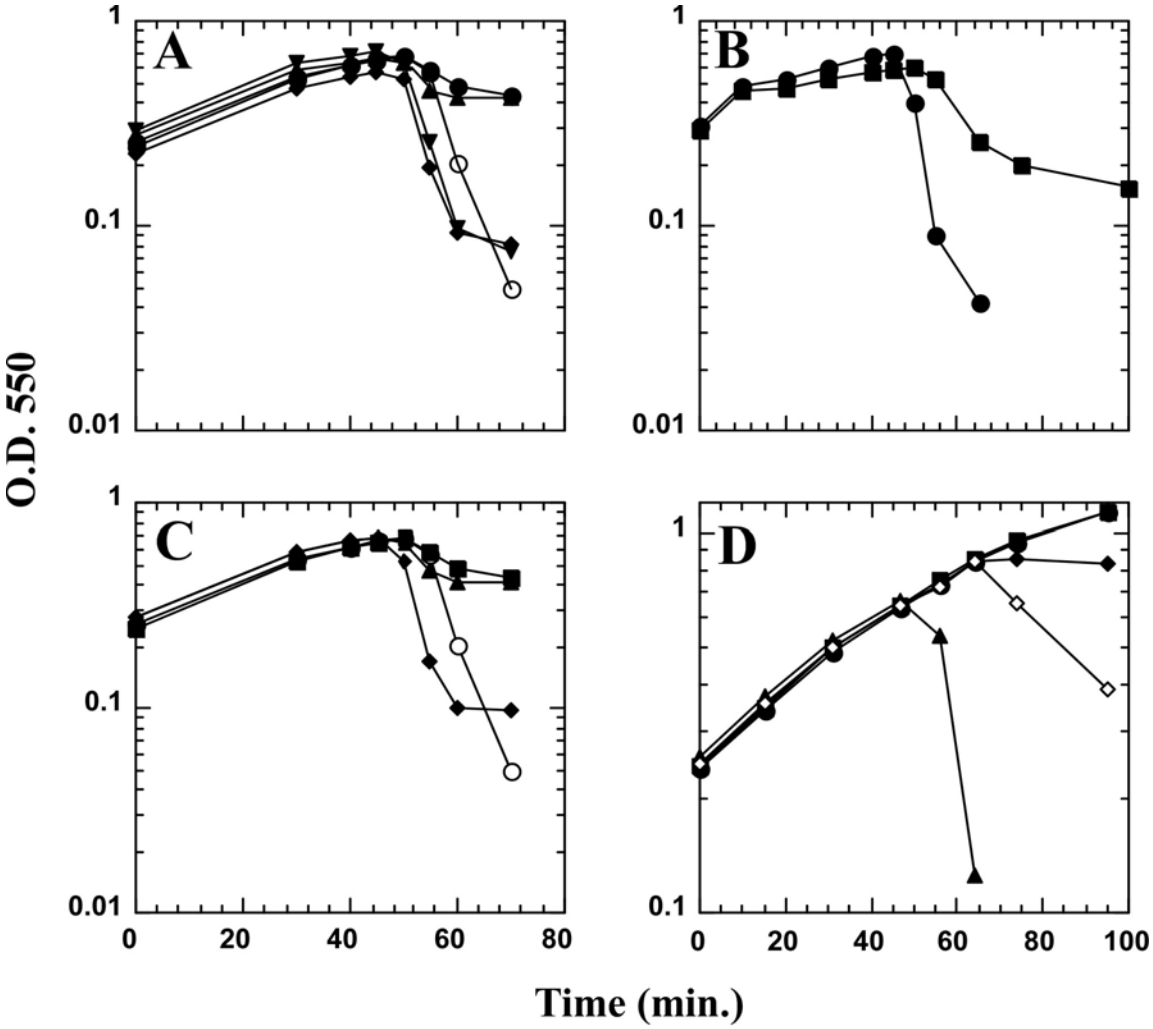


Figure 3.4. Rz1 function requires its OM localization signal. Growth of the indicated cultures after lysogenic (A-C) and/or IPTG (B and D) induction was monitored as described in *Materials and Methods*. The open symbols indicate standard LB media while the filled symbols indicate LB supplemented with 10 mM $MgCl_2$.

A. MC4100(λ900$Rz_{am}Rz1^{+}$) carrying pRE (○,● ); pRE-RzIRS (▼); pRE-PhoAΦ$Rz^{IRS}$ (▲); pRE-FtsIΦ$Rz^{IRS}$ (◆).

B. MC4100(λ900) carrying pJF118EH (●), pJF- PhoAΦ$Rz^{IRS}$ (■).

C. MC4100(λ900$Rz^{+}Rz1$) carrying pRE (○,■); pRE-$Rz1^{AU1}$ (◆); pRE-$Rz1^{AU1}{}_{T21D,S22D}$ (▲).

D. RY17299$lacI^{Q}$ carrying pRW (●) ; pRE-RzRz1 (■); pRW-$Lyz_{C13S,C44S}$ (◇,◆); pRW-RzRz1-$Lyz_{C13S,C44S}$ (▲).

In contrast, replacement of the TMD of Rz with that of FtsI, a type II membrane protein involved in cell division (Guzman *et al.*, 1997), produced a chimera that functioned similarly to Rz in cell lysis (Fig. 3.4A). Next, we altered the Rz1 sequence at the two codons immediately distal to the $Cys_{20}$ residue at which the lipoprotein precursor cleavage and processing occurs, replacing $Thr_{21}Ser_{22}$ with Asp-Asp. As predicted from the specificity of the LOL system (Terada *et al.*, 2001), this alteration redirected Rz1 to the IM (Fig. 3.5). Importantly, this Rz1 derivative was no longer functional (Fig. 3.4C).

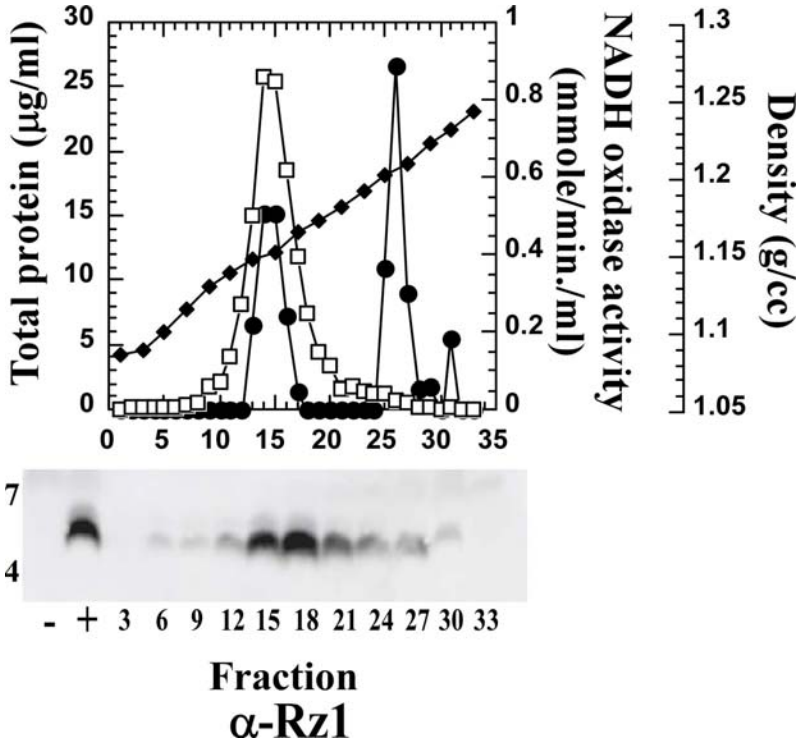


Figure 3.5. The non-functional Rz1Au1T21DS22D mutant localizes to the IM. Membranes from induced RY17299(λ901$Rz_{am}Rz1_{am}$) cells carrying the plasmid pRE-$Rz1^{AU1}_{T21D,S22D}$ were analyzed by sucrose gradient and Western blot, as described for Figure 3.2. Selected MW standards are indicated to the left of the blot.

The function of the Rz-R1 complex is independent of the holin protein

Many dsDNA phage encode SAR-endolysins which are capable of eliciting host lysis in the absence of a holin (Xu et al., 2004). In our studies of Lyz, the SAR-endolysin of bacteriophage P1, we observed that when *E. coli* expressed the *lyz* gene in media containing 10mM $MgCl_2$, they were converted to spherical forms rather than undergoing overt lysis (Fig. 3.4D). This sensitivity to $Mg^{+2}$ clearly mirrored the phenotype of *Rz*$^-$ or *Rz1*$^-$ mutants of bacteriophage λ. Strikingly, cells expressing the *Rz/Rz1* gene pair in addition to *lyz* no longer showed a $Mg^{+2}$-dependent lysis defect (Fig. 3.4D). In fact, cultures expressing the three genes showed an earlier and sharper lysis than those expressing *lyz* alone. These results demonstrate that Rz-Rz1 function, and by extension, also the function of spanins, is independent of holin function.

**Discussion**

Rz and Rz1 localization

Here, we demonstrate that, at physiological levels of expression, Rz and Rz1 are localized to the IM and OM, respectively, with their C-terminal domains predicted to lie in the periplasm. Importantly, when *Rz* and *Rz1* are co-expressed, a large fraction of Rz redistributes to the OM fractions in isopycnic sucrose gradients, likely due to an association between the Rz and Rz1 proteins. This result is at variance with several

other reports showing that Rz and Rz1 accumulate in fractions of density intermediate between the IM and OM (Hanych et al., 1993, Kedzierska et al., 1996, Taylor et al., 1996). However, in all but one case, these experiments were done using either induced $S^+$ lysogens or over-expression of the *Rz* or *Rz1* genes from T7 promoters. Both approaches are problematical. As noted above, separation of the membranes by isopycnic gradient centrifugation depends on spheroplast formation, and stable spheroplasts cannot be obtained if the lambda holin is expressed. In the one experiment using a thermally induced λ*cI857*$S_{am7}$ lysogen, Rz1 was found to be restricted to the OM fraction (Taylor *et al.*, 1996). Significantly, in the same report, Rz1 was found in all cellular fractions if it was over-produced from a hyper-expression T7 plasmid vector.

It is also worth noting that a previous study claimed that the IM and OM completely lose separability in induced lambda lysogens, with essentially all the membranes converted to an intermediate density fraction (Kucharczyk et al., 1991). The change was shown to occur progressively during the infection cycle and to be dependent on late gene expression. However, recent work has shown that the S holin is triggered to hole formation by small decreases in membrane potential (Grundling et al., 2001), which will occur regardless of which method is used to harvest cells prior to spheroplast formation. Thus, these findings are also likely to be artifacts of unsuccessful spheroplasting, especially in view of our results showing that the membranes retain distinct densities in inductions of *Sam7* lysogens (Fig. 3.2).

Structure and topological requirements of Rz-Rz1 complexes

We have shown that Rz-Rz1$_{his}$ complexes can be isolated from detergent-solubilized spheroplasts (Fig. 3.3) and that these complexes appear to mask a proteolysis-sensitive site in the C-terminal third of the Rz periplasmic domain (Fig. 3.2B). Based on the 12 kDa size of the proteolysis fragment, the protease-sensitive site (ca. residues 90 - 115) is, according to secondary structure analysis, in an unstructured region separating two α-helices that occupy most of the Rz periplasmic domain (Fig. 3.1B). Since protection of Rz from proteolysis did not require the co-expression of a functional holin/endolysin gene pair, the interaction between Rz and Rz1 can occur in vivo in the presence of the normal complement of peptidoglycan. These observations are also consistent with results from yeast two-hybrid assays that indicated the C-termini of the Rz and Rz1 equivalents of bacteriophage T7 interact (Bartel et al., 1996).

Significantly, the function of this complex is lost if either protein is improperly localized (Fig. 3.4). Redirecting Rz1 to the IM by changing the lipoprotein sorting signal eliminated function (Fig. 3.4C). Moreover, when the C-terminal domain of Rz is exported to the periplasm using a cleavable signal sequence instead of its normal type II signal anchor domain, it also loses function (Fig. 3.4A), and, in this case, actually antagonizes the function of the wild type protein (Fig. 3.4B). In contrast, Rz function was maintained when its N-terminus was replaced with the type II signal anchor of FtsI (Fig. 3.4A), indicating that being physically tethered to the IM is necessary and sufficient for Rz to carry out its normal function.

A model for the role of Rz-Rz1 in lysis

Our findings are inconsistent with a recent model for the function of Rz/Rz1-like proteins stemming from the study of bacteriophage PRD1 (Krupovic et al., 2008). In this scheme, the Rz/Rz1 complex transmits mechanical stress from holin-mediated lesion formation in the IM to the OM, resulting in its disruption. Here, we show that holin-independent cell lysis brought about by SAR endolysins is blocked by millimolar concentrations of divalent cations and that this blockage is relieved by co-expression of a non-cognate *Rz/Rz1* lysis gene pair. This would appear to rule out any direct role for holin proteins in the function of the Rz/Rz1 complex. Note that this does not rule out an effect of the converse: i.e., effects of Rz/Rz1 on holin function. Indeed missense changes in *lysC*, the *Rz1* gene of phage P2, significantly delay the onset of lysis (Markov et al., 2004). However, without information about the expression of the nearby P2 holin gene under these conditions, these results cannot yet be interpreted in terms of effects of a mutant Rz-Rz1 complex on the IM, and thus potentially, on holin function.

The simplest interpretation of the results reported here might be that the Rz-Rz1 complex improves the efficiency of endolysin degradation of the murein layer. Since the OM is covalently attached to the cell wall by $>10^5$ oligopeptide linkages between Lpp and the murein, a complex that spans the periplasm could conceivably push the IM away from the murein layer. This might make endolysin-mediated murein degradation more efficient, similarly to the requirement for sucrose-mediated plasmolysis in spheroplast formation (Birdsell & Cota-Robles, 1967). We think this is unlikely to be the basis of

Rz-Rz1 function. With phage lambda (R. Young, unpublished; also, see Fig. 3 of Gründling et al. (2001)) and with cells undergoing lysis via a SAR endolysin (M. Xu, unpublished observations), cells pass through a brief spherical stage just before lysis. In the absence of Rz-Rz1 function and the presence of moderate levels of divalent cations, they progress no further. It is difficult to conceive of murein structures uniformly distributed in the spherical cell periplasm that are somehow resistant to the endolysin, especially considering the diversity of enzymatic activities that are manifested among phage endolysins.

An alternative model, which we favor, is that the Rz-Rz1 complex mediates a third and final step in host lysis. In this view, the first step is the temporally-programmed permeabilization of the cytoplasmic membrane by the holin, resulting in the release of a cytoplasmic endolysin or the activation of a SAR endolysin. The second stage is the endolysin-dependent degradation of the murein layer. We propose that this is followed by a third stage involving the fusion of the IM and OM mediated by the Rz-Rz1 complexes. This would cause the cytoplasm and the environment to become topologically equivalent and, thus, all conceivable barriers to the release of the progeny virions would be eliminated. We suggest that the initial Rz-Rz1 complexes are metastable but are competent to undergo conformational changes that bring the two membranes in contact and facilitate their fusion, analogous to the function of SNARE complexes in eucaryotic systems (Jahn & Scheller, 2006). However, premature membrane fusion is prevented since the peptidoglycan meshwork would interfere with the proposed conformational changes and, obviously, prevent close apposition of the IM

and OM. Although this final step is not required in typical laboratory medium lacking sufficient divalent cations to stabilize the OM, the lack of Rz or Rz1 function is noticeable as a diminution in the sharpness of lysis profiles, not only in lysis mediated by SAR endolysins (Fig. 3.4D) but also with the canonical lambda *SR* holin-endolysin lysis (e.g., see Fig. 4 of Summer et al. 2007). The fact that genes for Rz-Rz1 equivalents are found in nearly all phages of Gram-negative hosts (Summer et al., 2007a), indicates that in the osmotic and ionic conditions found in nature, the OM is a significant barrier even after holin-endolysin mediated destruction of the cell wall.

The model predicts that the Rz-Rz1 complex must exist in at least two conformations, with the final form more conformationally stable but inhibited from formation as long as the murein layer is present. How the peptidoglycan barrier interferes with the conformational change is unclear, but the simplest notion would be that the final complexes are too large to be formed as long as the meshwork of the murein is still present. It should be noted that membrane-fusion activity for Rz1 has been suggested before, based on studies with purified, SDS-solubilized Rz1 protein and artificial liposomes (Bryl et al., 2000). However, it is unclear whether any small, proline-rich, N-terminally lipoylated polypeptide might not show this effect, since no controls with mutant Rz1 proteins lacking the putative activity were undertaken. Indeed, our results indicate that Rz1 acting alone has no biological activity. Our model can be tested in a number of ways, including, most directly, by high-resolution cryo-electron microscopy, which may allow visualization of the Rz-Rz1-dependent membrane fusion event.

Finally, we note that while the three steps of phage lysis mediated by holins, endolysins and Rz-Rz1 complexes form a sequential pathway, in which holin function is required for endolysin function, which is in turn required for Rz-Rz1 function, they are mechanistically independent (i.e., do not require heterotypic interactions with each other). This likely accounts for the remarkable diversity and mosaicism found in phage lysis cassettes, which are composed of many unrelated families of holins and Rz-Rz1 proteins, and at least three types of endolysins (Wang *et al.*, 2000, Young, 2002, Young, 2006, Summer et al., 2007a). If there is no direct interaction between the three components of the pathway that assault the three elements of the cell envelope, there would be no restriction on recombinational assortment of the three functions, other than the recently discovered requirement that pinholins must serve SAR endolysins (Park et al., 2007).

# CHAPTER IV

# THE LAMBDA SPANIN COMPONENTS RZ AND RZ1 UNDERGO TERTIARY AND QUATERNARY REARRANGEMENTS UPON COMPLEX FORMATION

## Introduction

The process of λ host cell lysis has three sequential yet phenotypically discrete steps (Fig. 4.1A). The λ holin (S105) forms large hole(s) in the IM at a genetically programmed time and its absence prevents not only cell death, but also lysis by restricting endolysin release from the cytoplasm to the periplasm (Young, 1992). The λ endolysin (R) is a soluble enzyme which degrades the peptidoglycan layer making the cell susceptible to lysis as a result of internal osmotic pressure. Absence of a functional endolysin prevents lysis but not death (Young, 1992) and also results in an apparent block of the as yet to be defined two-component Spanin (Rz and Rz1) function (Berry *et al.*, 2008). The lack of either Spanin component leads to an absolute block of lysis only if the OM is stabilized by mM concentrations of a divalent cation such as magnesium (Zhang & Young, 1999).

The small Spanin subunit reading frame of *Rz1* is entirely embedded in the +1 reading frame of the larger Rz subunit. Rz is a 153 residue IM protein with an N-terminal TMD (Fig. 4.1B). The final 123 residues constitute a C-terminal periplasmic domain. This region of Rz is highly amphipathic in nature and charged residues are

distributed evenly throughout the entire domain. Secondary structure predictions indicate the majority of the periplasmic domain (70%) consists of two stretches of alpha-helix interrupted by a short non-helical linker region (Berry et al., 2008). The mature Rz1 protein is a 40 residue OM lipoprotein with an uncommonly high percentage of proline residues (25%), and thus is devoid of any predictable secondary structure (Fig. 4.1C) (Kedzierska et al., 1996, Summer et al., 2007a).

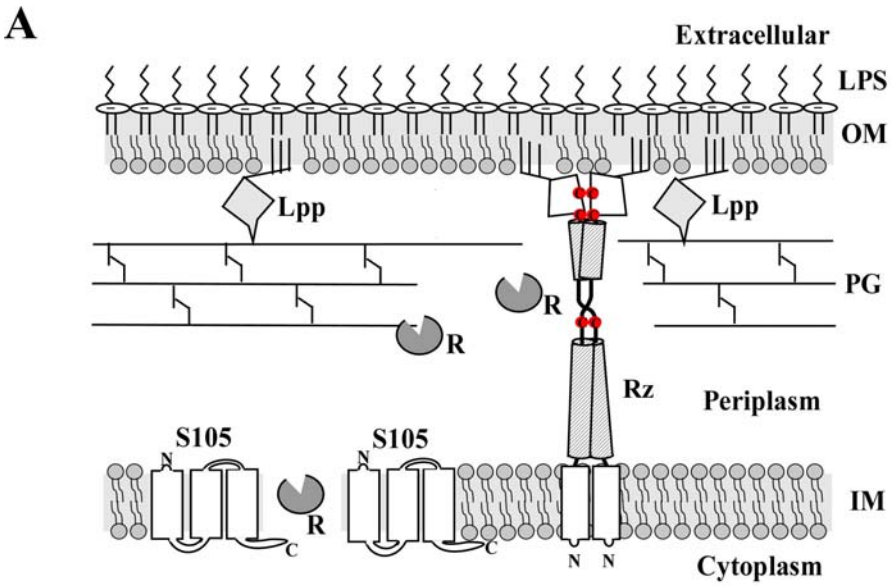


Figure 4.1. The holin-endolysin-spanin model for λ lysis
A. Three step model for lambda lysis. Approximate location of crosslinking disulfide bonds indicated by letter C highlighted in red. See text for details.
B. Rz amino acid sequence. Charged residues are indicated. The predicted N-terminal TMD is highlighted and the predicted α-helical regions are underlined (Summer et al., 2007a). The region of Rz which was deleted during the construction of $pSRzH_6$ is indicated by a cross bar and Δ symbol. Regions containing a heptad repeat are indicated above the sequence. The sequence and location of the C-terminal his tag is also indicated.
C. Rz1 amino acid sequence. Charged residues are indicated. The predicted lipoprotein signal sequence is highlighted in grey with the processed Cys residue is highlighted in black (Juncker et al., 2003). The region of Rz1 which was deleted during the construction of $pSumo\Phi sRz1H_6$ is indicated by a cross bar and Δ symbol. The site at which a SUMO tag was fused to the Rz1 protein during construction of $pSumo\Phi sRz1H_6$ is indicated by an arrow. The sequence and location of the C-terminal his tag is also indicated.

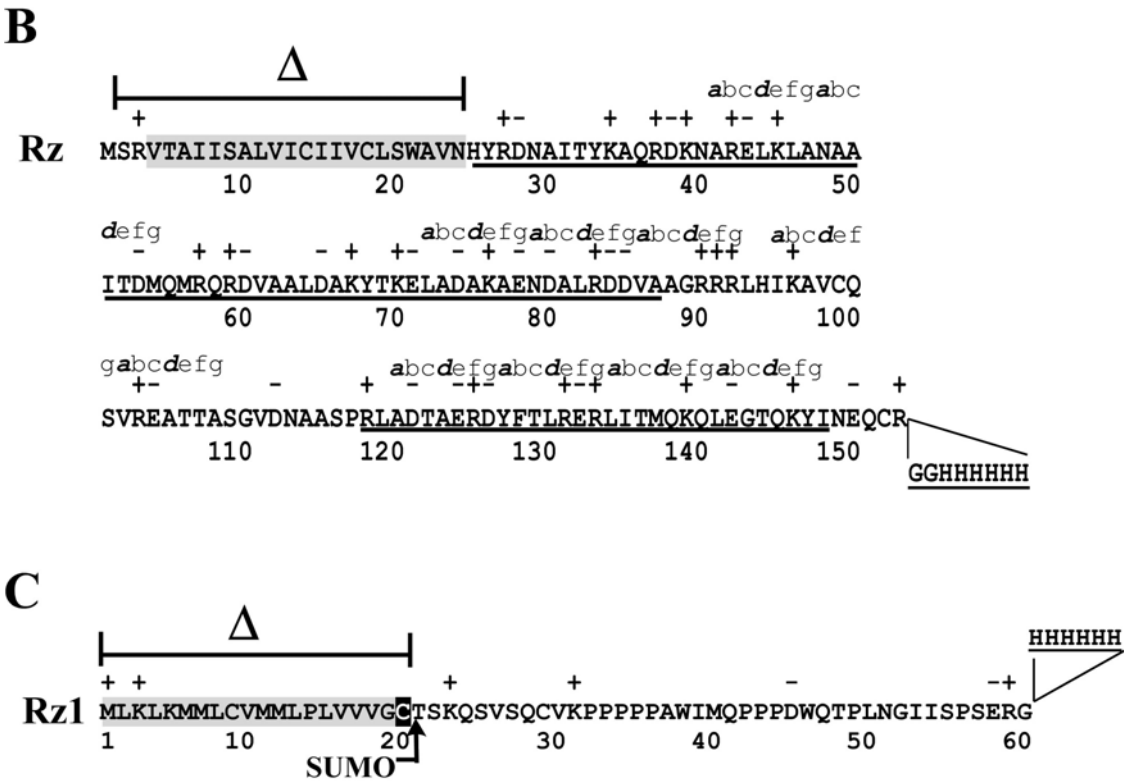


Figure 4.1. Continued.

Prior genetic evidence indicates that Rz and Rz1, which are tethered to apposing membranes, may interact via their C-terminal domains to form a periplasm spanning complex (Markov et al., 2004). In support of this finding, a protein linkage map of the T7 genome indicates that Rz/Rz1 equivalents (18.5/18.7) can interact through their last 50 and 10 residues respectively (Bartel et al., 1996). A detergent-solubilized Spanin complex was isolated from *E. coli* spheroplasts (Berry et al., 2008), but this finding does not rule out the possibility of an indirect interaction. Furthermore, Rz1 was found to prevent proteolysis of the Rz periplasmic domain. This protection occurred in the

absence of the holin/endolysin gene products indicating the Rz-Rz1 complex occurs prior to endolysin mediated PG degradation (Berry et al., 2008).

The divalent-cation dependent phenotype indicates that spanin function is related to destruction of the OM. To date, all attempts to reconcile the phenotype with a molecular mechanism for spanin mediated OM destruction have been purely speculative and none of the resulting models have been verified through direct experimentation. As an initial step toward future biochemical and structural characterization of the Spanin complex, C-terminal HIS-tagged alleles of the Rz and Rz1 periplasmic domains were over-expressed and purified to milligram quantities. The approximate molecular mass of the individual proteins in solution was determined by size exclusion chromatography (SEC) and their secondary structure was evaluated by circular dichroism (CD) analysis. The ability of the soluble Rz periplasmic domain (sRz) and soluble Rz1 periplasmic domain (sRz1) to form a complex was assessed by CD analysis and transmission electron microscopy (TEM). The macromolecular structure of the Spanin complex will be discussed in terms of computer assisted tertiary structure predictions for Rz as well as a model for spanin mediated OM disruption.

## Materials and methods

### Bacterial growth and induction

The bacterial strains and plasmids used in this study are listed in Table 4.1. Bacterial cultures were grown in standard LB media supplemented with $MgCl_2$ (10 mM), ampicillin (100 μg/ml), kanamycin (40 μg/ml), and chloramphenicol (10 μg/ml) when appropriate. Culture growth and lysis profiles were monitored as previously described (Smith et al., 1998a). Briefly, overnight and starter cultures were diluted 300:1 and grown with aeration at 30ºC for lysogenic cultures and 37ºC for cultures of BL21(DE3). Lysogens were thermally induced at A550 ~0.3 by aeration at 42ºC for 20 min, followed by continued growth at 37ºC. Small scale starter cultures intended for inoculation of large scale batch cultures were started from slurry of ~ 100 fresh overnight colonies and grown to mid-log phase prior to sub-culture. Large scale batch cultures carrying the indicated plasmids were induced for expression by the addition of 1mM final concentration of isopropyl β-D-thiogalactosidase (IPTG) at an O.D. of 0.6.

For complementation experiments, the plasmids carrying *Rz* or *Rz1*mutant alleles are derivatives of the medium-copy plasmid pRE carrying the λ late promoter, pR'. In all cases, the λ late gene activator Q is supplied *in trans* from an induced prophage (Zhang & Young, 1999).

Table 4.1. Strains and vectors

| **Strain** | **Description** | **Source** |
|---|---|---|
| XL-1 Blue | *recA endA1 gyrA96 thi1 hsdR17 supE44 relA1 lac* [F' *proAB lacZ*$_{\Delta M15}$::*Tn*10] | Stratagene |
| BL21(DE3) | (*P*$_{lac}$*UV5::*T7 *gene1*) *slyD::Kan tonA::tn10* | Lab stock |
| **Plasmid** | **Description** | **Source** |
| pTB145 | *lacI*$^{Q}$ *P*$_{T7}$*:: H*$_6$*-ulp1*(403-621) *bla* | (Bendezu *et al.*, 2009) |
| pTB146 | *lacI*$^{Q}$ *P*$_{T7}$*::H*$_6$*-sumo bla,* carries a unique sapI cloning site for seamless fusion to SUMO tag | (Bendezu et al., 2009) |
| pRE | Derivative of pJF118EH with *lacI*$^{Q}$ and P$_{tac}$ promoter replaced with pR' promoter region from λ; transcriptionally activated by lambda Q | (Park, *et al.,* 2006) |
| pRE-Rz | *Rz*$^{+}$ cloned in pRE with *Rz1*$_{W38am}$ null mutation | This study, see Ch. III |
| pRE-Rz1 | *Rz1*$^{+}$ cloned in pRE | This study, see Ch. III |
| pETduet | *lacI P*$_{T7}$*::*MCS1*P*$_{T7}$*::*MCS2 *bla* | Novagen |
| pRzH$_6$ | pET duet carrying *Rz* with a GGHHHHHH tag following residue 153 | This Study |
| pSRzH$_6$ | pET duet carrying residues 25-153 of Rz with a C-terminal GGHHHHHH tag and the mutations C99S and C152S | This Study |
| pH$_6$SumoΦsRz1 | pTB146 with residues 21-60 of Rz1 fused to the C-terminus of Sumo tag | This Study |

Table 4.1. Continued

| Plasmid | Description | Source |
|---|---|---|
| pET11a | *lacI,* T7 RNA polymerse promoter*, bla* | Novagen |
| pSumoΦsRz1H$_6$ | pET11a carrying *SumoΦRz*(21-60) with HHHHHH tag placed after codon 60 of *Rz1,* Rz1 carries mutation C29S | This Study |

Standard DNA manipulations, PCR, site directed DNA mutagenesis and DNA Sequencing

Isolation of plasmid DNA, DNA amplification by PCR, DNA transformation, and DNA sequencing were performed as previously described (Tran et al., 2005). Oligonucleotides (primers) were obtained from Integrated DNA Technologies (Coralville, Ia.) and were used without further purification. Restriction and DNA-modifying enzymes were purchased from New England Biolabs (Ipswich, Ma.); all reactions using these enzymes were performed according to the manufacturer's instructions. Site-directed mutagenesis was performed using the QuikChange kit from Stratagene (La Jolla, Calif.) as described previously (Grundling et al., 2000). Oligonucleotide (primer) sequences are listed in Table 4.2. Inverse PCR was carried out through a modified version of quick change site-directed mutagenesis. Forward and reverse primers which anneal to regions flanking the desired deletion region were generated. These forward and reverse primers, unlike traditional forward and reverse

QuickChange primers, anneal to the plus and minus strands respectively. The entire inverse PCR reaction is then treated with DpnI. The PCR product is purified with a PCR purification kit (Qiagen) and treated with T4 polynucleotide kinase (NEB) prior to ligation. The DNA sequence of all constructs was verified by automated fluorescence sequencing performed at the Laboratory for Plant Genome Technology at the Texas Agricultural Experiment Station.

Table 4.2. Cloning-primer sequences

| **Primer** | **Sequence** |
|---|---|
| RzC99SFor | TTGCACATCAAAGCAGTCTCTCAGTCAGTGCGTGAAGCC |
| RzC99SRev | GGCTTCACGCACTGACTGAGAGACTGCTTTGATGTGCAA |
| RzHISFor-2 | GGAATTCCATATGAGCAGAGTCACCGCG |
| RzHISRev-2 | CGCAGATCTCTAGCCGCCGTGATGGTGATGATGGTGGCC GCCTCTGCACTGCTCATTAATATACTTCTGGG |
| RzHISdelFor | CATTACCGTGATAACGCCATT |
| RzHISdelRev | CATATGTATATCTCCTTCTTA |
| RzHISC152SFor | CAGAAGTATATTAATGAGCAGTCTAGAGGCGGCCACCAT CATCAC |
| RzHISC152SRev | GTGATGATGGTGGCCGCCTCTAGACTGCTCATTAATATA CTTCTG |
| SumoRz1For | TATGGTTGCTCTTCCGGTACATCAAAGCAGTCTGTC |
| SumoRz1Rev | ATCTCGAGGCCTCTCTCTGAGGGTGA |
| SumoRz1For-2 | GGGAATTCCATATGTCGGACTCAGAAGTCAATCAAGAA |
| SumoRz1Rev-2 | GCCAAGCTTCTAGTGATGGTGATGATGGTGGCCTCTCTCT GAGGGTGAAA |
| SumoRz1C29SFor | CACAGAGAACAGATTGGTGGTTGCACATCAAAGCAGTCT GTCAG |
| SumoRz1C29SRev | CTGACAGACTGCTTTGATGTGCAACCACCAATCTGTTCTC TGTG |

Plasmid construction

All plasmids used and generated in the course of this study are listed in Table 4.1. The plasmid pSRzH$_6$ used for overexpression of sRz was generated by Inverse PCR using pRzH$_6$ as a template. The plasmid pRzH$_6$ was generated by direct PCR using a forward primer (RzHISFor-2) which contains an NdeI site and a reverse primer (RzHISRev-2) which contains a GGHHHHHH tag followed by a BglII site. Using pRE-Rz as a template, these forward and reverse primers were used to amplify the *Rz* gene. The *RzHIS* fragment was then ligated to a pETduet backbone which was previously subjected to NdeI and BglII digestion. The nucleotides of pRzH$_6$ corresponding to residues 2-24 of the *Rz* reading frame were then deleted by Inverse PCR using the primers RzHISdelFor and RzHISdelRev. Residue C99 of Rz was converted to Serine by site-directed mutagenesis using the primer pair RzC99SFor/Rev. The second Cysteine to Serine substitution was made using the primer pair RzHISC152SFor/Rev resulting in the plasmid pSRzH$_6$.

Two plasmids, pH$_6$SumoΦsRz1 and pSumoΦsRz1H$_6$, were generated for the overexpression and purification of the soluble Rz1 (residues 21-60) periplasmic domain. The plasmid pH$_6$SumoΦsRz1 was produced by first amplifying codons 21-60 of *Rz1* using primer pair SumoRz1For/Rev and pRE-Rz1 as a template. The resulting fragment and the plasmid pTB146 were digested with SapI and XhoI. The cleaved fragment was then ligated to the pTB146 backbone. Use of a SapI site junction between the *sumo* and *Rz1* reading frames results in a seamless in-frame fusion of the two respective gene

fragments. The plasmid pSumoΦsRz1$H_6$ was generated in order to relocate the HIS tag from the N-terminus of *sumo* to the extreme C-terminus of the *Rz1* fragment. Using p$H_6$SumoΦsRz1 as a template, the primer pair SumoRz1For-2/Rev-2 was used to amplify the *sumoΦRz1* region. The forward primer contained an NdeI site and annealed to the template beginning at the start codon of *sumo*, just downstream of the HIS tag. The reverse primer contains a HindIII site followed by a HHHHHH tag. The resulting fragment which contains the *sumoΦRz1* region and a HIS tag following codon 60 of *Rz1* was ligated to pET11a following digestion of both with NdeI and BamHI. The mutation resulting in a substitution of Cysteine at position 29 for Serine was produced with site-directed mutagenesis using the primer pair SumoRz1C29SFor/Rev.

Protein purification

Six one liter cultures of BL21(DE3) carrying the plasmid pSumoΦsRz1$H_6$, pSRz$H_6$ or pTB145 ($H_6$-SUMO tag protease) were harvested approximately five hours post induction by centrifugation in a Beckman JA-10 rotor at 8,000 rpm for 10 minutes. Unless indicated otherwise, all following steps were conducted at or near 4ºC. Cell pellets were resuspended in 60 ml's of 20mM sodium phosphate, 300 mM Nacl, pH7.5 supplemented with 1mM PMSF, Protease Inhibitor Cocktail (Sigma-Aldrich, P8849), and 100 μg/mL final concentrations of DNase and RNase (Sigma Aldrich). Cells were broken by passage through a French pressure cell (Spectronic Instruments, Rochester, N.Y.) at 16,000 lb/in$^2$ and the resulting lysate was cleared by centrifugation in a Sorvall

SS-34 rotor at 15,000 rpm for 20 minutes. Cleared lysates were passed successively through a 5 μm and 0.45 μm filter prior to the addition of 1M Imidazole pH7.5 to a final concentration of 20mM Imidazole. Lysates were then passed over 1 mL bed volume of Talon metal affinity resin (Clontech) which was pre-equilibrated with 20 mM sodium phosphate, 300 mM Nacl, 20mM Imidazole pH7.5. The resin bed was then washed with 10 bed volumes of equilibration buffer. Bound protein was eluted with 6 bed volumes of 20 mM sodium phosphate, 300 mM Nacl, 500mM Imidazole pH7.5. Elution fractions were pooled and concentrated to 3 mL final volume with an Ultra-4 3,000 MWCO centrifugal filter device (Amicon) and loaded onto a prep grade HiLoad 16/60 Superdex-75 column (GE healthcare) pre-equilibrated at room temperature with 10 mM Sodium Phosphate, 100 mM NaCl, pH 7.5. The peak $A_{280}$ fractions were collected and assessed for purity by SDS-PAGE and coomassie blue staining prior to pooling.

Cleavage of the N-terminal SUMO tag to yield residues 21-60 of Rz1 followed by a C-terminal HIS tag required treatment of the fusion protein with the yeast derived Ulp-1 protease (pTB145). Pooled S-75 peak elution fractions containing the N-terminal Sumo tagged Rz1(21-60)HIS were concentrated to 1 mL with an Ultra-4 3,000 MWCO centrifugal filter device (Amicon) and dialyzed extensively against Ulp-1 protease reaction buffer (50 mM Tris-Cl, 150 mM NaCl, 10% glycerol, 1mM DTT, 0.05 % Triton X-100, pH 8) prior to the addition of Ulp-1 protease to a 1:100 molar ratio. The reaction was incubated overnight on ice. The C-terminal His tagged Rz1 fragment was separated from the Ulp-1 protease and the freed Sumo tag by loading the reaction on a Superdex-75 column (Amersham) pre-equilibrated with 10 mM Sodium Phosphate, 100 mM NaCl,

pH 7.5. Specificity of the cleavage reaction was confirmed by automated Edman protein sequencing of the purified Rz1(21-60)HIS protein. N-terminal protein sequencing was performed by the Protein Chemistry Laboratory at Texas A&M University, Dept. of Biochemistry/Biophysics.

Size exclusion chromatography

Size exclusion chromatography was carried out using an Superdex 75 10/300 GL column (GE Healthcare)on a AKTA FPLC (GE Healthcare). The column was calibrated with the Low Molecular Weight Gel Filtration Calibration Kit (GE Healthcare).

Transmission electron microscopy

Extinction coefficients for the sRz and sRz1 proteins were calculated using the ExPASy Proteomics server (Gasteiger *et al.*, 2005). Protein concentrations of purified sRz and sRz1 stock solutions were determined using the molar extinction coefficients 7450 M-1 cm-1 and 11000 M-1 cm-1, respectively, at 280 nm. Purified sRz and sRz1 dialyzed extensively against TBS buffer pH 7.4 were mixed at a molecular ratio of 4:1 (6.3μM sRz: 1.5μM sRz1) respectively and left to incubate for approximately 10 min. Specimens were prepared for EM according to the method of Valentine (Valentine *et al.*, 1968). Briefly, a 50-100 μl drop of sample was placed on parafilm and carbon on mica was floated onto the surface of the drop for 60 seconds to allow the protein complexes to

adhere. The carbon was subsequently floated onto a 100 μl drop of 2% (w/v) aqueous uranyl acetate for 15 seconds and finally picked up with a 400 mesh copper grid and blotted dry. Specimens were observed using a JEOL 1200EX transmission electron microscope operating at 100kV. Images were recorded at a nominal magnification of 25,000X on Kodak 4489 film and developed using standard procedures. Negatives were scanned using a Leafscan 45 scanner. The final pixel size was 4.08 Å on the specimen scale.

Single particle averaging

Approximately 1300 Rz-Rz1 particles were manually boxed using the Boxer software in the EMAN package (Ludtke *et al.*, 1999). Particle images were then low-pass filtered to remove spatial frequencies beyond 15 Å. Particles were then subjected to rotational and translational alignment using an artificial image of a rod as a reference. Finally reference-free class averages were calculated using the refine2d.py routine in EMAN.

Circular dichroism measurements

CD measurements were made using an Aviv model 202SF spectropolarimeter. The sRz and sRz1 proteins were dialyzed extensively against 10mM NaPi 100 mM NaCl pH 7.5. Samples were loaded into a 0.1 cm quartz cuvette and equilibrated to 25ºC for 5

minutes prior to being scanned. Scans from 260-190 nm with a 1 nm step size and 5 sec averaging time were applied to all samples in triplicate. Protein concentrations for stock solutions of sRz and sRz1 were determined by absorption at 280 nm using the molar extinction coefficients listed above. CD and difference spectra were fit by nonconstrained multiple linear regression (MLR) (Greenfield, 1996) using a polypeptide reference set (Brahms & Brahms, 1980). Spectra of the individual sRz and sRz1 proteins were also fit using the CONTINLL (Provencher & Glockner, 1981, van Stokkum *et al.*, 1990) and CDSSTR (Sreerama & Woody, 2000) programs available on the DICHROWEB server (Whitmore & Wallace, 2008).

**Results**

Purification of the Rz and Rz1 periplasmic domains

Following overexpression, the subsequent purification of full-length $Rz^{HIS}$ (residues 1-153) is complicated by poor solubility in detergent(s) (data not shown) and formation of large oligomers due to intermolecular disulfide formation between nonessential periplasmic cysteine residues (see Chapter II). Furthermore, the mature Rz1 lipoprotein, which is also subject to intermolecular disulfide formation (see Chapter II) does not accumulate to appreciable levels when expressed from a T7 promoter (data not shown). The requirement for detergent solubilization in the case of Rz and the low accumulation of Rz1 can both be nullified by simply ridding each protein of its

respective membrane localization signal (Fig. 4.1B and C). Nonessential periplasmic Cysteine residues for Rz and Rz1 (see Chapter II) were substituted with Serine to preempt possible complications due to covalent modification of the thiol groups during the course of IMAC (Dewey *et al.*, 2009).

The respective genetic and biochemical evidence indicates the Rz TMD functions solely in a tethering capacity (Berry et al., 2008) and that the secreted-soluble form of Rz, while non-functional regarding lysis, is still capable of forming a complex with the membrane tethered Rz1 (Berry et al., 2008). We constructed the plasmid pSRz$H_6$ which contains a C-terminal HIS tagged allele of *Rz,* Serine substitutions at C99 and C152, and lacks codons 2-24 which correspond to the TMD. The protein, soluble Rz (sRz), accumulated in the cytoplasm, migrated as a single monomeric species upon SDS-PAGE, and could be purified to near homogeneity by IMAC with 1-2 mg/liter yields (Fig. 4.2A). When the purified sRz protein was chromatographed on S75 resin (fractionation range, 3-100 kDa) a single peak corresponding to a molecular weight of ~ 36 kDa was observed, indicating the sRz is a dimer at room temperature (Fig. 4.2C).

During the course of sRz purification the cleared lysate (Material and Methods) was observed to become cloudy in response to being placed on ice. Allowing the solution to warm to room temperature resulted in a visible clearing of the lysate without any apparent precipitation. The cold-induced cloudiness persisted after 0.2 μm filtration indicating that sRz is present in the filtrate (data not shown).

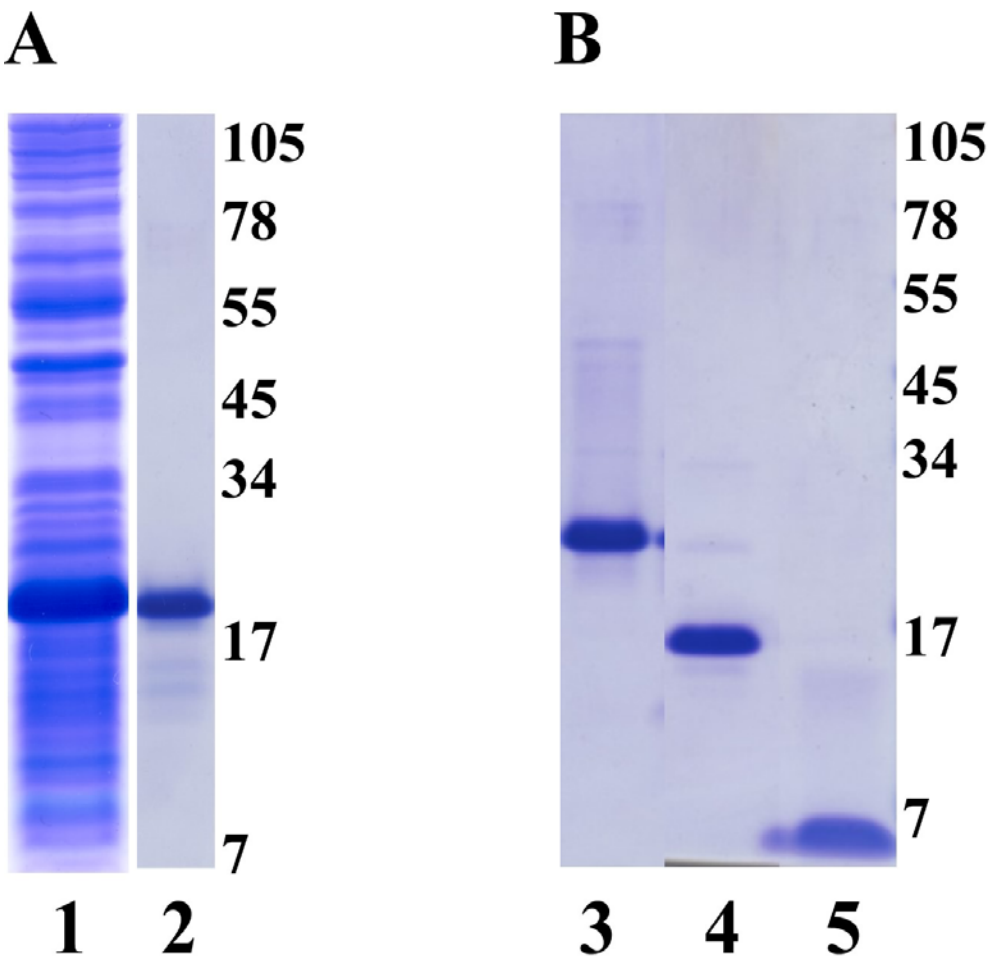


Figure 4.2. Purification of the Rz and Rz1 periplasmic domains.
A. Coomassie blue stained SDS gels showing total protein from the crude lysate following overexpression of sRz (lane 1) and IMAC pooled elution fractions (lane 2). MW standards are indicated to the right of lane 2.
B. Coomassie blue stained SDS gels showing total protein from pooled IMAC elution fractions following overexpression of SumoΦsRz1 (lane 3), freed SUMO tag (lane 4) and sRz1 protein (lane 5) following ULP-1 cleavage and gel filtration, see (C). MW standards are indicated to the right of lane 5.
C. Gel filtration. Elution profiles of SumoΦsRz1(circles) and SumoΦsRz1 ULP-1 cleavage reaction (squares).

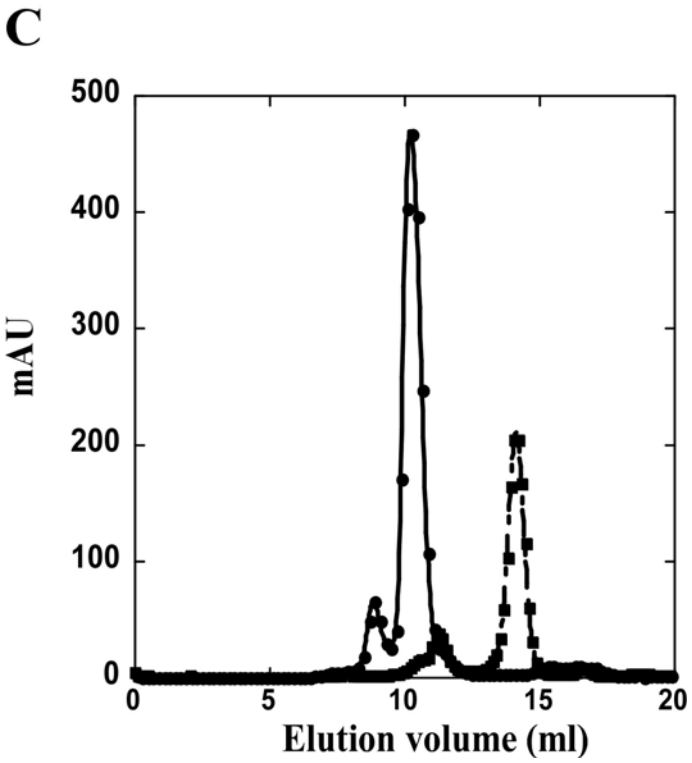


Figure 4.2. Continued.

It was later confirmed that sRz was the responsible agent as near homogenous solutions containing high concentrations (> 5 mg/ml) of the purified sRz protein were found to exhibit an apparently reversible cold-induced aggregation state (data not shown). So far, attempts to visualize these cold-induced sRz aggregates by Cryo-EM have been unsuccessful. For all intensive purposes the protein appears to be stable at working temperature and concentrations.

The lipoylated N-terminal Cysteine at position 20 not withstanding, the proteinaceous component of Rz1 should be entirely periplasmic. However, simply ridding Rz1 of its lipoprotein signal sequence and post-translationally modified C20 did

not resolve the issue of very low accumulation (data not shown). Due to its small size (40 residues) and probable lack of secondary structure due to high proline content (16%) (Fig. 4.1C), the C-terminal HIS tagged Rz1 peptide could be subject to cytoplasmic degradation. In response, the construct $pH_6$SumoΦsRz1 was generated which carries an *$H_6$-Sumo* tag fused to 21$^{st}$ codon of *Rz1C29S*. The $H_6$SumoΦsRz1 protein was found to undergo extensive C-terminal degradation (data not shown) so the N-terminal HIS tag was relocated to the extreme C-terminus of Rz1 (Fig.4.1C). Full-length SumoΦsRz1 accumulated to appreciable levels upon overexpression and could be purified to near homogeneity through IMAC (Fig. 4.2B, lane 3). Efficient cleavage of the Sumo tag was achieved (Fig. 4.2B, lane 4) and the freed soluble Rz1 (sRz1) protein was separated from the ulp-1 protease and sumo tag (Fig. 4.2B, lane 5) by S75 gel chromatography (Fig. 4.2C). The elution volume of the sRz1 peak indicates the protein is monomeric in solution.

CD analysis of the Rz and Rz1 periplasmic domains

The secondary structures of the sRz and sRz1 proteins were estimated by CD spectroscopy. Fig. 4.3A shows the CD spectra of the individual sRz and sRz1 proteins. Three methods were applied to estimate secondary structure content of the proteins (Materials and Methods) and all methods were in good agreement. Multiple linear regression (MLR) analysis of the spectra indicates the sRz dimer is 27% helical, well short of the expected (75%) based on secondary structure predictions, while the sRz1

protein is only 6% helical. All programs agree that the sRz1 protein consists primarily of a random (57-33%) conformation. This result was expected given the high proline content of the sRz1 peptide.

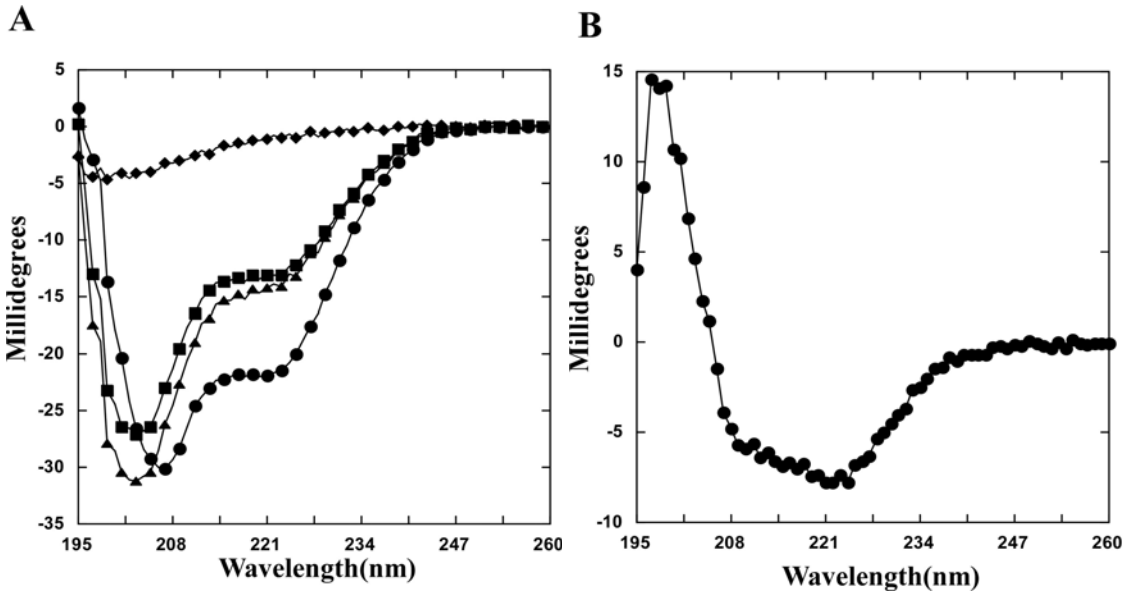


Figure 4.3. The sRz and sRz1 proteins form a complex.
A. CD analysis of sRz, sRz1, and sRz-sRz1 mixture. The individual sRz (■) and sRz1 (◆) spectrum at a final concentration of 20 and 5 μM, respectively. Theoretical spectrum for non-interacting sRz and sRz1 (▲). Spectrum for a 4:1 molar ratio (20μM sRz:5μM sRz1) mixture of sRz and sRz1 (●).
B. Difference plot for sRz-sRz1 complex. Spectrum shown was generated by subtracting mixture spectrum from the sum of the individual sRz and sRz1spectrums shown in (A).

Upon combining sRz and sRz1 an increase in negative ellipticity was observed which is greater than that achieved by simply combining the two individual spectra (Fig. 4.3A). A four to one mixture of the two proteins has a helical content of 33% while

simply combining the sRz and sRz1 spectrums results in a helical content of only 24%. The difference spectrum shows that binding of sRz and sRz1 produces an increase in negative ellipticity at 222, 218, and 208 nm (Fig. 4.3B). The changes at 222 and 208 nm are characteristic of increase in alpha-helical conformation while the change at 218nm is indicative of an increase in Beta-sheet conformation (Greenfield & Fowler, 2002). MLR analysis of the difference spectrum indicates that the changes in secondary structure due to sRz-sRz1 complex formation are primarily helical (50%). Deconvolution of the mixture and difference spectrums to attain secondary structure estimates for sRz and sRz1 are not possible without prior knowledge of complex stoichiometry (personal communication with M. Scholtz and N. Greenfield).

TEM and single particle analysis of the Rz-Rz1 complex

Images of negative-stained Rz-Rz1 complexes revealed a field of mono-dispersed rod-shaped particles (Fig. 4.4A). The length of the rods varied from 14 to 45 nm with an average length of 25 nm and a width of ~4 nm. Although a lengthwise heterogeneity existed, single particle analysis of ~1300 particles revealed some class averages with a coil-like or helical pattern (Fig. 4.4B) and a repeat length of ~4nm. This pattern, although noisier, was also apparent in raw images of the complexes (Fig. 4.4A). No structures were visible by TEM for either sRz or sRz1 alone at the concentrations used for complex formation.

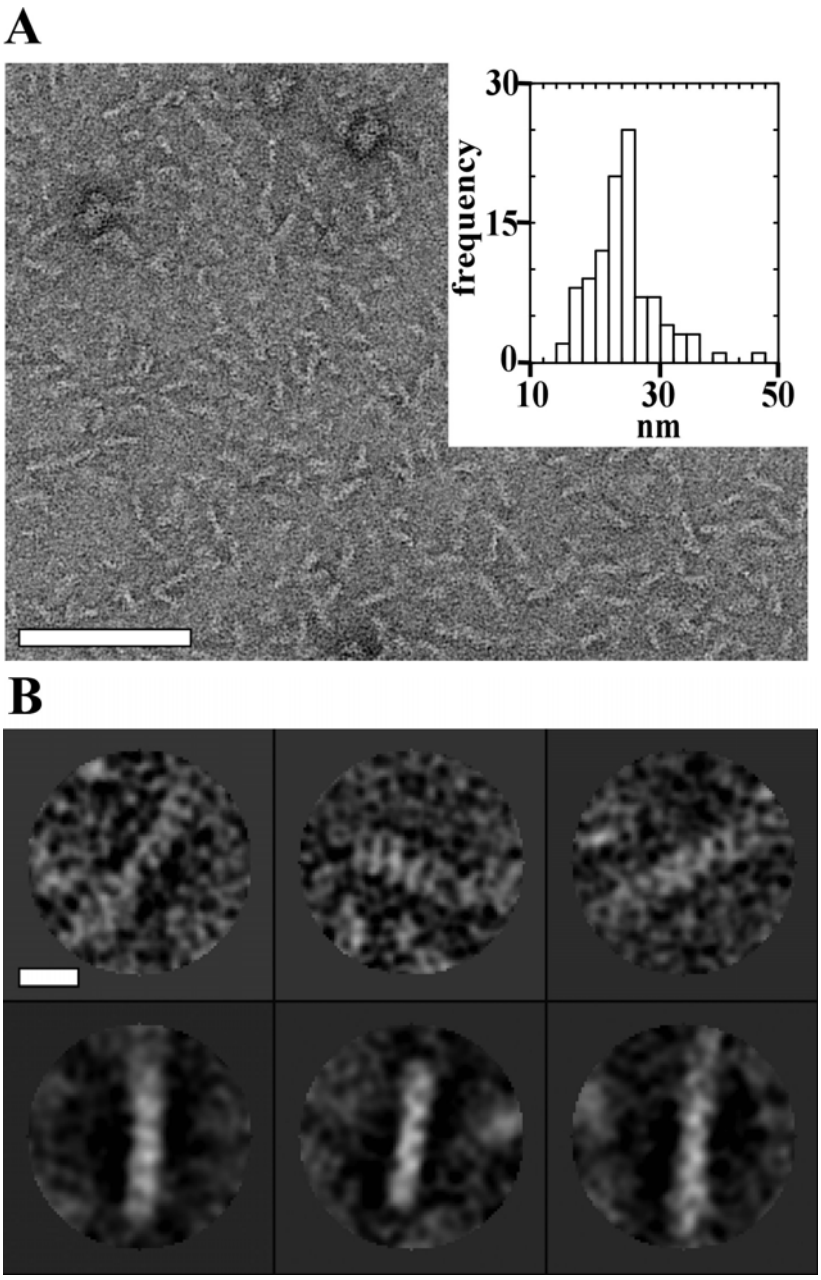


Figure 4.4. TEM and single particle analysis of sRz-sRz1 complex.
A. The sRz-sRz1 complex is an extended rod shaped structure. Image is of a negative stained sample containing a 4:1 molar ratio of sRz:sRz1. Scale bar, 100 nm. Inset, histogram representing the length distribution of the sRz-sRz1 complexes.
B. Single particles and characteristic class averages of the sRz-sRz1 complex. Panels 1-3 are single particles while panels 4-6 are class averages. Scale bar, 10 nm.

Coiled coil prediction for the Rz periplasmic domain

The Rz-Rz1 complex must span a distance of roughly 25 nm (Matias et al., 2003) from the periplasmic-face of the IM to that of the OM. The two predicted alpha helical regions of Rz alone (Summer et al., 2007a) could cover ~14 nm of this required distance if fully extended. In search of further support for an extended conformation of the Rz periplasmic domain, the sequence of λ Rz and known functional equivalents were examined for their propensity to form coiled coils through visual inspection and/or the use of COILS (Lupas *et al.*, 1991) and PairCoil (Berger *et al.*, 1995). Rz (Fig. 4.1B) and functional equivalents from other well characterized phage (data not shown) (e.g. T4, P2, P22, and PRD1) contain regions within their respective periplasmic domains which conform strongly to the heptad repeat. Only one Rz functional equivalent (T7 18.5) is not predicted by COILS or PairCoil to adopt a coiled coil conformation. However, two T7 homologues from phages phiYe03-02 and gh1 do show significant coiled coil prediction (data not shown). The variation in predictions or lack there of in some cases could indicate that these proteins do not form coiled coils. Another possible explanation however is that they simply form non-canonical structures which can not be detected by visual inspection or current search programs.

## Discussion

### sRz and sRz1 purification to high yield

Our primary goal is to understand the biological function of Rz and Rz1 as it relates to host cell lysis. Dissecting the structure of the Rz/Rz1 complex through biochemical and biophysical approaches could provide key insight regarding their function *in vivo*. This work represents the first attempt to purify the soluble periplasmic domains of the λ Rz and Rz1 proteins. We have not ceased work on the purification of the full-length Rz and the mature-lipoylated Rz1, but eliminating the need for detergent during their purification should accelerate progress toward structural characterization via biophysical approaches. The initial attempts at purification of both periplasmic domains were plagued by their susceptibility to proteolytic degradation. In the case of sRz, proteolytic activity was prevented by keeping the sample at or below 4ºC through the completion of the IMAC step of purification. As for sRz1, the extensive C-terminal degradation of the $H_6$SumoΦsRz1 fusion protein was prevented by relocating the $H_6$ tag to the C-terminus. The resultant high yield purification of sRz (2mg/L) and sRz1 (1mg/L) described in this work (Fig. 4.2A-C) will surely aid in the future structural characterization of the two proteins individually and the complex.

The sRz-sRz1 complex

The occurrence of two interacting gene products which are encoded by the same DNA in different reading frames is unprecedented in biology. Although a detergent solubilized Rz/Rz1 complex was isolated after lysogenic induction, this finding did not rule out the possibility of an indirect interaction (Berry et al., 2008). Both our CD and TEM analysis of the sRz and sRz1 mixtures indicate the detergent solubilized complexes consist solely of Rz and Rz1. SEC indicates that the sRz protein is a dimer in solution (Fig. 4.2C) and CD analysis indicates each sRz monomer consist of 26% or ~36 residues of alpha helix (Fig. 4.3A). The sRz1 monomer appears to be primarily unordered based on CD analysis and this finding is consistent with the lack of secondary structure prediction for the Rz1 (Fig. 4.3B). The presence of a poly-L-proline II helix is highly likely however due to a stretch of 5 consecutive proline residues.

We suspect the increase in alpha helical structure due to sRz-sRz1 binding is brought about by changes in sRz since the dimer falls well short of its predicted alpha helical content. We propose a possible scenario for explaining the changes observed by CD due to complex formation. The sRz1 proteins have a relatively weak affinity for self association and binding of a monomeric sRz1 to the C-terminal end of one primarily unordered sRz subunit effectively increases their local concentration to the ends of SRz subunits. Binding of a single sRz1 monomer to each C-terminal end of sRz dimer propagates the extension of coiled coil conformation in an N to C-terminal direction.

The propagation and stabilization of the coiled coil conformation is driven by the self association of sRz1.

TEM of a negative stained sRz-sRz1 mixture revealed the presence of possibly supramolecular rod shaped particles. Regardless, these particles confirm that structural changes observed by CD are due to complex formation. The extended particles which display a distinctive left handed helical pattern could be indicative of parallel coiled coil sRz dimers arranged longitudinally with respect to one another. The biological relevance of these particles is unknown but the average length for the long dimension of approximately 25 nm is in good agreement with the periplasmic width of E.coli K-12.

Determining the molecular mass of the complex and the ratio of sRz to sRz1 within it has been hampered by the tendency of the proteins to aggregate and precipitate upon mixing. The proteins tendency to aggregate upon mixing may be related to the heterogeneous appearance and length of the particles. The presence of heptad repeats throughout sRz could contribute to this behavior if adjacent monomers of sRz dimers are interacting out of register. It is important to note that the Rz protein functions as an IM protein therefore Rz self association is normally much more restricted. The soluble periplasmic domains however can sample infinitely more interaction surfaces. The formation of a supramolecular complex might be analogous to the manner in which α-keratin coiled coil molecules associate into protofilaments. We are however considering the possibility that the rod complex is made up of a 2sRz to 2sRz1 stoichiometry. This conclusion is based solely on TEM based measurements of another dimeric coiled coil

protein which is comparable in size to sRz (Steinmetz *et al.*, 1998). The matter of complex stoichiometry is a subject of future experimental inquiry.

## The biological role of Rz and Rz1

The biological function of Rz and Rz1 is undetermined but genetic evidence indicates the two proteins compromise the structural integrity of the OM (Zhang & Young, 1999). We have demonstrated conclusively in this work that Rz and Rz1 interact directly and that this interaction leads to significant structural rearrangements in one or both proteins. We have also provided a first glimpse at the potential structure of this unique membrane tethering complex. One model for Rz-Rz1 function proposed by Krupovič et al. (2008) states that the sudden lateral movement of holin proteins during hole formation forces the lateral movement of the proximal membrane tethered Rz subunit of the Spanin complex. The force applied to Rz is transferred to the OM through Rz1 and results in a localized disruption of the bilayer. However, we provided strong evidence that Rz-Rz1 function is not holin dependent but rather it relies solely on the absence of the PG (Chapter III; Berry, Summer et al. 2008). So in the course of a normal lambda infection, Rz-Rz1 function is only indirectly reliant on holin mediated hole formation due to its requirement for endolysin release.

# CHAPTER V

## DISCUSSION AND CONCLUSIONS

The work presented in this dissertation provides significant insight into the physiological and biochemical basis of large dsDNA phage lysis. Our understanding of this pervasive biological phenomenon is currently incomplete. The canonical model based primarily on the phage λ consists of two steps. The first step of λ lysis has been the focus of intense investigation. It is now known that the S105 protein accumulates in the IM during vegetative growth until, at a time determined by it primary structure, it oligomerizes to form a large, non-specific hole(s). The host, while still intact but physiologically dead, is now susceptible to the second step. The previously cytoplasmic R proteins diffuse through the S-hole(s) into the periplasm and begin degrading the rigid PG layer of the cell envelope. Under standard laboratory conditions the insult on the PG due to R activity is sufficient to bring about phage release. It is primarily for this reason that the contribution of Rz and Rz1 to lysis has gone undetermined for 30 years. The work presented in the preceding chapters and summarized below allows us to conclude that the Rz and Rz1 proteins interact directly in order to carry out the **essential** and final step of host cell lysis (Fig. 4.1A).

Chapter II addresses three important questions. The first is what does λ lysis look like on the microscopic level. This question has never been addressed directly prior to this work. What we learned from comparing λ and λ$Rz_{am}$ lysis (Fig. 2.1 and 2.2), in

the absence of 10 mM $Mg^{++}$, has fundamentally changed our understanding of phage lysis. The Rz and Rz1 proteins are required for rapid lysis so they can no longer be accurately viewed as accessory lysis proteins. They are in fact necessary for rapid and abrupt lysis.

The Rz/Rz1 phenotype has been masked since its discovery by the flask-induced mechanical shearing of the extremely labile spherical cells. The importance of Rz and Rz1 regarding rapid lysis may prove to be the selective advantage which has resulted in nearly every large dsDNA phage which infects a Gram-negative host to carry *Rz/Rz1* equivalents. All things considered, the OM appears to be a formidable barrier outside of the flask. Thus phages have acquired the means to overcome it. It will be interesting to see if lysis involving a pinholin and SAR endolysin looks the same as λ lysis. Theoretically, SAR endolysin release will result in a disperse assault on the PG as opposed to the localized variety involving canonical holins and endolysins. If lysis does differ between these two lysis systems, it may eventually provide some valuable insight into Rz- Rz1 function.

The second question we address in Chapter II relates to the Cys residue(s) located in the periplasmic domains of Rz and Rz1. Are these periplasmic Cys residues essential? Based on complementation analysis, the answer is no (Fig. 2.3A and 2.4A). However, subsequent SDS-PAGE and Western blotting revealed that both Rz (Fig. 2.3B) and Rz1 (Fig. 2.3B) have a Mr consistent with that of a homodimer under non-reducing conditions. We concluded through the use of Cys to Ser substitution mutants that both Rz and Rz1 are substrates for the formation of intermolecular disulfide bonds.

*In vivo*, Rz and Rz1 exist as a covalent homodimer due to interchain disulfides from C99 to C99, C152 to C152, and C29 to C29 linkages, respectively. To our knowledge this represents the first example of intermolecular disulfide formation occurring between proteins, of native or viral origin, in *E. coli*. Why are the disulfide bonds non-essential? We currently do not have an for answer this question, but perhaps a phenotype will be apparent if λ*RzC99S,C152S* or λ*Rz1C29S* lysis was observed under the microscope. Also yet to be tested is the complementation of λ$Rz_{am}Rz1_{am}$ by RzC99S, C152S and Rz1C29S simultaneously. Furthermore the Rz mutants RzC99S and RzC99S, C152S display an increasing susceptibility of to proteolytic degradation respectively. This suggests that the disulfide bonds may serve to stabilize a conformation of Rz which is more capable of interacting with Rz1.

The final question addressed in Chapter II is based on an unexpected discovery. Seven potential single gene equivalents of *Rz/Rz1* were identified based on genomic location and primary structure analysis (Summer et al., 2007a). Can a single gene product complement the Rz and Rz1 proteins? The answer is yes. The T1 gp11 was found to complement the λ$Rz_{am}Rz1_{am}$ lysis defect (Fig. 2.5). The clear implication, which was subsequently confirmed (see Chapters III and IV), is that Rz and Rz1 interact directly to form a periplasm spanning complex. Another still unresolved implication is that gp11 disrupts the OM in a different manner than a two component spanin such as λ Rz and Rz1. The periplasmic domain of gp11 has drastically different secondary structure predictions from that of Rz and Rz1. The gp11 periplasmic domain is predicted to have five short stretches of β-sheet conformation (Summer et al., 2007a).

At least superficially, the potential difference in secondary structure suggests that while gp11 function is complementary to Rz-Rz1 it has a different mechanism for OM disruption.

The most significant contribution of Chapter III is based on a single but longstanding question. Do Rz and Rz1 form a periplasm spanning complex? The question first arose when it was discovered that null mutations in *Rz* or *Rz1* result in an identical lysis defect (Zhang & Young, 1999). First we addressed the subcellular localization of Rz. The N-terminus of Rz contains a putative signal peptidase I cleavage site leading some to speculate that Rz is in fact a soluble periplasmic protein (Young *et al.*, 2000). However, replacing the N-terminus of Rz with the signal sequence from the *E. coli* phoA protein, a signal peptidase I processed protein, actually produced a partial dominant-negative phenotype (Fig. 3.4B). The non-functionality of phoAΦRz, the IM localization of Rz in the absence of Rz1 (Fig. 3.2B), and the net positive charge of the N-terminal residues proximal the TMD (Fig. 3.1B) (von Heijne, 1992) allows us to conclude that Rz is an type-II IM protein. The Rz1 protein was localized to the OM post lysogenic induction (Fig. 3.1C) providing a partner for a periplasm spanning complex. We isolated a detergent soluble Rz-Rz1 complex (Fig. 3.3 C) and also determined that the Rz and Rz1 proteins must be tethered to their respective membranes in order for the complex to be functional (Fig. 3.4 A and C).

An auxiliary conclusion can also be drawn from results in Chapter III. Krupovič et al. (2008) introduced a holin independent model for Rz/Rz1 function. Our results directly refute two aspects of this model. We found that replacement of the Rz TMD

with a non-cognate TMD had no affect on function (Fig. 3.4A). However, the Krupovič model relies on the co-localization of Rz and the holin. The only conceivable way that Rz and the holin could interact in order to co-localize is through their respective TMDs. This scenario regarding co-localization is highly unlikely given that the FtsIΦRz protein is functional. Furthermore, the Rz and Rz1 proteins appear to disrupt both the inner and OM based on the growth curve of cells co-expressing P1 *lyz* ( a SAR endolysin) and *Rz/Rz1* (Fig. 3.4D). So Rz and Rz1 appear to function without a holin! We conclude that Rz and Rz1 are only indirectly reliant on the holin because hole formation leads to endolysin release. Therefore, it is the resulting PG degradation, not hole formation, which triggers Rz/Rz1 activity.

There is currently no published account concerning the high yield purification of Rz or Rz1. Accordingly, the overexpression and purification of Rz and Rz1 has been a point of focus throughout my entire tenure as a graduate student. The specific aim being to elucidate the mechanism of Rz/Rz1 function through x-ray crystallography and/or NMR analysis. The work described in Chapter IV details the overexpression and purification of the Rz and Rz1 periplasmic domains as well as their initial characterization through CD and TEM analysis. TEM analysis confirmed what CD analysis suggested. The Rz and Rz1 periplasmic domains form a complex. Complex formation is associated with significant changes in primarily α-helical secondary structure (Fig. 4.3B). Imaging of a negative stained sample containing a mixture of the Rz and Rz1 periplasmic domains revealed rod shaped particles with average dimensions of ~ 25nm x 4 nm (Fig. 4.4 A). The average longitudinal axis measurement for the Rz-

Rz1 complex is strikingly similar to our own measurements, ~26.7 nm, for the distance between the periplasmic faces of the inner and outer membranes. The length of these particles being in agreement with the width of the periplasm lends weight an argument that they are physiologically relevant. At this point, given the information we have, there is nothing to suggest that the particles do not accurately represent the Rz-Rz1 tethering complex as it occurs at some point during the process of lysis. The ratio of sRz to sRz1 in the complex is currently unknown, but will certainly be a focal point for future investigation. The particle dimensions are consistent with secondary and tertiary structure predictions for Rz. These predictions suggest that the periplasmic domain of Rz is an extended coiled coil structure. Genetic evidence indicates that Rz1 binds at the C-terminal end of the putative coiled coil structure. Experiments to determine if the rod particle possesses an Rz/Rz1 polarity are currently underway.

**A model for Rz-Rz1 function**

Given that Rz and Rz1 tether the inner and outer membranes, a single, obvious question arises. What happens next? The null phenotype and bioinformatic evidence indicate that the sole purpose of these proteins is to disrupt the OM. We favor a model for OM disruption through the fusion of the inner and outer membranes for the following reasons. Membrane fusion often begins with tethering of adjacent membranes. Also, the mechanism is holin independent. The independence from S105 rules out OM disruption due to consequential mechanical forces associated with hole formation as

proposed by Krupvic et al. (2008). The Rz protein also has features common among other membrane fusion systems. For example, the conserved hinge region and flanking heptad repeat containing α-helical regions are similar to that of the hemagglutinin HA2 region (Cohen & Parry, 1994). The conserved hinge region could possibly be the point at which a collapsing conformational change occurs. The similar HA2 region in hemagglutinin undergoes an extension, as opposed to a collapse in response to increase in pH. The rapid lysis observed by time lapse microscopy (Fig. 2.1 A-C) only in the presence of Rz and Rz1 is also consistent with membrane fusion. If the trigger for Rz-Rz1 activity is PG degradation, a rapid lysis event would be expected to immediately follow the onset of R activity as opposed to a delayed response. A complex mechanism, such as one involving large conformational changes is supported by some of the available *Rz/Rz1* genetics. Mutations isolated in the P2 Rz1 equivalent *LysC* result in significant lysis delays despite the fact that lysis timing is thought to rely solely on holin activity. So how does an OM lipoprotein affect the activity of an IM protein? LysB, the Rz equivalent provides a bridge to the IM, but our evidence suggests that the Rz protein does no interact with the holin. If LysB and LysC are simply a static membrane tether, it is difficult to explain how missense changes in LysC could delay lysis.

We plan to test the membrane fusion hypothesis directly through an *in vitro* system. The first step would be to purify full length Rz and the lipid modified Rz1. Both proteins could then be reconstituted independently to yield separate populations of proteoliposomes. Fluorescence based fusion assays can then be employed to monitor lipid and content mixing due to Rz-Rz1 induced vesicle fusion. If the membrane fusion

hypothesis can be validated, a powerful phage genetics based approach could be developed to isolate mutants. These mutants could be employed in the *in vitro* system to dissect the mechanism of membrane fusion.

## REFERENCES

Bartel, P. L., Roecklein, J. A., SenGupta, D.and Fields, S., (1996) A protein linkage map of *Escherichia coli* bacteriophage T7. *Nat Genet* **12**: 72-77.

Bayer, M. E., (1974) Ultrastructure and organization of the bacterial envelope. *Ann N Y Acad Sci* **235**: 6-28.

Bendezu, F. O., Hale, C. A., Bernhardt, T. G.and de Boer, P. A., (2009) RodZ (YfgA) is required for proper assembly of the MreB actin cytoskeleton and cell shape in *E. coli*. *EMBO J* **28**: 193-204.

Bendtsen, J. D., Nielsen, H., von Heijne, G.and Brunak, S., (2004) Improved prediction of signal peptides: SignalP 3.0. *J Mol Biol* **340**: 783-795.

Berger, B., Wilson, D. B., Wolf, E., Tonchev, T., Milla, M.and Kim, P. S., (1995) Predicting coiled coils by use of pairwise residue correlations. *Proc Natl Acad Sci U S A* **92**: 8259-8263.

Berry, J., Summer, E. J., Struck, D. K.and Young, R., (2008) The final step in the phage infection cycle: the Rz and Rz1 lysis proteins link the inner and outer membranes. *Mol Microbiol* **70**: 341-351.

Bienkowska-Szewczyk, K., Lipinska, B.and Taylor, A., (1981) The R gene product of bacteriophage lambda is the murein transglycosylase. *Mol Gen Genet* **184**: 111-114.

Bienkowska-Szewczyk, K.and Taylor, A., (1980) Murein transglycosylase from phage lambda lysate. Purification and properties. *Biochim Biophys Acta* **615**: 489-496.

Birdsell, D. C.and Cota-Robles, E. H., (1967) Production and ultrastructure of lysozyme and ethylenediaminetetraacetate-lysozyme spheroplasts of *Escherichia coli. J Bacteriol* **93**: 427-437.

Blasi, U., Chang, C. Y., Zagotta, M. T., Nam, K. B.and Young, R., (1990) The lethal lambda S gene encodes its own inhibitor. *EMBO J* **9**: 981-989.

Blasi, U., Nam, K., Hartz, D., Gold, L.and Young, R., (1989) Dual translational initiation sites control function of the lambda S gene. *EMBO J* **8**: 3501-3510.

Blasi, U.and Young, R., (1996) Two beginnings for a single purpose: the dual-start holins in the regulation of phage lysis. *Mol Microbiol* **21**: 675-682.

Brahms, S.and Brahms, J., (1980) Determination of protein secondary structure in solution by vacuum ultraviolet circular dichroism. *J Mol Biol* **138**: 149-178.

Braun, V., Bosch, V., Hantke, K.and Schaller, K., (1974) Structure and biosynthesis of functionally defined areas of the *Escherichia coli* outer membrane. *Ann N Y Acad Sci* **235**: 66-82.

Broome-Smith, J. K.and Spratt, B. G., (1986) A vector for the construction of translational fusions to TEM beta-lactamase and the analysis of protein export signals and membrane protein topology. *Gene* **49**: 341-349.

Bryl, K., Kedzierska, S., Laskowska, M.and Taylor, A., (2000) Membrane fusion by proline-rich Rz1 lipoprotein, the bacteriophage lambda Rz1 gene product. *Eur J Biochem* **267**: 794-799.

Campbell, A.and Delcampillo-Campbell, A., (1963) Mutant of lambda bacteriophage producing a thermolabile endolysin. *J Bacteriol* **85**: 1202-1207.

Casadaban, M. J., (1976) Transposition and fusion of the lac genes to selected promoters in Escherichia coli using bacteriophage lambda and Mu. *J Mol Biol* **104**: 541-555.

Casjens, S., Eppler, K., Parr, R.and Poteete, A. R., (1989) Nucleotide sequence of the bacteriophage P22 gene 19 to 3 region: identification of a new gene required for lysis. *Virology* **171**: 588-598.

Cayley, D. S., Guttman, H. J.and Record, M. T., Jr., (2000) Biophysical characterization of changes in amounts and activity of *Escherichia coli* cell and compartment water and turgor pressure in response to osmotic stress. *Biophys J* **78**: 1748-1764.

Chang, C. Y., Nam, K.and Young, R., (1995) S gene expression and the timing of lysis by bacteriophage lambda. *J Bacteriol* **177**: 3283-3294.

Cohen, C.and Parry, D. A., (1994) Alpha-helical coiled coils: more facts and better predictions. *Science* **263**: 488-489.

Danovaro, R., Dell'Anno, A., Corinaldesi, C., Magagnini, M., Noble, R., Tamburini, C.and Weinbauer, M., (2008) Major viral impact on the functioning of benthic deep-sea ecosystems. *Nature* **454**: 1084-1087.

Dewey, J. S., Struck, D. K.and Young, R., (2009) Thiol protection in membrane protein purifications: a study with phage holins. *Anal Biochem* **390**: 221-223.

Furste, J. P., Pansegrau, W., Frank, R., Blocker, H., Scholz, P., Bagdasarian, M.and Lanka, E., (1986) Molecular cloning of the plasmid RP4 primase region in a multi-host-range tacP expression vector. *Gene* **48**: 119-131.

Gasteiger, E., Hoogland, C., Gattiker, A., Duvaud, S., Wilkins, M. R., Appel, R. D.and Bairoch, A., (2005) Protein identification and analysis tools on the ExPASy server. In The Proteomics Protocols Handbook. J. M. Walker (ed). Totowa, N.J.: Humana Press, pp. 571-607.

Greenfield, N. J., (1996) Methods to estimate the conformation of proteins and polypeptides from circular dichroism data. *Anal Biochem* **235**: 1-10.

Greenfield, N. J.and Fowler, V. M., (2002) Tropomyosin requires an intact N-terminal coiled coil to interact with tropomodulin. *Biophys J* **82**: 2580-2591.

Groman, N. B.and Suzuki, G., (1962) Relation of endolysin to lysis by lambda bacteriophages. *J Bacteriol* **84**: 596-597.

Grundling, A., Blasi, U.and Young, R., (2000) Biochemical and genetic evidence for three transmembrane domains in the class I holin, lambda S. *J Biol Chem* **275**: 769-776.

Grundling, A., Manson, M. D.and Young, R., (2001) Holins kill without warning. *Proc Natl Acad Sci U S A* **98**: 9348-9352.

Guzman, L. M., Weiss, D. S.and Beckwith, J., (1997) Domain-swapping analysis of FtsI, FtsL, and FtsQ, bitopic membrane proteins essential for cell division in *Escherichia coli*. *J Bacteriol* **179**: 5094-5103.

Hanych, B., Kedzierska, S., Walderich, B., and Taylor, A., (1993) Molecular cloning, overexpression of Rz lysis Gene of bacteriophage lambda and subcellular localization of its protein product. In Bacterial Growth and Lysis: Metabolism and Structure of the Bacterial Sacculus. M.A. de Pedro, J.V. Höltje, and W. Löffelhardt (ed). New York: Plenum Press, pp. 269-276.

Hara, T., Matsuyama, S.and Tokuda, H., (2003) Mechanism underlying the inner membrane retention of *Escherichia coli* lipoproteins caused by Lol avoidance signals. *J Biol Chem* **278**: 40408-40414.

Harris, A. W., Mount, D. W., Fuerst, C. R.and Siminovitch, L., (1967) Mutations in bacteriophage lambda affecting host cell lysis. *Virology* **32**: 553-569.

Holtje, J. V., (1998) Growth of the stress-bearing and shape-maintaining murein sacculus of *Escherichia coli*. *Microbiol Mol Biol Rev* **62**: 181-203.

Jahn, R.and Scheller, R. H., (2006) SNAREs--engines for membrane fusion. *Nat Rev Mol Cell Biol* **7**: 631-643.

Johnson-Boaz, R., Chang, C. Y.and Young, R., (1994) A dominant mutation in the bacteriophage lambda S gene causes premature lysis and an absolute defective plating phenotype. *Mol Microbiol* **13**: 495-504.

Juncker, A. S., Willenbrock, H., Von Heijne, G., Brunak, S., Nielsen, H.and Krogh, A., (2003) Prediction of lipoprotein signal peptides in Gram-negative bacteria. *Protein Sci* **12**: 1652-1662.

Kadokura, H., Katzen, F.and Beckwith, J., (2003) Protein disulfide bond formation in prokaryotes. *Annu Rev Biochem* **72**: 111-135.

Kedzierska, S., Wawrzynow, A.and Taylor, A., (1996) The Rz1 gene product of bacteriophage lambda is a lipoprotein localized in the outer membrane of *Escherichia coli*. *Gene* **168**: 1-8.

Kennedy, E. P.and Rumley, M. K., (1988) Osmotic regulation of biosynthesis of membrane-derived oligosaccharides in *Escherichia coli*. *J Bacteriol* **170**: 2457-2461.

Krupovic, M., Cvirkaite-Krupovic, V.and Bamford, D. H., (2008) Identification and functional analysis of the Rz/Rz1-like accessory lysis genes in the membrane-containing bacteriophage PRD1. *Mol Microbiol* **68**: 492-503.

Kucharczyk, K., Laskowska, E.and Taylor, A., (1991) Response of *Escherichia coli* cell membranes to induction of lambda cl857 prophage by heat shock. *Mol Microbiol* **5**: 2935-2945.

Leive, L., (1974) The barrier function of the gram-negative envelope. *Ann N Y Acad Sci* **235**: 109-129.

Ludtke, S. J., Baldwin, P. R.and Chiu, W., (1999) EMAN: semiautomated software for high-resolution single-particle reconstructions. *J Struct Biol* **128**: 82-97.

Lupas, A., Van Dyke, M.and Stock, J., (1991) Predicting coiled coils from protein sequences. *Science* **252**: 1162-1164.

Lutz, R.and Bujard, H., (1997) Independent and tight regulation of transcriptional units in *Escherichia coli* via the LacR/O, the TetR/O and AraC/I1-I2 regulatory elements. *Nucleic Acids Res* **25**: 1203-1210.

Markov, D., Christie, G. E., Sauer, B., Calendar, R., Park, T., Young, R.and Severinov, K., (2004) P2 growth restriction on an rpoC mutant is suppressed by alleles of the Rz1 homolog lysC. *J Bacteriol* **186**: 4628-4637.

Matias, V. R., Al-Amoudi, A., Dubochet, J.and Beveridge, T. J., (2003) Cryo-transmission electron microscopy of frozen-hydrated sections of *Escherichia coli* and Pseudomonas aeruginosa. *J Bacteriol* **185**: 6112-6118.

Nikaido, H., (1996) Outer membrane. In *Escherichia coli* and *Salmonella*: Cellular and Molecular Biology. F. C. Neidhardt (ed). Washington, D.C.: American Society for Microbiology, pp. 29-47.

Oliver, D. B., (1996) Periplasm. In *Escherichia coli* and *Salmonella*: Cellular and Molecular Biology. F. C. Neidhardt (ed). Washington, D.C.: American Society for Microbiology, pp. 88-103

Osborn, M. J.and Munson, R., (1974) Separation of the inner (cytoplasmic) and outer membranes of Gram-negative bacteria. *Methods Enzymol* **31**: 642-653.

Owen, P., Graeme-Cook, K.A., Crowe, B.A., and Condon, C., (1982) Bacterial membranes: preparative techniques and criteria of purity. In Techniques in Lipid and Membrane Chemistry. T. R. Hesketh, Kornberg, H.L., Metcalfe,andJ.C., N., D., Pogson, C.I., and Tipton, K.F. (eds). Amsterdam: Elsevier/North Holland Scientific Publishers, pp. 1–69.

Park, J. T., (1996) Cytoplasmic membrane. In *Escherichia coli* and Salmonella: Cellular and Molecular Biology. F. C. Neidhardt (ed). Washington, D.C.: American Society for Microbiology, pp. 58-87.

Park, T., Struck, D. K., Dankenbring, C. A.and Young, R., (2007) The pinholin of lambdoid phage 21: control of lysis by membrane depolarization. *J Bacteriol* **189**: 9135-9139.

Park, T., Struck, D. K., Deaton, J. F.and Young, R., (2006) Topological dynamics of holins in programmed bacterial lysis. *Proc Natl Acad Sci U S A* **103**: 19713-19718.

Provencher, S. W.and Glockner, J., (1981) Estimation of globular protein secondary structure from circular dichroism. *Biochemistry* **20**: 33-37.

Raab, R., Neal, G., Garrett, J., Grimaila, R., Fusselman, R.and Young, R., (1986) Mutational analysis of bacteriophage lambda lysis gene S. *J Bacteriol* **167**: 1035-1042.

Raab, R., Neal, G., Sohaskey, C., Smith, J.and Young, R., (1988) Dominance in lambda S mutations and evidence for translational control. *J Mol Biol* **199**: 95-105.

Reader, R. W.and Siminovitch, L., (1971) Lysis defective mutants of bacteriophage lambda: genetics and physiology of S cistron mutants. *Virology* **43**: 607-622.

Schindler, M.and Osborn, M. J., (1979) Interaction of divalent cations and polymyxin B with lipopolysaccharide. *Biochemistry* **18**: 4425-4430.

Smith, D. L., Chang, C. Y.and Young, R., (1998a) The lambda holin accumulates beyond the lethal triggering concentration under hyperexpression conditions. *Gene Expr* **7**: 39-52.

Smith, D. L., Struck, D. K., Scholtz, J. M.and Young, R., (1998b) Purification and biochemical characterization of the lambda holin. *J Bacteriol* **180**: 2531-2540.

Sreerama, N.and Woody, R. W., (2000) Estimation of protein secondary structure from circular dichroism spectra: comparison of CONTIN, SELCON, and CDSSTR methods with an expanded reference set. *Anal Biochem* **287**: 252-260.

Steinmetz, M. O., Stock, A., Schulthess, T., Landwehr, R., Lustig, A., Faix, J., Gerisch, G., Aebi, U.and Kammerer, R. A., (1998) A distinct 14 residue site triggers coiled-coil formation in cortexillin I. *EMBO J* **17**: 1883-1891.

Stock, J. B., Rauch, B.and Roseman, S., (1977) Periplasmic space in Salmonella typhimurium and *Escherichia coli*. *J Biol Chem* **252**: 7850-7861.

Summer, E. J., Berry, J., Tran, T. A., Niu, L., Struck, D. K.and Young, R., (2007a) Rz/Rz1 lysis gene equivalents in phages of gram-negative hosts. *J Mol Biol* **373**: 1098-1112.

Summer, E. J., Gill, J. J., Upton, C., Gonzalez, C. F.and Young, R., (2007b) Role of phages in the pathogenesis of Burkholderia, or 'Where are the toxin genes in Burkholderia phages?'. *Curr Opin Microbiol* **10**: 410-417.

Sun, Q., Kuty, G. F., Arockiasamy, A., Xu, M., Young, R.and Sacchettini, J. C., (2009) Regulation of a muralytic enzyme by dynamic membrane topology. *Nat Struct Mol Biol* **16**: 1192-1194.

Taylor, A., (1971) Endopeptidase activity of phage lamba-endolysin. *Nat New Biol* **234**: 144-145.

Taylor, A., Benedik, M.and Campbell, A., (1983) Location of the Rz gene in bacteriophage lambda. *Gene* **26**: 159-163.

Taylor, A., Kedzierska, S.and Wawrzynow, A., (1996) Bacteriophage lambda lysis gene product modified and inserted into *Escherichia coli* outer membrane: Rz1 lipoprotein. *Microb Drug Resist* **2**: 147-153.

Terada, M., Kuroda, T., Matsuyama, S. I.and Tokuda, H., (2001) Lipoprotein sorting signals evaluated as the LolA-dependent release of lipoproteins from the cytoplasmic membrane of *Escherichia coli*. *J Biol Chem* **276**: 47690-47694.

Tokuda, H.and Matsuyama, S., (2004) Sorting of lipoproteins to the outer membrane in *E. coli*. *Biochim Biophys Acta* **1693**: 5-13.

Tran, T. A., Struck, D. K.and Young, R., (2005) Periplasmic domains define holin-antiholin interactions in t4 lysis inhibition. *J Bacteriol* **187**: 6631-6640.

Valentine, R. C., Shapiro, B. M.and Stadtman, E. R., (1968) Regulation of glutamine synthetase. XII. Electron microscopy of the enzyme from *Escherichia coli*. *Biochemistry* **7**: 2143-2152.

van Stokkum, I. H., Spoelder, H. J., Bloemendal, M., van Grondelle, R.and Groen, F. C., (1990) Estimation of protein secondary structure and error analysis from circular dichroism spectra. *Anal Biochem* **191**: 110-118.

von Heijne, G., (1992) Membrane protein structure prediction. Hydrophobicity analysis and the positive-inside rule. *J Mol Biol* **225**: 487-494.

Wagner, P. L., Livny, J., Neely, M. N., Acheson, D. W., Friedman, D. I.and Waldor, M. K., (2002) Bacteriophage control of Shiga toxin 1 production and release by *Escherichia coli*. *Mol Microbiol* **44**: 957-970.

Wang, I. N., Smith, D. L.and Young, R., (2000) Holins: the protein clocks of bacteriophage infections. *Annu Rev Microbiol* **54**: 799-825.

White, R., Tran, T. A., Dankenbring, C. A., Deaton, J.and Young, R., (2009) The N-terminal transmembrane domain of lambda S is required for holin but not antiholin function. *J Bacteriol* **192**: 725-733.

Whitmore, L.and Wallace, B. A., (2008) Protein secondary structure analyses from circular dichroism spectroscopy: methods and reference databases. *Biopolymers* **89**: 392-400.

Wilson, D. B., (1982) Effect of the lambda S gene product on properties of the *Escherichia coli* inner membrane. *J Bacteriol* **151**: 1403-1410.

Xu, M., Arulandu, A., Struck, D. K., Swanson, S., Sacchettini, J. C.and Young, R., (2005) Disulfide isomerization after membrane release of its SAR domain activates P1 lysozyme. *Science* **307**: 113-117.

Xu, M., Struck, D. K., Deaton, J., Wang, I. N.and Young, R., (2004) A signal-arrest-release sequence mediates export and control of the phage P1 endolysin. *Proc Natl Acad Sci U S A* **101**: 6415-6420.

Young, I., Wang, I.and Roof, W. D., (2000) Phages will out: strategies of host cell lysis. *Trends Microbiol* **8**: 120-128.

Young, R., (1992) Bacteriophage lysis: mechanism and regulation. *Microbiol Rev* **56**: 430-481.

Young, R., (2002) Bacteriophage holins: deadly diversity. *J Mol Microbiol Biotechnol* **4**: 21-36.

Young, R., (2005) Phage lysis. In Phages: Their Role in Bacterial Pathogenesis and Biotechnology. D. I. F. Matthew K. Waldor, and Sankar L. Adhya (ed). Washington D.C.: ASM, pp. 92-127.

Young, R.and Blasi, U., (1995) Holins: form and function in bacteriophage lysis. *FEMS Microbiol Rev* **17**: 191-205.

Young, R., and Wang, I.N., (2006) Phage lysis. In The Bacteriophages. R. Calendar (ed). Oxford: Oxford University Press, pp. 104–126.

Young, R., Way, J., Way, S., Yin, J.andSyvanen, M., (1979) Transposition mutagenesis of bacteriophage lambda: a new gene affecting cell lysis. *J Mol Biol* **132**: 307-322.

Zhang, N.andYoung, R., (1999) Complementation and characterization of the nested Rz and Rz1 reading frames in the genome of bacteriophage lambda. *Mol Gen Genet* **262**: 659-667.

Zheng, Y., Struck, D. K., Dankenbring, C. A.andYoung, R., (2008) Evolutionary dominance of holin lysis systems derives from superior genetic malleability. *Microbiology* **154**: 1710-1718.

# VITA


Name: Joel Dallas Berry

Permanent Address: 300 Olsen Blvd.
TAMU 2128
Bio./Bio. Rm. 315
College Station, Tx 77843

Email Address: j_berry@tamu.edu


Education: B.S., Biochemistry
Mississippi State University
Starkville, Mississippi

Ph.D., Biochemistry
Texas A&M University
College Station, Texas